DEVELOPMENT OF NOVEL POROUS CARBONS USING AGRICULTURAL BIOMASS FOR HIGH PERFORMANCE AND COST-EFFECTIVE ELECTRODES FOR SUPERCAPACITOR APPLICATION

Submitted in partial fulfilment of the requirements for the award of the degree of

Doctor of Philosophy

by

T. RAMESH

(Roll No: 714051)

Under the supervision of

Prof. L. RAM GOPAL REDDY
Internal Supervisor
Professor
Department of Physics

Dr. N. RAJALAKSHMI
External Supervisor
Team Leader & Senior Scientist
CFCT-ARCI, Chennai

DEPARTMENT OF PHYSICS
NATIONAL INSTITUTE OF TECHNOLOGY
WARANGAL - 506004, (T. S.), INDIA

September – 2020

*I would like to thank my **parents** for allowing me to be independent and strongly believing in my thoughts and supporting me to pursue Ph. D degree to fulfill my dreams.*

I dedicate this research work for their unconditional love, support, and encouragement.

CERTIFICATE

This is to certify that the work presented in the thesis entitled "**Development of Novel Porous Carbons Using Agricultural Biomass for High Performance and Cost-Effective Electrodes for Supercapacitor Application**" is a bonafide work carried out by **Mr. T. Ramesh (Roll No. 714051)** under our supervision and was not submitted elsewhere for the award of any degree.

19-09-2020

Prof. L. RAM GOPAL REDDY
RESEARCH SUPERVISOR
Professor
Department of Physics
National Institute of Technology
Warangal

PROFESSOR
Department of Physics
N.I.T., Warangal-4.

N. Rajalakshmi Sep 2020

Dr. N. RAJALAKSHMI
RESEARCH SUPERVISOR
Team Leader & Senior Scientist
Centre for Fuel Cell Technology
(CFCT-ARCI)
Chennai

Warangal
September, 2020

DECLARATION

This is to certify that the work presented in the thesis entitled "**Development of Novel Porous Carbons Using Agricultural Biomass for High Performance and Cost-Effective Electrodes for Supercapacitor Application**" is a bonafide work done by me under the supervision of Prof. L. Ram Gopal Reddy and Dr. N. Rajalakshmi and was not submitted elsewhere for the award of any degree.

I declare that this written submission represents my ideas in my own words and where others' ideas or words have been included, I have adequately cited and referenced the original sources. I also declare that I have adhered to all principles of academic honesty and integrity and have not misrepresented or fabricated or falsified any idea / data / fact / source in my submission. I understand that any violation of the above will be a cause for disciplinary action by the Institute and can also evoke penal action from the sources which have thus not been properly cited or from whom proper permission has not been taken when needed.

T. Ramesh.

T. RAMESH

Roll No. 714051

Date: 18-09-2020

ACKNOWLEDGEMENTS

First and foremost, I would like to thank the Almighty for giving me this opportunity, strength, and good health to carry out all my research work without any hassles.

I would like to express my sincere gratitude to my supervisor **Prof. L. Ram Gopal Reddy**, National Institute of Technology Warangal (NITW), for his guidance, constant support, and motivation which helped me to go forward and to complete my Ph.D. His valuable guidance and comments always helped me to focus and achieve the research objectives. Equally, I would like to extend my sincere thanks to my supervisor, **Dr. N. Rajalakshmi**, Team Leader, Centre for Fuel Cell Technology (CFCT), ARCI for her constant guidance, support, and encouragement throughout my Ph.D. She helped me to learn and utilize all the experimental facilities at CFCT-ARCI, which has boosted my confidence as a researcher. Her valuable comments, critical suggestions, analytical opinions have always propelled me to achieve the aimed research objectives.

I extend my sincere thanks to my Doctoral Scrutiny Committee (DSC) members **Prof. K. V. Gobi**, Department of Chemistry **and Prof. R. L. N. Sai Prasad, Dr. D. Paul Joseph** Department of Physics, NITW, for their valuable comments and suggestions which helped in the progress of my Ph. D work.

I would like to express my sincere gratitude to **Dr. K. S. Dhathathreyan**, Former Associate Director, CFCT-ARCI for his motivating and inspiring words. His diverse research thoughts and opinions always inspired me to approach a scientific problem in a simple and effective manner.

I would also like to express my gratitude to **Dr. G. Padmanabham**, for providing me with the ARCI fellowship and all the facilities to carry out the research work at the Institute. I express my deep sense of gratitude to **Dr. R. Gopalan**, Regional Director, ARCI-Chennai, for the critical technical reviews, moral support, and constant encouragement extended throughout my research tenure.

I thank **Prof. N. V. Ramana Rao**, Director, NITW for giving me an opportunity to register my Ph. D at the esteemed institute. I also thank **Prof. D. Dinakar**, Head, Department of Physics, NITW for providing the necessary support during my Ph. D tenure. I take this opportunity to sincerely acknowledge all the faculty members at the Department of Physics NITW. I am also thankful to all the non-teaching staff, NIT-W for their support.

I am sincerely thankful to **Dr. K. Ramya**, Senior Scientist, **Dr. R. Balaji**, Senior Scientist at CFCT for their support and valuable suggestions during our lab meetings.

I would like to specially thank **Dr. Raman Vedarajan**, Scientist at CFCT, for his guidance, support, and motivation, also for spending his valuable time to correct my thesis.

I am grateful to Late **Mr. Parthasarathy, Mr. Vasudevan, Mr. Kannadasan, Mr. Sudalai and Mr. Velmurugan** for their technical support without whom the experiments could not have been completed effectively. I am also thankful to **Mr. P. Sampath Kumar** and **Mrs. Geetha Sundar** for their administrative support at CFCT-ARCI. I would like to thank our **housekeeping** people and **securities** for keeping our lab environment always clean and safe during my stay at CFCT-ARCI.

I specially thank **Dr. Anusree Unnikrishan** and **Dr. N. Manjula**, both of whom have always supported my thoughts, had kept me motivated, and had kept my spirits boosted up even during the sober periods of my life.

I am also indebted to the following friends for various reasons related to my Ph. D work, all of whom deserve special mention: **Dr. Anusree Unnikrishan, Dr. N. Manjula, Dr. K. Naga Mahesh, Mrs. J.A. Prithi, Mr. B. V. Sasank, Mr. M. Deenadayalan, Dr. Harigopi, Mr. Rajkumar, Dr. Abha Bharti, Mr. Tamil Selvan, Dr. P. M. Pratheeksha, Mr. M. Nagaraju, Dr. M. Mohan Babu, Dr. Ramarajan, Mr. N. Purushotham Reddy, Mr. G. Buchaiah, Mr. R. Muniramaiah.** I also express my thankfulness to all the present and past research scholars of NITW and CFCT-ARCI.

I am infinitely indebted to my loving parents **Mrs. T. Pathmavathy** and **Mr. S. Thangavel**, without whose motivation I would not have been what I am. Their unconditional love and affection always inspired me to achieve my goals and beyond and gave strength and confidence to complete impossible tasks more than my strength, including my Ph.D.

I would like to thank my brother **Mr. T. Thanapal**, and sister-in-law **Mrs. T. Priya** for their moral support, and special thanks to my niece **Ms. Thisasree** for making my family happy and nursing my ailing father, which was the greatest booster for completing my Ph. D degree successfully.

ABSTRACT

Development of a highly efficient and cost-effective supercapacitor system with good energy characteristics is crucial for the growth of the supercapacitor market. Physical and electrochemical properties of the electrode and electrolyte materials play a vital role in the energy characteristic of the supercapacitor. Carbon materials derived from various renewable (biomass resources) and non-renewable precursors have shown promising electrochemical behavior in the supercapacitor application. This work reports the development of novel porous carbon electrode materials using agricultural biomass wastes. Agricultural biomasses with different chemical compositions were identified for the synthesis of carbons with novel morphological features using the three main strategies and further an efficient diagnostic tool has been developed for the rapid evaluation of new electrode materials for supercapacitor. The salient features of the research work are as follows:

- Cellulose and hemicellulose rich jute fibre with intrinsic micro-tubular structure is converted into **activated carbon fibre** using the process of direct carbonization.
- Tannin rich tamarind seed coat is converted into **porous carbon microfibers** using hydrothermal method.
- The third strategy included Xyloglucan rich tamarind seed kernel as precursor to synthesize **carbon microspheres** and **carbon aerogels** using hydrothermal method and sol-gel method, respectively.
- The textural properties of these different morphological carbons are optimized by chemical activation method using KOH. A symmetric two electrode cell was fabricated using the synthesized carbon materials and an aqueous 6 M KOH as an electrolyte. The electrochemical behavior of the assembled cell was systematically studied using cyclic voltammetry (CV), galvanostatic charge-discharge (GCD), and electrochemical impedance spectroscopy (EIS) techniques. The synthesized electrode materials have shown very high specific capacitance and the results compare well with the other biomass derived carbon materials.
- To improve the energy density, 1-butyl 3-methyl imidazolium bistrifluoro sulfonyl imide (BmIm-TFSI), an ionic liquid is used as the electrolyte owing to its high ionic conductivity and large potential window. The electrochemical results have shown a

remarkable enhancement in the energy density with the ionic liquid electrolyte based systems.

The energy densities of the synthesized samples have shown promising values both in the aqueous and ionic liquid electrolyte systems. The highest energy density value of 25.7 W h $kg^{-1}$is obtained for carbon aerogels compared to other samples because of its high surface with multimodal pore size distribution. Further, an energy density of as high as 119.2 W h kg^{-1} is obtained for the ionic liquid electrolyte system with the carbon microfibres as electrode. Whereas the 6M KOH aqueous electrolyte system with the same electrode material has only a low energy density of 21.1 W h kg^{-1}

Further, a novel method of using dynamic electrochemical impedance spectroscopy (DEIS) has been developed for identifying the new electrode materials with potential for high performance for supercapacitor application, through rapid evaluation.

CONTENTS

ABBREVIATIONS & SYMBOLS

ACF	: Activated carbon fibres
ASC	: Asymmetric supercapacitor
BET	: Brunauer–Emmett–Teller model
BMIM-TFSI	: 1-Butyl-3-methylimidazolium bis(trifluoromethylsulfonyl)imide
CAG	: Carbon aerogel
CF	: Carbon fibres
CNT	: Carbon nanotube
CV	: Cyclic voltammetry
DEIS	: Dynamic electrochemical impedance spectroscopy
DMF	: N, N Dimethyl formamide
DI	: Deionized water
EDLC	: Electric double layer capacitor
EIS	: Electrochemical impedance spectroscopy
EMIM-TFSI	: 1-Ethyl-3-methylimidazolium bis(trifluoromethylsulfonyl)imide
FTIR	: Fourier transform infrared spectroscopy
GCD	: Galvanostatic Charge discharge
GO	: Graphene oxide
HSC	: Hybrid supercapacitor
IL	: Ionic Liquid
IHP	: Inner Helmholtz plane
MOF	: Metal organic framework
OHP	: Outer Helmholtz plane
PANI	: Polyaniline
PCMF	: Porous carbon micro-fibres
PCMS	: Porous carbon micro-spheres
PPy	: Polypyrrole
PSC	: Pseudo supercapacitor

PTFE : Polytetrafluoroethylene

PVA : Polyvinyl alcohol

PVDF : Polyvinylidene fluoride

SC : Supercapacitor

SCE : Saturated calomel electrode

SEM : Scanning electron microscopy

SSHSC : Solid-state hybrid supercapacitor

SCCM : Standard cubic centimeters per minute

TEABF4 : Tetraethylammonium tetrafluoroborate

TEM : Transmission electron microscope

XRD : X-ray diffraction

ZIF : Zeolitic imidazolate framework

d : Distant between double layer electrode and double layer

n : Number of electron transfer

z : Charge of the ion

σ : Ionic conductivity

ε_r : Relative permittivity

k : Boltzmann constant

T : Temperature

T_b : Boiling point

T_m : Melting point

η : Viscosity

E_{red} : Reduction potential

E_{oxd} : Oxidation potential

C_{sp} : Specific capacitance

C_{dl} : Double layer capacitance

R_{ct} : Charge transfer resistance

R_s : Solution resistance

F : Faraday constant

V : Voltage

i : Current

t : Discharge time

dv/dt	: Scan rate
MW	: Molar weight
m	: Mass of each electrode
S_{mic}	: Micropore surface area
S_{tot}	: Total surface area
V_{mic}	: Micropore volume
V_{tot}	: Total pore volume

LIST OF FIGURES

List of Tables

CHAPTER 1

INTRODUCTION

1.1 Energy and Environmental Challenges

Availability of clean and low-cost energy is central to the techno-economic development of human civilization. Abundant and inexpensive fossil fuels have been used for industrialization and human development for over 250 years. The global energy system currently relies 85.5% on fossil fuels, although reliance on fossil fuels ranges from 32.1% to 100% in different countries [1]. The rapid consumption of fossil fuels has led to CO_2 and other emissions resulting in drastic climate change and environmental pollution [2, 3]. Presently, the CO_2 emissions from various industries and the transport sector have become the greatest threat [4]. According to the Global Carbon Project, the amount of CO_2 produced was 37.1 gigatons in 2018 [5]. Further, carbon dioxide emissions from fossil fuel sources have risen by 2.7 percent in 2018, compared to 1.6 percent in 2017 [5].

Shifting away from fossil fuels and transforming to renewable energy sources will be a viable option to reduce global CO_2 emissions [6-7]. Renewable energy sources like solar [8], wind [9], tidal [10], hydro [11], etc., hold great promise to meet the ever-increasing demand for the energy. However, these renewable energy sources are dependent on the uninterrupted availability of driving force, which hinders the energy utilization. This issue can be effectively handled by the use of clean and efficient electrochemical energy storage systems (EES).

EES systems like batteries and supercapacitors are emerging as potential candidates for efficient energy and transport applications [12-14]. The demand for EES systems is increasing due to their high energy and power densities, long-term cyclic life, and low cost [12-14]. EES systems are generally characterized based on their energy characteristics and are represented by the Ragone plot, as shown in **Figure 1.1**. It shows that each EES system possesses its own advantages and disadvantages in terms of energy and power density [15, 16]. To fulfill the future energy requirements, it is imperative to develop an energy system that offers both high energy density and high power density capabilities. Supercapacitor or ultracapacitor has drawn significant interest in both industrial and transport applications because of its distinct features like high power density, fast charging / discharging and long cycle life compared to batteries [17-19]. It combines the features of both conventional dielectric capacitors and batteries like fast charging and long discharge ability, respectively [20].

The demand for supercapacitor market has increased tremendously as they are used in various industrial applications. As per, “Supercapacitor Market- Global Industry Analysis, Size, Share, Growth, Trends, and Forecast, 2018-2026” published by Transparency Market Research

(TMR), the supercapacitor market is expected to reach a compound annual growth rate (CAGR) of 15.24% from 2018 to 2026 [21].

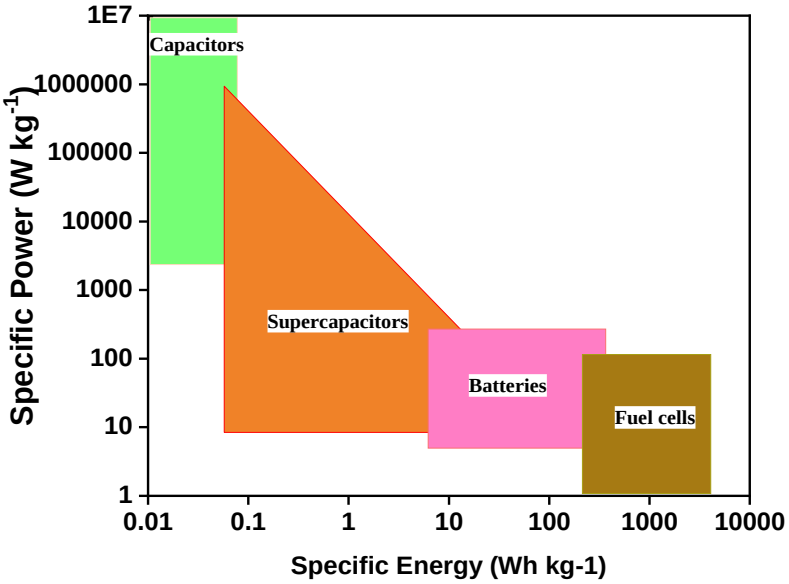

Figure 1.1 The Ragone plot showing energy density vs. power density of various energy storage and conversion devices.

1. 2 Supercapacitor

Supercapacitor (SC) or ultracapacitor is an electrochemical energy storage device, like a battery for the storage of electrical energy via electrochemical reactions at the interface of electrode and electrolyte. In 1853, the concept of charge accumulation at the interface of electrode and electrolyte known as "double layer" was first described by Hermann von Helmholtz. The amount of charge accumulated on the electrode surface is directly proportional to the applied voltage ($\Psi_0 = \Psi$) [22]. Extensive work has been carried out by Gouy-Chapman and Stern to explain the model for "electric double layer", shown in **Figure 1.2**. Gouy and Chapman developed a model called "*diffuse double layer"* in which the change in concentration of the counter ions near a charged surface follows the Boltzman distribution, $n = n_0 \exp(-ze\Psi_0/kT)$ {where, n- bulk concentration, z- charge on the ion, k - Boltzmann constant}. Later, Stern modified the Gouy-Chapan model by considering that ions do have finite size and cannot reach the electrode surface nearer than a few nm. Also, he assumed that some of the ions are specifically adsorbed on the electrode surface, and this layer is called as the Stern Layer shown in **Figure 1.2** [22]. Based on this concept various types of SCs are made using different electrode materials.

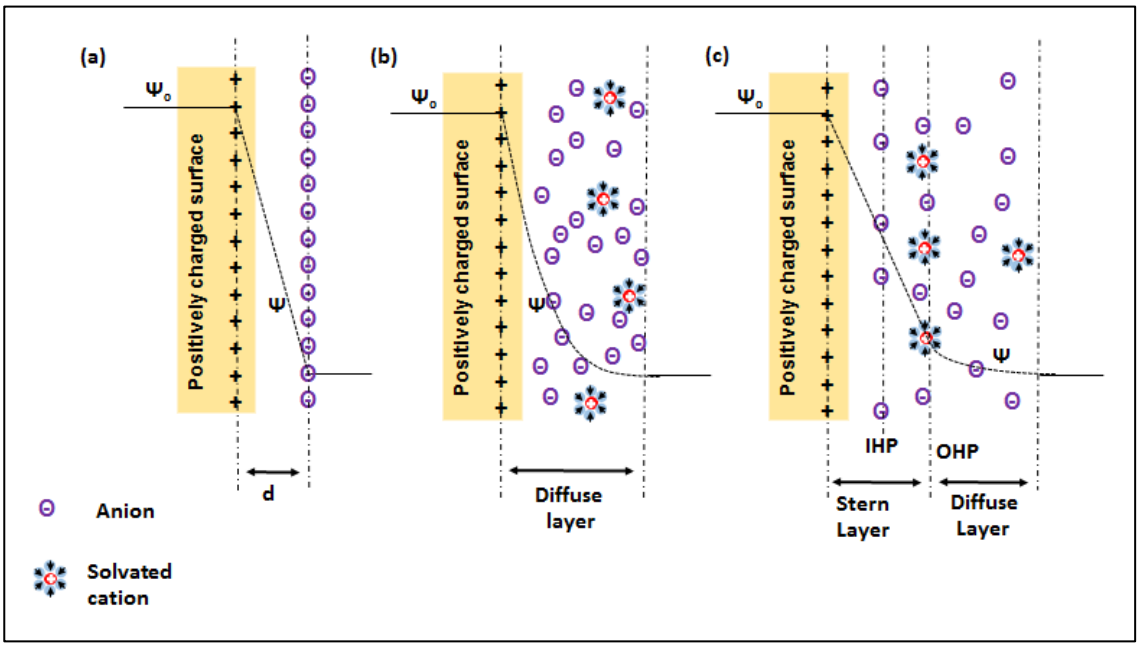

Figure 1.2 Electrochemical double layer models (a) Helmholtz (b) Gouy-Chapman, and (c) Stern.

A typical SC cell consists of two electrodes, each composed of a metal current collector coated with a conducting high surface area material and immersed in an electrolyte separated by a porous thin film separator. While charging, one electrode will be charged positively, and the other will be charged negatively. At this stage, anions and cations present in electrolyte are migrated towards the positive (anode) and negative (cathode) electrode surface, respectively. It has several advantages that includes:

High specific capacitance: It has the capability to store a lot of energy in the same space compared to dielectric capacitors.

High power density: It delivers very high power in a fraction of second due to its very low internal impedance.

High columbic efficiency: It has very high columbic efficiency (< 95%) than batteries and can be operated at wide temperature ranges (-35 °C to 65 °C).

Fast Charging: It takes less than a minute to charge a supercapacitor, unlike batteries which take several hours to charge.

Longevity: The lifetime of supercapacitors is much longer than that of batteries, usually between 10 and 20 years.

1. 3 Types of Supercapacitor

Currently, there are three major types of supercapacitors, classified based on the type of electrode material and charge storage mechanism, namely electric double layer capacitor (EDLC), pseudocapacitor (PSC), and hybrid supercapacitor (HSC).

1. 3. 1 Electric double layer capacitor (EDLC)

A schematic representation of typical EDLCs is shown in **Figure1.3**. It consists of two symmetric electrodes with a thin separator immersed in electrolyte solution separating them. EDLCs store charges by the non-faradaic process, and the charges are accumulated on the surface of the electrodes when a potential is applied between them [23-24]. For EDLCs, charging and releasing capacity are profoundly reversible. This results in extremely high cyclic stability. High surface area conducting materials with high chemical stability are utilized as electrodes in EDLCs. Activated carbon, carbon nanotube, graphene, carbon aerogel, templated carbon, zeolites, etc., are some of the commonly used EDLC electrode materials.

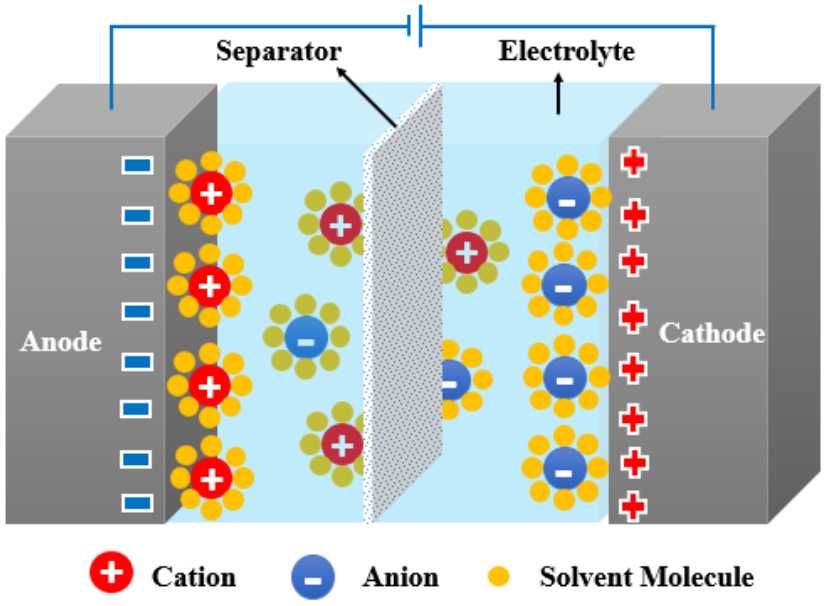

Figure 1.3 Schematic representation of electric double layer capacitor.

1. 3. 2 Pseudocapacitor (PSC)

The PSCs store the charge via faradaic process that is reversible. Mostly, metal oxides are used as electrode materials for PSCs (**Figure 1.4**). The merits of metal oxide electrodes are as follows: high theoretical specific capacitance, large potential window, environmental

friendliness, etc. Their limitations are poor conductivity (10^{-5} to 10^{-6} S cm^{-1}), poor chemical, and electrochemical stability [25]. The mechanism of charge storage on metal oxides is either via adsorption and (or) electron transfer at the electrode-electrolyte interface is given below [26-27],

$$(MO_2)_{surface} + C^+ + e^- \rightarrow (MO_2.C)_{surface} \quad (1)\ (Or)$$

$$MO_2 + C^+ + e^- \rightarrow MOOC \quad (2)$$

Where M is metal (Mn, Ru, and Ti, etc.) and C (H^+, Li^+, Na^+, and K^+, etc.,) is a cation present in the electrode and electrolyte, respectively.

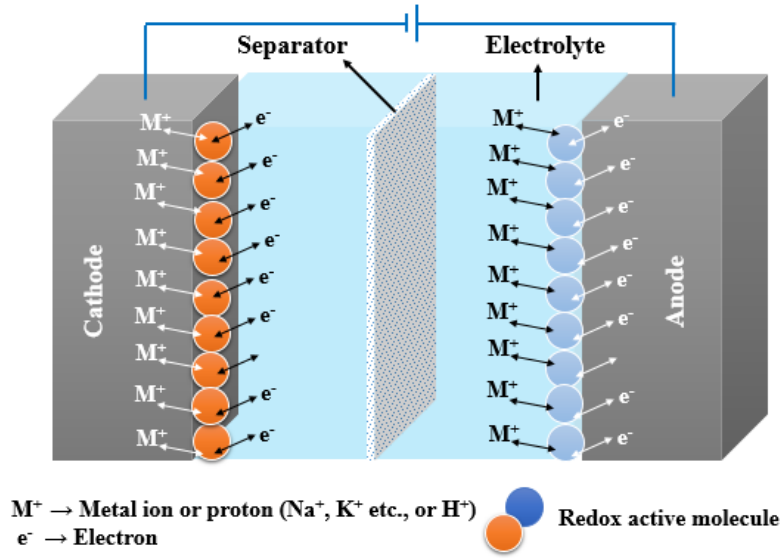

Figure 1.4 Schematic representation of pseudocapacitor.

Theoretical capacitance (C_{sp}) of the metal oxide systems can be calculated using the following formula [28],

$$Theoretical\ C_{sp} = \frac{n.F}{MW.V} \quad (F\ g^{-1}) \quad (3)$$

Where n is the number of electrons transferred, F is Faraday Constant, MW is Molecular weight, and V is applied potential.

1. 3. 3 Hybrid supercapacitors (HSC)

HSCs are fabricated to provide the combined advantage of EDLC and PSCs such as high power density and high energy density, respectively [29-30]. The HSCs consists of EDLC and PC type electrodes for anode and cathode, respectively. The commonly used HSC cathode

materials are metals oxides, composite electrode (MnO_2/C, RuO_2/C), and battery materials [31]. The high surface area carbon materials are used as anode materials. HSCs are having a better cyclic stability over PSCs and high energy density than EDLC. The configuration of the HSC is shown in **Figure 1.5**. The specific capacitance of the anode and cathode are measured separately using the cyclic voltammetry technique. Generally, the cell fabrication is based on the active mass required to store an equal amount of columbic charge ($q_{electrode}$) on both electrodes [32].

$$q_{electrode} = m_{anode}.C_{sp.anode}.\Delta V_{anode} = m_{cathode}.C_{sp.cathode}.\Delta V_{cathode} \quad (4)$$

where q is the columbic charge, ΔV is the potential window and m is the active mass of electrode.

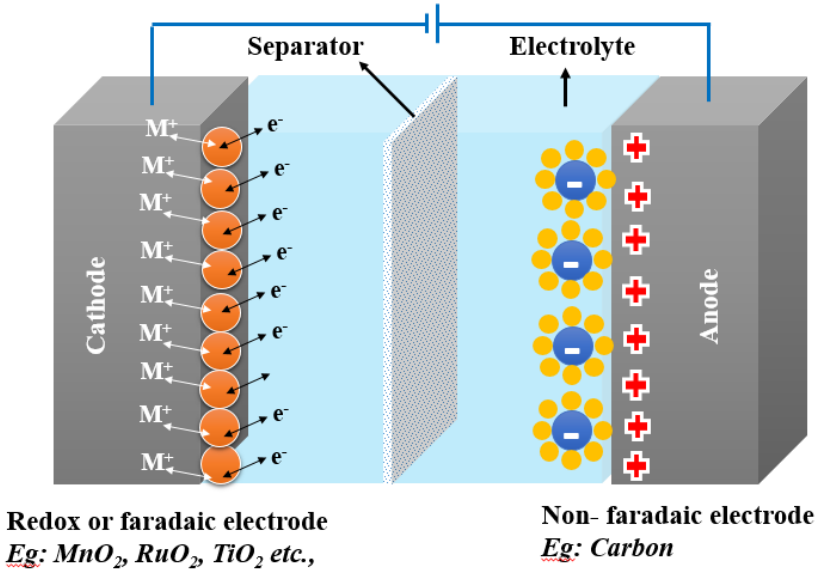

Figure 1.5 Schematic representation of hybrid supercapacitor.

The characteristic features of various energy storage systems along with their performance, cost, and electrolyte used, are listed in **Table 1.1**. Considering the merits and demerits of each one of the SC systems, EDLC is considered as a promising medium for energy storage owing to its offers high power density and long cycle life which are essential for stationary, portable devices, and transport applications. However, the use of EDLCs is impeded by its low energy density compared to other SCs systems. The energy density of EDLCs can be enhanced by increasing the specific surface area of the electrode material and optimization of pore size based on the electrolyte ion size, and using ionic liquid as an electrolyte to enlarge the potential window (< 3 V) of the SC ($E = \frac{1}{2}CV^2$).

Table 1.1 Summary and comparison between energy storage systems (Dielectric capacitor, Supercapacitor, and Li-ion Battery) [33-34].

Characteristics	Dielectric capacitor	Supercapacitor			Li-ion Battery
		EDLC	Pseudocapacitor	Hybrid	
Charge time (s)	10^{-12} – 10^{-3}	1-10	1-10	100	600
Cycle life	> 100000 cycles	100000	100000	500000	500
Cell Voltage (V)	6-800	2.7	2.3-2.8	2.3-2.8	3.6
Capacitance (F)	< 2.7	0.1- 30000	100 – 12000	300-3300	-
Specific Energy (W h kg^{-1})	0.01 – 0.05	3-5	10	180	250
Cost per kWh (USD)		˜ 10000	˜ 10000	˜	˜ 140
Operating Temperature (°C)	20-100	-40 to 65	40-65	40-65	20-60
Self-discharge per month (%)		60	60	a	4
Efficiency (%)	99	95	95	90	90
Type of electrolyte	-	Aprotic or Protic (TEABF4 or H2SO4)	Protic (H2SO4)	Aprotic TEABF4	Aprotic (EC:DMC)

The capacitance of value of the commercial supercapacitor mostly represented in Farad or F. Whereas, the specific capacitance considered only for the materials and represented in F g^{-1} or F/cm^2. In this thesis, the specific capacitance of the materials is represented in F g^{-1} taking account of active materials weight or loading.

As mentioned, the electrochemical performance of EDLCs is mainly dependent on the electrode material as well as the electrolyte. Mostly, porous carbon (PC) materials are used as electrode due to its high surface area, tunable pore size, high conductivity, high chemical stability, and low cost. PC materials are generally produced using carbon-rich raw materials

like animal wastes, agricultural wastes, and their byproducts which are available in abundance. The carbon conversion process usually consists of direct carbonization followed by activation, which results in high surface area and porosity. So far, various approaches have been attempted to form a structured porous carbon from biomass and agricultural wastes based on experimental method and nature of the raw materials used.

In this work, we have used agricultural waste materials for the fabrication of PC due to their high carbon content, abundant availability, and fascinating chemical and physical properties. Jute fibres and tamarind seed constituents are chosen as raw materials to form a different microstructure using different experimental methods.

1. 4 Objectives of the present study

- The main objective of this thesis is to develop low-cost porous carbon materials using agricultural biomass, which is renewable and eco-friendly.
- To enhance the energy density of the SCsystem by using ionic liquid electrolyte.
- Rapid evaluation of new electrode materials for supercapacitor application through dynamic electrochemical impedance spectroscopy.

1. 5 Structure of this thesis

This thesis is organized into eight chapters,

Chapter 1 gives a brief introduction about the electrochemical energy systems, in general, and the supercapacitors for energy storage, in particular. The types of supercapacitor systems and their advantages and disadvantages have been discussed in detail. Further, it gives the objectives and scope of the present study.

Chapter 2 presents the literature review on supercapacitor systems, particularly the electrochemical double layer capacitors. In literature survey, both the electrode and electrolyte materials have been covered along with the choice of precursor materials and experimental procedures for the development of structural PCs [10-15].

Chapter 3 deals with the materials synthesis and characterization techniques used in the present study. It explains the synthesis techniques used to obtain the microstructural porous carbons from agricultural biomass under different experimental conditions. Various characterization techniques are used for studying the physical characteristics of the new carbon materials synthesized.

Chapter 4 describes in detail the synthesis of activated carbon fibres from raw jute by the direct carbonization process. The effect of carbonization temperature and chemical activation on the specific surface area has been discussed.

Chapter 5 describes in detail the process of conversion of tamarind seed kernel into porous carbon microspheres and presents its electrochemical performance for supercapacitor applications.

Chapter 6 describes the preparation of hierarchical porous carbon micro-fibres from tamarind seed coat using hydrothermal method. Electrochemical performance was studied in both aqueous and ionic liquid electrolytes. The relation between surface area, pore size, and electrochemical performance are analyzed.

Chapter 7 presents the preparation of advanced porous carbon aerogels from tamarind seed kernel by a simple synthesis scheme. The effect of temperature on the surface area and pore size distribution has been evaluated. The outstanding capacitive electrode was identified using dynamic electrochemical impedance spectroscopy.

Finally, **chapter 8** summarizes the work along with performance highlights and gives the scope for future work.

References

[1] Ediger VS, *Energy Procedia.*, **2019**, *156*, 2.

[2] Teixeira ACR and Sodre JR, *Transp. Res. D*, **2018**, *59*, 375.

[3] Quéré CL, Korsbakken JI, Wilson C, Tosun J, Andrew R, Andres RJ, Canadell JG, Jordan A, Peters GPand van Vuuren DP, *Nature Climate Change*, **2019**,*9*, 213.

[4] Zhang Y, Chen X, Wu Y, Shuai C, Shen L, *Environ. Impact Assess. Rev.*, **2019**, *79*, 106303.

[5] Quéré CL, Andrew R. M, Friedlingstein P, and Sitch S et al., *Earth Syst. Sci. Data*,**2018**, *10*, 2141.

[6] Cho JH and Sohn SY, *J. Clean. Prod.*, **2018**,*193*, 290.

[7] Slater JD, Chronopoulos T, Panesar RS, Fitzgerald FD, and Garcia M, *Int. J. Greenh. Gas Control.*,**2019**, *91*, 102818.

[8] Kumavat PP, Sonar P, and Dala DS, *Renew. Sustain. Energy Rev.*, **2017**, *78*, 1262.

[9] Hooper T, Beaumont N and Hattam C, *Renew. Sustain. Energy Rev.*, **2017**, *70*, 230.

[10] Mohanty A, Viswavandy M, Ray PK, Mohanty S, *J. Ocean Engi. Sci.*, **2016**, *1*, 256.

[11] Dallinger B, Schwabeneder D, Lettner G and Auer H, *Renew. Sustain. Energy Rev.*, **2019**, *107*, 482.

[12] Chong LW, Wong YW, Kumar R, Rajkumar RK, and Isa D, *Renew. Sustain. Energy Rev.*, **2016**, *66*, 174.

[13] Liu C, Neale ZG, and Cao G, *Mater. Today*, **2016**, *9*, 109.

[14] Wang L, Han Y, Feng X, Zhou J, Qi P, and Wang B, *Coord. Chem. Rev.*,**2016**, *307*, 361.

[15] Yoo HD, Markevich E, Salitra G, Sharon D and Aurbach D, *Mater. Today*, **2014**, *17*, 110.

[16] McCloskey BD, *J. Phys. Chem. Lett*.,**2015**, *6*, 3592.

[17] Chen J, Li C, and Shi G, *J. Phys. Chem. Lett.*, **2013**, *4*, 1244.

[18] Liu T, Zhang F, Songa Y, and Li Y, *J. Mater. Chem.A*, **2017**,*5*, 17705.

[19] Sun MH, Huang SZ, Chen LH, Li Y, Yang XY, Yuan ZY, and Su BL, *Chem. Soc. Rev.*, **2016**,*45*, 3479.

[20] Teng Y, Liu E, Ding R, Liu K, Liu R, Wang L, Yang Z, and Jiang H, *Electrochim. Acta*, **2016**, *194*, 394.

[21] https://www.transparencymarketresearch.com/supercapacitor-market.html.

[22] Conway BE, *Academic Publishers/Plenum Press, Dordrecht/New York*, **1999**.

[23] Salunkhe RR, Kamachi Y,Torad NL, Hwang SM, Sun Z, Dou SX,Kim JH, and Yamauchi, *J. Mater. Chem.A*, **2014**, *2*, 19848.

[24] Wang D, Fang G, Xue F, Ma J, and Geng G, *J. Power Sources*, **2016**, *307*, 401.

[25] Lang X, Hirata A, Fujita T and Chen M, *Nat. Nanotechnol.*, **2011**, *6*, 232.

[26] Toupin M, Brousse T and Belanger D, *Chem. Mater.*,**2004**, 16, *16*, 3184.

[27] Iamprasertkun p, Tanggarnjanavalukul C, Krittayavathananon A, Khuntilo J, Chanlek N, Kidkhunthod P, and Sawangphruk M, *Electrochimi. Acta*, **2017**, *249*, 26.

[28] Zhi M, Xiang C, Li J, Li M, and Wu N, *Nanoscale*, **2013**, *5*, 72.

[29] Wang J, Liu S, Zhang X, Liu X, Li N, Zhao J, and Li Yao, *Electrochim. Acta*, **2016**, *213*, 663.

[30] Bretesche NG, Crosnier O, Buvat G, Favier F, and Brousse T, *J. Power sources*, **2016**, *326*, 695.

[31] Muzaffar A, Ahamed MB, Deshmukh K, and Thirumalai J, *Renew. Sustain. Energy Rev.*,**2019**, *101*, 123.

[32] Roldan S, Barreda D, Granda M, Menendez R, Santamaria R, and Clara Blanco, *Phys. Chem. Chem. Phys.*, **2015**,*17*, 1084.

[33] Libich J, Maca J, Vondrak J, Cech O, and Sedlarikova M, *J. Energy Storage*, **2018**, *17*, 224.

[34] Afif A, Rahman SMH, Azad AT, Zaini J, Islan MA, and Azad AK, *J. Energy Storage*, **2019**, *25*, 100825.

CHAPTER 2

LITERATURE REVIEW ON NATURAL CARBON SOURCES

2.1 Brief History

The first working prototype supercapacitor (SC) was fabricated using activated carbon (high surface area) as an electrode and aqueous ion-conducting solution (NH_4Cl and H_2SO_4) as electrolyte by General Electric Corporation in the year 1975 [1]. This work has led to the growth and commercialization of a variety of SC cells with novel high surface area electrode materials and large potential window electrolytes. Subsequently, different companies have successfully commercialized the SC cell with capacitance ranging from 7 to 4000 F and maximum operating voltage ranging from 2 to 6 V [2]. Over the past several decades, enormous efforts have been made to improve the energy and power densities of SCs by incorporating advanced nanoporous carbon electrodes with highly ionic conducting electrolyte solutions.

A survey of publications shows that the number of research articles in this particular field has been increasing enormously with every passing year indicating the massive growth and advancement of SC in the energy storage sector as depicted in **Figure 2.1**. This survey includes the work carried out both in electrode and electrolyte materials.

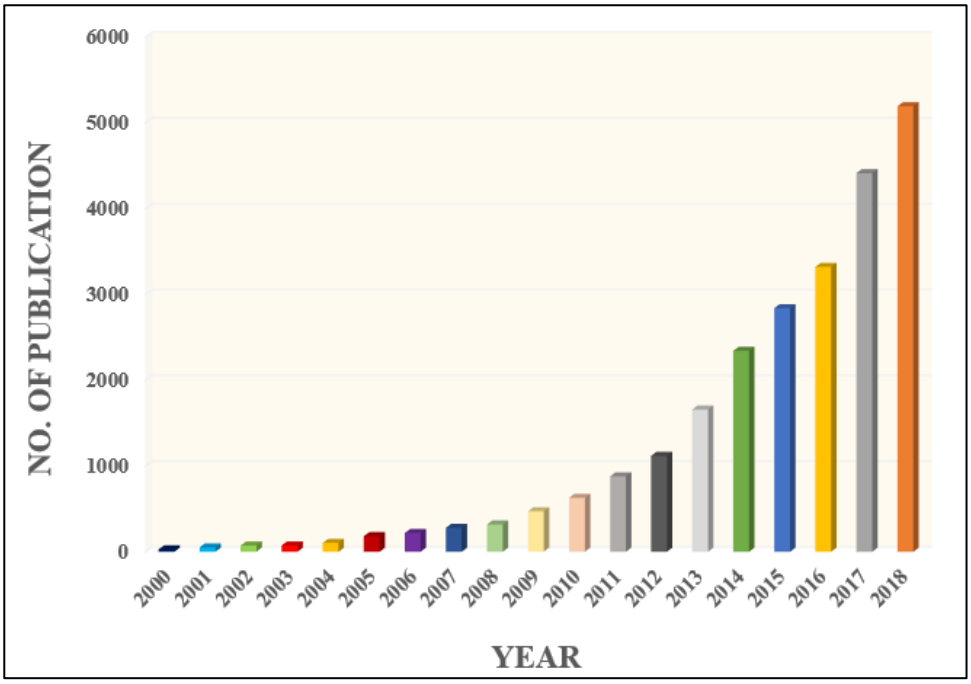

Figure 2.1 Publication on supercapacitors during the past two decades (Search Engine – Scopus; Keyword- Supercapacitor) (Date accessed on Aug 2019) (includes journal articles, reviews, book chapters).

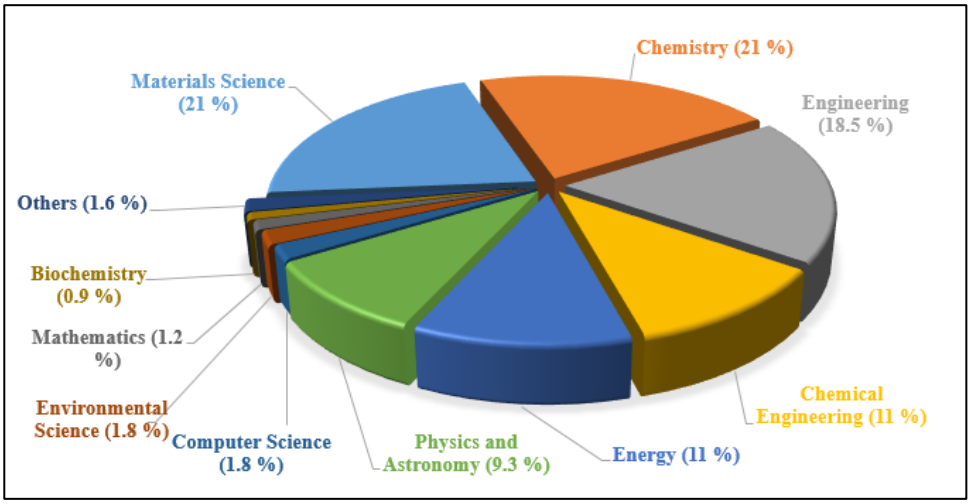

Figure 2.2 Discipline wise publication on supercapacitors (source – Scopus search engine).

Figure 2.2 shows the pie chart of various disciplines in SC projects. It can be seen that the material science (21%) and chemistry disciplines (21%) together account for the highest proportion, followed by engineering (18.5%) and chemical engineering (11%), energy (11%), physics (9.3%) and all other disciplines put together (9.2%). A significant effort has been made in both material science and chemistry fields towards achieving high performing electrodes and electrolytes.

This chapter elaborately explains the synthesis of various electrode materials along with their electrochemical performance. In addition, the electrolyte materials used for improving the energy density of the supercapacitor are also discussed.

2.2 Type of carbon electrodes

The specific capacitance and power density of a supercapacitor depends on the specific surface area of the electrode material, and the matching between the pore size and the electrolyte ion size. As a result, electrode materials play a vital role in the enhancement of electrochemical performance [3, 4]. The desired properties of the electrodes materials can be summarized as (i) high surface area, (ii) high electrochemical stability (iii) high conductivity, and (iv) optimized pore size distribution.

Different types of carbon materials have been studied as electrodes for SCs, such as carbon nanofibers (CNFs), graphene, carbon nanotubes (CNTs), template carbons, carbon aerogels, and biomass-derived carbons. The following sections summarize the recent progress in these materials along with the challenges associated with them.

2.2.1 Carbon fibres

Electrospun derived carbon fibres usually involves the use of polymers such as poly(vinyl alcohol) (PVA), Poly(methyl methacrylate) (PMMA), poly(vinylidene fluoride) (PVDF), phenolic resin, polyacrylonitrile (PAN), polyvinylpyrrolidone, polycarbosilane, polyphenylsilane (PPS), polyaniline and polyimide (PI) [5, 6]. It is a direct process, wherein the polymer is dissolved in a suitable solvent and electrospinned at the high potential difference, to obtain polymer fibres with uniform thickness. Further, it is carbonized at high temperature to obtain the carbon fibres. The thickness of the carbon fibres are range from micro to nanometers depending on the electrospinning and pyrolysis conditions.

Table 2.1 Literature survey of various carbon fibres and their electrochemical performance.

Precursor	**Specific capacitance ($F\ g^{-1}$)**	**Scanning conditions**	**Electrolyte/ Electrode**	**Reference**
Polyacrylonitrile (PAN), poly(acrylonitrile-co-butadiene (PAN-co-PB)	170.2	5 mV s^{-1}	2 M KOH / 3 electrode	Ya, 2014 [10]
Protein + Lignin	410	1 A g^{-1}	6 M KOH / 3 electrode	Yang, 2015 [11]
PVA modified resorcinol/phenolic resin	251.2	0.1 A g^{-1}	6 M KOH / 3 electrode	Tian, 2015 [9]
Polyacrylonitrile@ polyaniline core-shell nanofibers	577	5 mV s^{-1}	1 M H_2SO_4/ 3 electrode	Miao, 2015 [12]
	151	1 A g^{-1}	(PVA)/H2SO4 / 2 electrode	
Polyaniline/multi-walled carbon nanotube	180	0. A g^{-1}	(PVA)/H2SO4 / 2 electrode	Liang, 2016 [13]
Graphene oxide-reinforced electrospun carbon nanofibers	140.1	1 A g^{-1}	6 M KOH / 2 electrode	Chee, 2017 [14]

The pristine carbon fibres and activated carbon fibres have been widely used as electrode materials for supercapacitors, which show reasonable specific capacitance value due

to the long-range fibrous structure and high surface area [5]. Recently, extensive work has been carried out by many researchers to improve the electrochemical performance of carbon fibres by doping with heteroatoms such as nitrogen, boron, sulfur, and phosphorus [6-8]. The inclusion of heteroatoms in the carbon fibres increases the electrical conductivity and wettability, and also enhances the capacitance via a reversible Faradaic process (e.g Pseudocapacitance). Tian et al. reported superior electrochemical performance from nitrogen-doped electrospun carbon nanofibers in alkaline electrolyte [9]. Many research groups have worked on electrospun carbon nanofibers and demonstrated reasonable specific capacitance values [9-12].

Further, the carbon fibres are blended with other conducting polymer and nanostructured carbon materials (e. g CNT, Graphene and GO) to enormously improve the electrochemical performance [13-14]. Junsheng et al. fabricated polyaniline/multi-walled carbon nanotubes via the electrospun method. They reported that the specific capacitance of prepared electrospun carbon fibres has varied from 129 to 180 F g^{-1}, with a good rate capability and cyclic stability [14]. The following **Table 2.1** summarizes the research work on the development of carbon fibres.

2.2.2 Graphene

Graphene, a single layer to multilayer graphite sheet material, with a few nanometer thicknesses, has been extensively used as the electrode material owing to its high specific surface area (Theoretical ~ 2630 m^2 g^{-1}), high electrical, thermal conductivity, and mechanical strength. The theoretical specific capacitance of monolayer graphene is ~21 μF cm^{-2}, considering the complete utilization of monolayer, is about ~550 F g^{-1} [15]. However, the experimentally measured specific capacitance value of graphene is far lower than the theoretical value.

The pure graphene materials suffer from agglomeration and restacking of graphene sheets, which drastically decrease the active surface area and affects the electrochemical performance, and it is one of the main challenges faced in the electrode fabrication process. Various strategies have been adopted to overcome the restacking and agglomeration of graphene in order to effectively improve the electrochemically active surface area. The first approach involves the oxidation of graphene, which increases the oxygen functional groups and helps in improving the wettability. The increase in wettability results in improving the interaction between electrolytes and graphene electrodes [16].

The second approach is enhancing the electrochemical performance by doping the heteroatoms (Eg. N, B, S, etc) [17-21]. The addition of heteroatoms improves the wettability, electronic conductivity in addition to facilitating electrochemical reaction via the faradaic process (Eg. Pseudocapacitance). Dewei et al. reported an efficient way to prepare nitrogen doped graphene via hard and soft acids and bases (HSAB) theory [18]. They found that the presence of both nitrogen and oxygen functional groups have played a significant role in increasing the wettability and decreasing the intrinsic resistance of graphene electrodes which results in excellent capacitive performance even at high current densities.

Table 2.2 Literature survey of various graphene-based electrodes and their electrochemical performance.

Material	**Specific capacitance ($F\ g^{-1}$)**	**Operating Condition**	**Electrolyte/ Electrode**	**Reference**
Nitrogen-doped graphene	242	1 A g^{-1}	1 M H_2SO_4 / 2 electrode	Wang, 2014 [18]
Nitrogen doped reduced graphene oxide	96.4	0.1 A g^{-1}	1 M $LiPF_6$ / 2 electrode	Yang, 2014 [19]
Nitrogen-doped graphene aerogels	170.5	0.2 A g^{-1}	6 M KOH / 3 electrode	Ling, 2015 [20]
Nitrogen-doped graphene hydrogel	48.6	0.5 A g^{-1}	[BMIM]PF_6 / 2 electrode	Liu, 2016 [21]
Graphene sheets/polyaniline nanofibers composite	596	1 A g^{-1}	3 M NaOH/ 3 electrode	Tang, 2017 [22]
rGO-polyaniline	1084	3.22 mA cm^{-2}	1 M H_2SO_4/ 3 electrode	Nooshabadi, 2017 [23]
Polypyrrole/nickel hydroxide/sulfonated graphene oxide	1632.5	1 A g^{-1}	6 M KOH / 3 electrode	Li, 2018 [24]
	224	1 A g^{-1}	6 M KOH / 2 electrode (Asymmetric)	

The third approach involves the composite electrode fabrication using more than one electrochemically active component into the graphene matrix [22-24]. This results in improving the electrochemical performance by the synergistic interaction between the graphene matrix and electrochemical active substances. Li et al. reported fabrication of composite electrodes using polypyrrole, nickel hydroxide, and sulfonated graphene oxide. This composite electrode has shown extremely high specific capacitance value of 1632.5 F g^{-1} at 1 A g^{-1} in three-electrode system using 6 M KOH electrolyte [24]. An asymmetric supercapacitor cell was fabricated by considering the charge balance between the positive and negative electrodes and exhibited a very high capacitance value of 224 F g^{-1} at 1 A g^{-1} in two-electrode system using 6 M KOH electrolyte [24]. **Table 2.2** summarizes the research work on the development of graphene and its composite electrodes for SCs.

2.2.3 Carbon nanotubes (CNTs)

CNTs have been investigated as promising electrode materials for supercapacitor because of its very high electrical conductivity and electrochemical stability, and have the capacity to deliver very high-power densities [25]. Despite its potential application in SC, the CNT-based electrodes suffer from poor dispersion ability due to strong Vander Wall interaction with nanotube sidewalls resulting in agglomeration which affects the electrode fabrication process. This problem can be eliminated by acid oxidation and heteroatom doping of CNTs which increases the defect and tip opening, enhancing the wettability and electronic conductivity, respectively [26-30]. John et al. demonstrated the effect of nitrogen doping on CNT leading to a significant enhancement in specific capacitance compared to pristine CNT [26]. Further, CNT composite electrodes have been developed to improve the electrochemical performance [28-29, 31]. For instance, Abdah et al. reported the fabrication of a ternary nanocomposite consisting of polypyrrole (PPy), graphene oxide (GO), and multi-walled carbon nanotube (MWCNT), and reported a maximum capacitance value of 358 F g^{-1} at 100 mV s^{-1} in 1 M Na_2SO_4, the high capacitance value was obtained due to the synergistic interaction between the electro-active components [31].

Recently, Avasthi et al. fabricated a binder-free CNT electrode using a facile synthesis process [30]. They demonstrated the formation of vertically aligned CNT forests on stainless steel mesh using a high temperature method. They claimed a high areal specific capacitance of 16.24 mF cm^{-2} at an aerial current density of 1.67 mA cm^{-2} in 0.1 M Na_2SO_4 electrolyte. T**able 2.3** summarizes the research work on the development carbon nanotubes and its composite electrodes for SCs.

Table 2.3 Literature survey of various CNT based electrodes and their electrochemical performance.

Sample	Specific capacitance ($F\ g^{-1}$)	Experimental condition	Electrolyte/ Electrode	Reference
Nitrogen-doped carbon nanotubes	146	-	1 M KCl / 3 electrode	John, 2015 [26]
Polyaniline/carbon nanotube-COOH	381	1 A g^{-1}	1 M H_2SO_4 / 3 electrode	He, 2016 [27]
Flexible PANI/NCNT	128	2.47 A g^{-1}	PVA/H2SO4 hydrogel / 2 electrode	Malik, 2017 [28]
Reduced graphene oxide/carbon nanotube hybrid	243	0.2 A g^{-1}	6 M KOH/ 3 electrode	Zhang, 2017 [29]
Aligned CNT Forests on SS Mesh	16.24 mF cm^{-2}	1.67 mA cm^2	0.1 M Na_2SO_4 / 3 electrode	Avasthi, 2019 [30]
Polypyrrole/graphene oxide/multi-walled carbon nanotubes	358.69 F g^{-1}	100 mV s^{-1}	1 M Na_2SO_4/ 3 electrode	Abdah, 2018 [31]

2.2.4 Templated carbons

Templated carbons, a new and attractive carbon material have been extensively used as electrode SCs because of its tunable morphological and textural properties [32-34]. Most commonly used templates are mesoporous silica, metal organic frameworks (MOFs), zeolite imidazole frameworks (ZIFs), surfactant templates, and organic polymer templates, etc. The resultant morphology, size, and pore characteristics of these types of carbons mainly depend on the template, in which the precursor only acts as a carbon source. Various morphological carbons have been fabricated and the electrochemical properties were improved by optimizing the specific surface area [32-34]. Liang et al. prepared a hollow nest like nitrogen doped carbon using glucose by hard template (nickel hydroxide ($Ni(OH)_2$) method [32]. They reported a high specific capacitance value of 322 F g^{-1} at 1.0 A g^{-1}. Owing to its hollow nest-like structure and

nitrogen doping, a remarkably high rate capability (54.3% at 20 A g^{-1}) and cyclic stability (98% at 10 A g^{-1} over 10000 cycles) was achieved.

The MOFs and ZIFs play dual roles in carbon synthesis; it acts both as a carbon source and scaffold. Typically, the hierarchical porous carbons from MOFs and ZIFs are synthesized by the carbonization of the same in an inert environment. Khan et al. reported a synthesis of mesoporous carbon nanospheres from MOF-5 by controlled carbonization temperature, and presented a very high specific capacitance value of 300 F g^{-1} at 1.5 A g^{-1} [34]. Tang et al. fabricated core-shell structured hierarchical porous carbon spheres from core-shell MOF powders and demonstrated its suitability for supercapacitor electrodes [33]. T**able 2.4** summarizes the research work on the development of template carbon electrodes for supercapacitor

Table 2.4 Literature survey of various template carbons and their electrochemical performance.

Morphology	**Precursor**	**Template**	**Specific capacitance (F g^{-1})**	**Current density (A g^{-1})**	**Electrolyte/ Electrode**	**Reference**
Hollow nest	Glucose	$Ni(OH)_2$	322	1	3 electrode	Liang, 2015 [32]
Core-shell	ZIF-8 & ZIF-67	Self	270	2	1 M H2SO4/ 3 electrode	Tang, 2015 [33]
Mesoporous carbon nanospheres	MOF-5	Self	300	1.5	KOH/ 3 electrode	Khan, 2017 [34]

2.2.5 Carbon aerogels

Carbon aerogels are monolithic 3-dimensional hierarchical porous material synthesized from organic gel mixture of resorcinol-formaldehyde by freeze-drying process followed by high-temperature pyrolysis [35]. Carbon aerogels combine the advantage of high surface area, extremely low packing density, good electrical conductivity, and they can also be used as free-standing electrodes because of good structural stability [36-39]. Carbon aerogels prepared from various precursors are extensively studied as electrodes for supercapacitors. They have been shown to possess very high specific capacitance and energy characteristics compared to other carbon-based materials.

Zhang et al. reported a preparation method of N-doped carbon aerogel using commercial melamine sponge and an organic mixture of phenol-formaldehyde [35]. This material exhibited a superior specific capacitance value of 354 F g^{-1} at a current density of 0.2 A g^{-1} in 6 M KOH in three-electrode system, due to its synergetic role of the 3D porous networks and N doping. Yang et al. have prepared an activated carbon aerogel using the mixture of resorcinol-formaldehyde and studied the electrochemical performance in an organic electrolyte (1 M TEABF4) [39]. It demonstrated a comparable electrochemical performance with commercial activated carbon. Several other researchers have worked on carbon aerogels using different organic mixtures under different experimental conditions to improve the textural properties and enhance the electrochemical performance, as detailed in **Table 2.5.**

Table 2.5 Literature survey of various carbon aerogel electrodes and their electrochemical performance.

Raw Materials	**Specific surface area (m^2 g^{-1})**	**Specific capacitance (F g^{-1})**	**Current density (A g^{-1})**	**Electrolyte/ Electrode**	**Reference**
Phenol-formaldehyde resol, Melamine sponges	1626	354	0.2	6 M KOH/ 3 electrode	Zhang, 2015 [35]
PEA/PVA-H_3BO_3 complex	2016	467	1	1 M H_2SO_4/ 3 electrode	Wei, 2016 [36]
Phloroglucinol (P), resorcinol (R), and formaldehyde	450	151	0.5	6 M KOH/ 3 electrode	Xu, 2018 [37]
Pyrrole and formaldehyde	1450	166	0.1	1 M H_2SO_4/ 2 electrode	Zeng, 2018[38]
Resorcinol and formaldehyde	2690	33	0.1	1 M $TEABF_4$/ 2 electrode	Yang, 2018 [39]

2.2.6 Biomass Derived Carbons

Porous carbon prepared from biomass sounds interesting because of its extremely high carbon content, abundant availability, viability for large scale production, and low-cost investment compared to other carbon containing precursors [40]. Porous carbons from biomass have been prepared by various experimental methods such as pyrolysis or carbonization [41], hydrothermal carbonization [42], microwave heating [43], dehydration process [44], etc. The shape, size, and pore characteristics of the resultant porous carbons have been optimized by selective experimental processes [40-44].

2.2.6.1 Direct or Conventional Biomass

Biomass such as plants and animal matters are directly used to prepare carbons without any pretreatment process. Mostly, plant waste like woods, pruning's, seeds, leaves, and other parts are extensively used as a source because of its abundance and availability [45-50]. Generally, the direct carbonization or pyrolysis process was carried to convert the conventional biomass into porous carbons. This process involves a simple and effective heating of precursor at high temperatures in an inert environment which removes organic volatile content and leaves carbon-rich solid residue along with tar. The solid residue is then washed to remove impurities and dried. Later, this solid residue is activated by chemical or physical activation method at very high temperatures (600 ˚C to 1000 ˚C) in order to improve the surface area and pore size distribution.

Wang et al. prepared a porous carbon from celtuce leaves using the KOH activation method [45]. The prepared porous carbons exhibited a superior surface area of 3404 $m^2\ g^{-1}$, resulting in a very high specific capacitance value of 421 F g^{-1} at 0.5 A g^{-1} in a three-electrode system using 6 M KOH electrolyte. Misnon et al. prepared an activated carbon using an oil palm kernel shell (PKS) as a carbon source by direct carbonization and activation process [47]. They studied the effect of physical (CO_2) and chemical (KOH) activation strategies to effectively enhance the textural properties of the activated carbon. It was found that the chemical activation strategy has enormously increased the surface area compared to physical activation. A high specific capacitance value of 210 F g^{-1} for chemical activated carbon at 0.5 A g^{-1} in 1 M KOH is resulted due to its wider pore size distribution which is 2 times higher than physically activated carbon (123 F g^{-1}). The following T**able 2.6** summarizes the research work on biomass-derived from carbon using different activating agents for supercapacitor by direct carbonization process

Table 2.6 Porous carbon derived from direct biomass and their electrochemical performance.

Precursor	Activating agent	Specific surface area ($m^2 g^{-1}$)	Specific capacitance ($F g^{-1}$)	Electrolyte	Reference
Celtuce leaves	KOH	3404	421	2 M KOH	Wang, 2012 [45]
Rice husk	H_3PO_4	2009	176 ($0.05 A g^{-1}$)	6 M KOH	Wu, 2015 [46]
Oil palm kernel shell	KOH CO_2	462.1 727.3	210 ($0.5 Ag^{-1}$) 123 ($0.5 Ag^{-1}$)	1 M KOH	Misnon, 2015 [47]
Coniferous Pine	KOH	1515	90 ($0.1 A g^{-1}$)	1 M Na_2SO_4	Manyala, 2016 [48]
Metaplexis japonica	KOH	1394	256.5 ($20 mVs^{-1}$)	6 M KOH	Liang, 2017 [49]
Saccharum bengalense	$ZnCl_2$	2090	102.6 ($2 mVs^{-1}$)	1 M Li_2SO_4	Rawal, 2018 [50]

2.2.6.2 Biomass derivatives

Biomass derivatives are one of the most promising precursor materials for the synthesis of porous carbons because of their unique chemical compositions. The biomass derivatives such as cellulose, lignin, starch, carrageenan, etc have been used to prepare porous carbons [51-56]. These materials have been converted into very broad shaped carbons using hydrothermal carbonization process. During this process, the derivatives will be dissolved and recrystallized in water under very high pressure and temperature (< 300 ˚C). This process eliminates the formation of tar which is a major limitation of the pyrolysis process resulting in increased carbon conversion efficiency. The solid residue is well known as hydro char and mostly obtained in a spherical shape, and the size of the particles can also be optimized by experimental conditions.

For example, the natural polysaccharide carrageenan was used to synthesize the micro-mesoporous carbon sphere by hydrothermal method for supercapacitor application [52]. The open porous network and surface area of the samples were optimized by varying the chemical activation temperature. The sample carbonized at 900 ˚C exhibited a high surface area value of 2502 $m^2 g^{-1}$ with a pore volume of 1.43 $cm^3 g^{-1}$. The specific capacitance value of 230 F g^{-1} at

a current density of 1 A g^{-1} was attributed to its high surface area with narrow pore size distribution.

Ruibin et al. used starch derived from potato as a precursor for carbon microspheres preparation by hydrothermal method [54]. They used potato starch mainly based on the availability and low cost, essential for large scale commercialization. They reported a uniform microsphere with an average size of 500 nm after hydrothermal carbonization. The average particle size of the microsphere was said to be decreased to 250 nm after high-temperature treatment due to gasification which enhances the porosity of the sample. The carbonized sample showed a high specific surface area value of 456 $m^2 g^{-1}$ and a specific capacitance value of 245 F g^{-1} at a current density of 1 A g^{-1}. The capacitance value remained at 98% over 3900 cycles at 3 A g^{-1} indicating the good retention capacity and cyclic stability.

Table 2.7 Porous carbons derived from biomass derivatives and their electrochemical performance.

Precursor	**Morphology**	**Specific surface area ($m^2 g^{-1}$)**	**Specific capacitance (F g^{-1})**	**Current density (A g^{-1})**	**Electrolyte**	**Reference**
Sugar	Micro spheres	1216.78	179.2	1	30 wt% KOH	Kurniawan, 2013 [51]
Carrageenan	Micro spheres	2502	230	1	6 M KOH	Fan, 2014 [52]
White office paper	3D-interconnect pores	2341	179	1	$EMIMBF_4$	Puthusseri, 2014 [53]
Potato starch	Micro spheres	456	245	1	1 M KOH	Ruibin, 2015 [54]
Water hyacinth	Micro spheres	1010	182.2	-	6 N KOH	Kurniawan, 2015 [55]
Bamboo by-product	Beehive	1472	301	0.1	6 M KOH	Tian, 2015 [56]

Kurniawan et al. reported the use of water hyacinth as a carbon source to form carbon microspheres by hydrothermal method [55]. In this method, they directly converted the biomass water hyacinth into carbon microsphere with the help of the catalyst i.e dilute sulfuric acid.

Carbon particles having a smooth surface and spherical shape and average diameter value of 2-4 μm were formed at 200 ˚C for 10 h. The chemical activation process was carried out to optimize the surface area and pore size. The highest specific surface area value of 1010 $m^2 g^{-1}$ was achieved for the KOH to carbon ratio of 1:1. This sample exhibited a superior specific capacitance value of 182 F g^{-1} compared to commercial activated carbon (179 F g^{-1}, F-400 Calgon Carbon) because of its open porous structure. T**able 2.7** summarizes the research work on porous carbon derived from different biomass precursors and its by-products by hydrothermal carbonization process.

2.2.6.3 Cellulose and Lignin aerogel

An advanced form of carbon with an integrated pore structure is highly desirable to achieve high energy density and power density. Carbon aerogels are one of the integrated pore structured materials which are commonly prepared from organic materials. Recently, carbon aerogels have been prepared from cellulose and lignin by green chemistry using the sol-gel process [57-62]. Mostly, cellulose was used to synthesize carbon aerogels because of its solubility in various solvents. It can also be easily derived from various biomass by the alkaline extraction process. Cellulose-based carbon aerogels were synthesized by a systematic process which involves dissolution, gelation, carbonization, and activation. Initially, the cellulose is dissolved in a suitable solvent and made into a gel in an anti-solvent. Subsequent freeze-drying removes the water molecules and allows it to form a compact aerogel structure. Further, it will be carbonized and chemically activated to tailor the hierarchical porous structure with micropores, mesopores, and macropores.

Hao et al. synthesized hierarchical porous carbon aerogel using cellulose extracted from sugarcane bagasse [57]. Bagasse is a renewable and cost-effective byproduct obtained from the sugarcane industry which mainly contains cellulose derivatives and is used as a precursor to synthesize carbon aerogel. Initially, the lignin and hemicellulose contents present in the bagasse were removed by the alkaline hydrolysis process. The resultant product mainly contains cellulose, which was subject to the process described earlier to form a cellulose aerogel. This resultant cellulose aerogel was carbonized at different temperatures (700 ˚C, 800 ˚C, and 900 ˚C) to achieve high surface area and pore size distribution. The carbon aerogel prepared at 700 ˚C presented a nominal surface area value of 1892.4 $m^2 g^{-1}$; with a high degree of graphitization and a high specific capacitance value of 142.1 F g^{-1} at a current density of 0.5 A g^{-1} in a symmetric configuration. It has exhibited an excellent capacitance retention value of 93% over 5000 cycles at 1 A g^{-1} because of its hierarchical pore structure with integrated micropores and

mesopores. Following the research work by Hao and co-workers, numerous research articles have been published on cellulose-based carbon aerogels for its application in supercapacitors.

Yang et al. fabricated carbon aerogel from cellulose fibres derived from bamboo by following the simple experimental procedure [61]. In this work, the prepared carbon aerogel was subjected to KOH activation for altering the structural and textural properties. The resultant carbon aerogel exhibited an interlined fibrous network covered by porous nano-platelets with a high surface area value of 1085 m^2 g^{-1}. It has displayed a high specific capacitance value of 381 F g^{-1} at a scan rate of 5 mV s^{-1} and 90% of its capacitance was retained at 200 mV s^{-1}, because of its hierarchical porous texture.

Table 2.8 Cellulose and lignin-derived porous carbon aerogels and their electrochemical performance.

Precursor	**Specific surface area (m^2 g^{-1})**	**Specific capacitance (F g^{-1})**	**Scanning condition**	**Electrolyte**	**Reference**
Bagasse	1892.4	142.1	0.5 A g^{-1}	6 M KOH	Hao, 2014 [57]
Cellulose (Cotton linter)	615	225	0.5 A g^{-1}	1 M H_2SO_4	Hu, 2016 [58]
Cellulose	1364	328	0.5 A g^{-1}	1 M H_2SO_4	Zhuo, 2016 [59]
Cellulose	646	160	0.2 A g^{-1}	1 M H_2SO_4	Tian, 2017[60]
Bamboo	1085	381	5 mV s^{-1}	6 M KOH	Yang, 2018 [61]
Lignin/ Resorcinol+ formaldehyde	779	142.8	0.5 A g^{-1}	6 M KOH	Xu, 2018 [62]

Recently, Xu et al. utilized natural lignin derived from crop waste as source material for carbon aerogel synthesis [62]. Lignin is one of the most abundant materials available in biomass after cellulose. It is similar to phenolic resins and extracted from crop waste by enzymatic hydrolysis process. They prepared lignin aerogel by mixing lignin (L) with resorcinol (R) and formaldehyde (F) at different weight ratios and followed an ambient drying process to eliminate

the use of freeze-drying process which is quite expensive. The high surface area value of 779 m^2 g^{-1} was obtained for the carbon aerogel with L/ (L+R) ratio of 20%. The lignin aerogel exhibited a high specific capacitance value of 142.8 m^2 g^{-1} at a current density of 0.5 A g^{-1}, 78% of its capacitance was reported to be retained even at a high current density value of 10 A g^{-1}. This superior performance of lignin-based carbon aerogel was attributed to its interconnected hierarchical porous network structure with a high degree of graphitization. The following T**able 2.8** summarizes the research work on porous carbon aerogels derived from different biomass precursors and its byproducts by the green chemistry method. These research studies open a new pathway to synthesize hierarchical porous carbon directly from biomass precursor.

2.3 Types of Electrolytes

Electrolyte is an ionic conducting solution which consists of anions and cations. Electrolytes play a major role in the formation of a "double layer" in EDLC, shown in **Figure. 1.2**. The electrochemical performance of an EDLC system depends on electrolyte properties, the ion conductivity, and ion size matching with electrode pore size. Generally, the electrolytes used in EDLCs must satisfy the essential parameters like wide operating potential window, high electrochemical stability, high ionic conductivity, and low cost. It is very difficult to have an electrolyte which satisfies all these parameters; this encourages fabricating a novel electrolyte system for achieving the best performing supercapacitor system [63]. The electrolyte solutions are classified into three major families based on their solvent, namely aqueous, non-aqueous, and ionic-liquid electrolytes.

2.3.1 Aqueous Electrolyte

Aqueous electrolyte is a solution containing a mixture of water with acid or base or neutral salts. The aqueous electrolytes are classified as acidic, basic, and neutral electrolytes based on the solute present in the system. Initially, aqueous electrolytes were used to examine the capacitive behavior of newly developed electrode materials, as they can be easily handled in ambient conditions without any pretreatment. The electrochemical performance of the aqueous electrolyte systems is dependent on the choice of anion, cation, and concentration of electrolyte, which strongly influence the specific capacitance and capacitance retention [64]. The properties such as the size of bare and hydrated anions, cations, and ionic conductivity, are listed in **Table. 2.9**. Aqueous electrolytes have less possibility for commercial device purposes due to its low operating potential compared to other electrolyte systems which limit it's in a commercial application.

Commonly used aqueous electrolytes

- Acid electrolytes: H_2SO4, K_2SO_4, HCl, KCl, etc. The most commonly used acidic electrolyte is H_2SO_4 because of its high cationic conductivity
- Basic Electrolytes: LiOH, NaOH, KOH, etc. Widely used electrolyte is KOH because of its high ionic conductivity.
- Neutral Electrolytes: Na_2SO_4

In this work, the aqueous 6M KOH is used as the electrolyte owing to its non-toxic, non-flammable, cost-effective, and safe to handle in an air environment property.

2.3.2 Non-Aqueous Electrolyte

The electrochemical stability of non-aqueous solvents such as propylene carbonate and acetonitrile are very high than the aqueous electrolyte due to the low dielectric constant. Further, these solvents can be operated in a very high potential window <3 V compared to aqueous electrolytes (<1 V) due to their low dielectric constant. Typical non-aqueous electrolytes consist of conductive salts dissolved in solvent.

Commonly used non-aqueous electrolyte is tetraethylammonium tetrafluoroborate ($TEABF_4$) dissolved in propylene carbonate or acetonitrile [64, 65]. The non-aqueous electrolyte based EDLCs can be operated at a potential window of up to 3 V. The use of propylene carbonate and acetonitrile as a solvent in non-aqueous electrolytes has its own merits and demerits because of its physical and electrochemical properties. **Table 2.10** shows the electrochemical properties of 0.65 M $TEABF_4$ dissolved in propylene carbonate and acetonitrile.

Though the non-aqueous electrolytes provide a large potential window, their applications are limited because of its high cost, low specific capacitance, low ionic conductivity, flammability, and toxicity. Further, the non-aqueous electrolytes require sophisticated instruments for cell assembly and complicated purification processes to remove impurities and moisture.

Table 2.9 Physical and electrochemical properties of electrolyte ions [64].

Ion	**Bare ion size (Å)**	**Hydrated ion size (Å)**	**Ionic Conductivity (S cm^2 mol^{-1})**
H^+	0.115	2.8	350.1

Li^+	0.60	3.82	38.69
Na^+	0.95	3.58	50.11
K^+	1.33	3.31	73.5
Mg^{2+}	0.72	4.28	106.12
Ba^{2+}	1.35	4.04	127.8
NH^{4+}	1.48	3.31	73.7
Ca^{2+}	1.00	4.12	119
ClO_4^-	2.92	3.38	67.3
CO_3^{2-}	2.66	3.94	138.6
Cl^-	1.81	3.32	76.31
OH^-	0.176	3.00	198.0
SO_4^{2-}	2.90	3.79	160.0
NO_3^-	2.64	3.35	71.42
PO_4^{3-}	2.23	3.39	207

Table 2.10 Physical and electrochemical Properties of $TEABF_4$ in different solvent [64].

Solvent	**ε_r**	**η (cp)**	**T_b (°C)**	**T_m (°C)**	**MW (g)**	**σ (mS cm^{-1})**	**E_{red} (V vs. SCE)**	**E_{oxd}**
Propylene Carbonate	65	2.5	242	-49	102	10.6	-3.0	3.6
Acetonitrile	36	0.3	82	-49	41	49.6	-2.8	3.3

ε_r - Relative permittivity **η - Viscosity**

T_b – Boiling Point **T_m - Melting point**

MW- Molecular weight **σ – Conductivity**

E_{red} – Reduction potential **E_{oxd} – Oxidation potential**

2.3.3 Ionic-Liquid Electrolyte

Ionic liquid is a salt that exists in a molten state at room temperature because of its low melting point. It is free from solvent and contains only anions and cations. High thermal stability, low vapor pressure, low toxicity, non-flammable, non-corrosive, and easy to handle properties of ionic liquids makes them suitable for electrolyte application [66]. Commonly used

anions and cations are given in **Table. 2. 11**. Among them, the imidazolium and pyrrolidinium are having superior qualities like low viscosity and moderate ionic conductivity, respectively.

Table 2.11 Commonly used anions and cations in ionic liquids.

Anions	Cations
Tetrafluroborate [BF_4]	Imidazolium
Hexafluorophosphate [PF_6]	Pyrrolidinium,
bis(trifluoromethanesulfonyl)imide [TFSI]	Ammonium,
	Sulfonium,
bis(fluorosulfonyl)imide [FSI]	Phosphonium
dicyanamide [DCA]	

Generally, imidazolium-based ILs are extensively studied as an electrolyte because of its high ionic conductivity and reasonable potential window which suits well for supercapacitors application. Table 2.12 provides the physical properties of the commonly used imidazolium (1-Ethyl-3-methylimidazolium-[EMIM] based ILs [67]. Largeot et al. studied the relation between electrochemical performances of the ionic size of EMIM-TFSI electrolyte with pore size for carbon electrode materials [68]. It was reported that the matching of the pore size of the electrode material with the electrolyte ion size (~ 0.7 nm) significantly improves the specific capacitance. They also observed a notable loss in specific capacitance for the electrode materials with pore sizes that were larger or smaller compared to the ion size, and have suggested that the pore size must be matched with ions size to achieve very high specific capacitance [68].

Table 2.12 Physical properties of commonly used EMIM cation based ionic liquids at 25 ˚C [67].

Electrolyte	Viscosity (cP)	Ionic conductivity (mS cm^{-1})
EMI-FSI	17.9	15.5

EMI-TFSI	28.0	8.4
EMIm-BF_4	32	13.6
EMIM-B(CN4)	16.3	15.91
$EMImPF_3(C_2F-)_3$	32.8	5.35
EMImSCN	20.0	22.05
$EMImN(SO_2CF_3)_2$	32.1	9.12
$EMImN(SO_2F)_2$	12.5	17.7

2.4 Types of Symmetric Supercapacitor Cells

Symmetric supercapacitor cells are considered to be one of the best practicing methods to evaluate the performance of newly developed carbon-based electrode materials. This evaluation method provides capacitive behavior and resembles the real-time capacitors because of its two-electrode configuration. Typically, the symmetric supercapacitor cells consist of two electrodes separated by electrolyte filled porous membrane separator, as shown in **Figure 1.3**. Many types of symmetric cells such as Coin cells, HS flat cells, and in-house developed cells have been used to study the capacitive behavior of electrode materials. The details of each cell system and its advantages are discussed in the following section.

2.4.1 Coin cells

Coin cells or button cells are simple and effective symmetric cells. It has several advantages like light weight, high voltage stability, easy stackability, and long cycle life. It is mainly used to evaluate the electrochemical performance of non-aqueous electrolyte-based supercapacitor systems. Sometimes, neutral aqueous electrolytes have also been used because of its neutral pH value which will not corrode the metal casing of the coin cell. For example, Bissett et al. have studied the capacitive behavior of flexible PVDF membrane coated with exfoliated MoS_2 and graphene on both side as supercapacitor electrodes in coin cell configuration using 1 M Na_2SO_4 as an electrolyte which is shown in **Figure 2.3**. The composite membrane has shown a very high specific capacitance of 11 mF cm^{-2} at 5 mV s^{-1} and presented a very low self-discharge over 1 h [69].

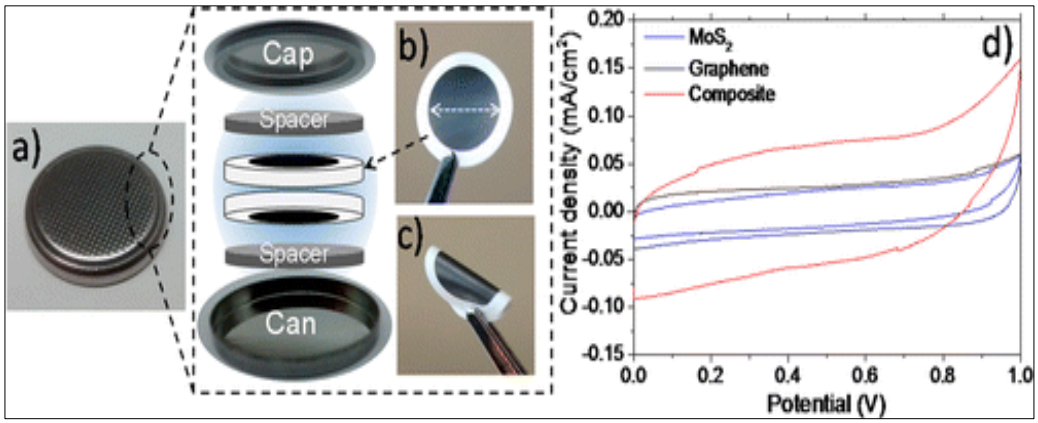

Figure 2.3 (a) Assembly of coin cell CR2032, (b & c) flexible MoS2 electrode, and (d) the cyclic voltammogram of assembled coin cells, at scan rate of 50 mV s^{-1} [69].

2.4.2 HS Flat cell

Specially designed HS flat cell fabricated by Hohsen Corporation, Japan is recently being used to evaluate the electrochemical performance of electrodes for supercapacitors and batteries [70]. It is very compact and can easily be assembled and disassembled. It is similar to that of a coin cell, it can be reused many times because it's simple design with O-rings and a spring, and is shown in **Figure 2.4.**

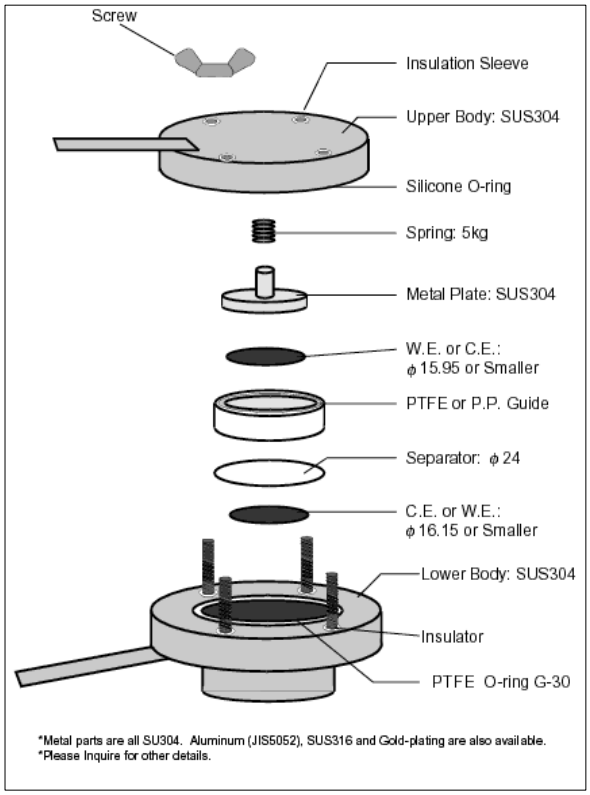

Figure 2.4 Block diagram of HS flat cell [70].

It has been extensively used by many researchers to evaluate the electrode performance using non-aqueous and ionic liquids, because it limits the diffusion of oxygen from the environment which increases the cyclic stability of the cell. For example, Bhattacharjya et al.

evaluated the electrochemical performance of hollow mesoporous carbon capsules using an airtight HS-Flat test cell from Hohsen Corporation. The cell has shown very good cycle stability over 2000 cycles and preserves 88% of the original capacitance [71].

2.4.3 In-house designed cells

In-house developed cells are simple, inexpensive, and easy to fabricate. Unlike, coin cell and HS flat cell it does not require specialized instruments for assembly, and the electrode area can be varied based on our requirement. These cells can be fabricated at the lab level to conduct the electrochemical capacitive behavior of samples in aqueous electrolyte solution (Acidic or basic). Electrolyte drying is the major drawback of these homemade cells because of its open structure which decreases the cyclic stability, and it can be minimized by continuous refilling of additional electrolytes to the system. For example, Lal et al. fabricated a homemade two-electrode cell using composite electrode (Cu/CuO/PCNF/TiO2) as an active material coated on carbon cloth (2 x 2 cm^2) and used it as an electrode [72].

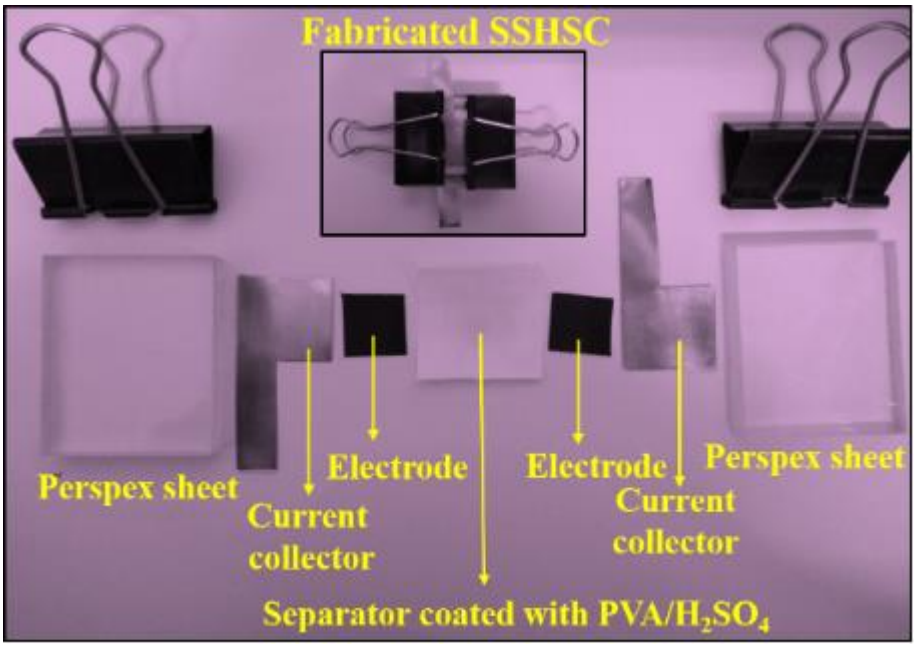

Figure 2.5 Photograph of in house designed symmetric supercapacitor cell [72].

The PVA/H2SO4 polymer gel was prepared and used as a solid electrolyte. The polymer gel electrolyte was placed between the two electrodes and the L shaped stainless steel plate is placed on both sides for the current collection. Then, the assembly was placed between the non-conducting support materials and clamped firmly to reduce the internal resistance, as shown in **Figure 2.5**. The resultant polymer gel electrolyte based solid-state hybrid supercapacitor (SSHSC) has exhibited a high specific capacitance value of (330 F g^{-1} @1 A g^{-1}) with high capacitance retention (78.8% up to 10,000 cycles).

The type shown in **Figure 2.5** is useful only to evaluate the electrochemical performance in the aqueous electrolytes. This type of cell is not useful to evaluate the performance in non-aqueous electrolytes and ionic liquid electrolytes. Mostly, the non-aqueous and ionic liquid electrolytes are sensitive to water molecules and oxygen, which will decrease the operating potential window and oxidize the electrolytes. Thus, the capacitive performances of these electrolytes should be evaluated in an air-free environment. The homemade Swagelok cell can fulfill these criteria and can provide proper sealing for the electrolyte which can minimize the diffusion of air [73]. The assembly of the Swagelok cell is shown in **Figure 2.6**. For example, Lin et al. studied the electrochemical performance of the eutectic ionic liquid mixture electrolyte using graphene-based electrodes by Swagelok cell [73]. The electrolyte mixture consists of N-methyl-N-propylpiperidinium bis(fluorosulfonyl)imide and N-butyl-N-methylpyrrolidinium bis(fluorosulfonyl)imide) in the weight ratio of 1:1. The cell was tested in the temperature range from -30 °C to 80 °C. The highest specific capacitance value of 175 F g^{-1} was obtained at 0.085 Ah g^{-1} (80 °C).

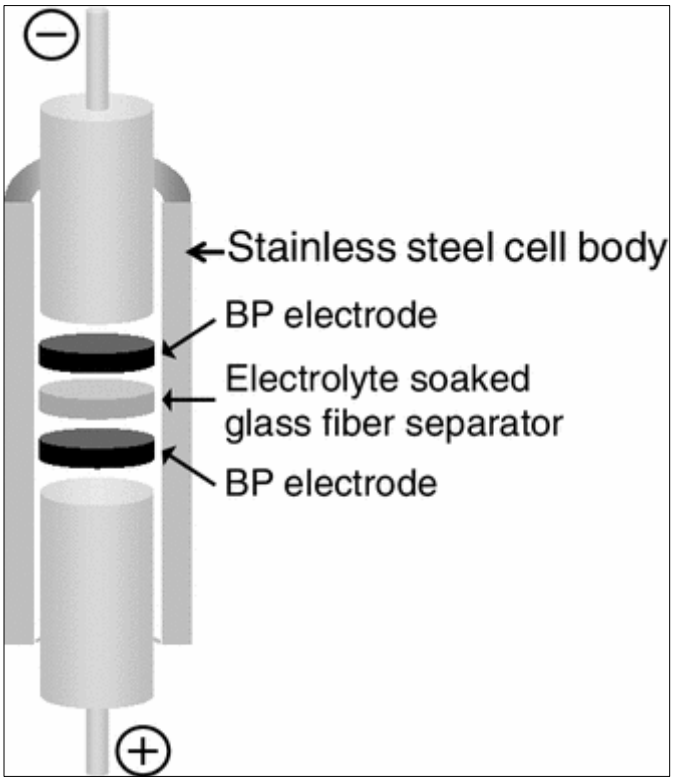

Figure 2.6 Block diagram of in house designed Swagelok cell [73].

Symmetric supercapacitor cells are given much attention over asymmetric supercapacitor cells. The symmetric supercapacitor cell can provide long term cyclic stability with very less capacity fading compared to asymmetric supercapacitors. Moreover, the energy

density could be enhanced by replacing the wide potential window electrolytes, which makes them highly suitable for commercial device fabrication applications.

Three-electrode system is specifically used to measure the electrochemical characteristics of the electrode materials, whereas the two-electrode systems is valuable for determining electrochemical-specific material characteristics, a two-electrode systems cell mimics the physical configuration, internal voltages and charge transfer that occurs in a packaged ultracapacitor and thus provides the best indication of an electrode material's performance. The two-electrode system was chosen in this thesis to identify the suitability of the electrode towards device and real time application analysis. As the current flowing through the electrodes is insignificantly small, the changes it causes in the applied voltage can be treated as insignificant [74].

2.5 Summary

The literature survey provides a detailed report on the significant developments that have taken place in electrode and electrolyte materials for the advancement of supercapacitor systems. It could be seen from the literature survey that extensive work has been carried out in graphene, carbon nanotube, carbon fibres, carbon aerogels, and template carbon-based materials (**Figure 2.7**). Most of these materials have shown promising electrochemical performances in terms of specific capacitance, rate capability, and cyclic stability.

Though, these materials have shown promising results, the use of fossils and non-renewable precursors for the synthesis have been a blemish on the otherwise green energy storage device, supercapacitor. Considering the aforementioned problem, the development of novel porous carbons from renewable and non-toxic precursors has become the most sought research material for supercapacitors. As discussed in section 2.2.6, biomass-based carbons are being considered as one of the potential candidates for porous carbon synthesis.

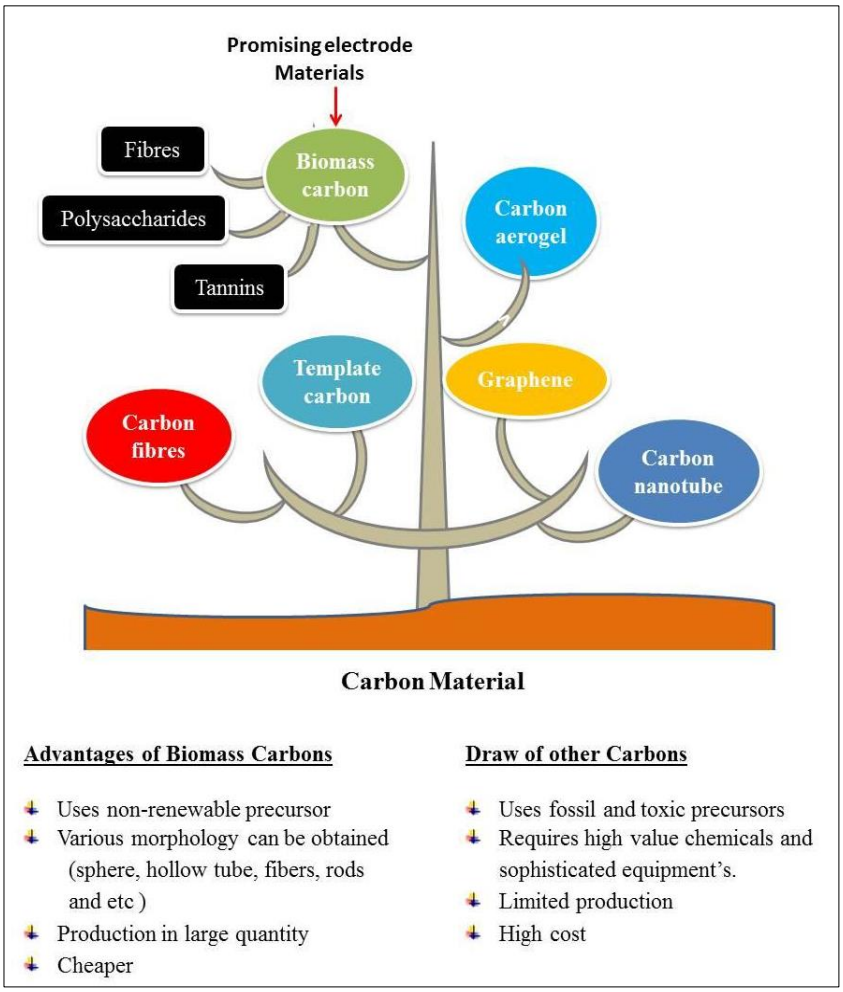

Figure 2.7 Type of carbon materials used for supercapacitors.

In the present work, various forms of porous carbons have been fabricated using different precursors by different experimental processes.

1. Jute fibres were chosen to prepare activated carbon due to its long-range fibrous structure with abundant cellulose and lignin content.
2. The tannin-rich tamarind seed coat was converted into carbon micro-fibres by hydrothermal method.
3. The Xyloglucan rich tamarind seed kernel was used to prepare carbon microsphere and carbon aerogels by hydrothermal and sol-gel method, respectively.

The homemade two-electrode symmetric cell and HS flat cell has been used to evaluate the electrochemical performance of aqueous 6 M KOH and the ionic liquid electrolyte (BmIm-TFSI), respectively.

References

[1] Becker H, *US Pat. 2800616A*, **1957**.

[2] Zhang R, Ph. D. Thesis, *Brunel University London*, **2016.**

[3] Kondrat S, Pérez CR, Presser V, Gogotsi Y, and Kornyshev AA, *Energy Environ. Sci.*, **2012,** *5*, 6474.

[4] Sun J, Iakunkov A, Rebrikova AT, and Talyzin AV, *Nanoscale*, **2018**, *10*, 21386.

[5] Peng S, Li L, Lee JKY, Tian L, Srinivasan M, Adams S, and Ramakrishna S, *Nano Energy*, **2016**, *22*, 361.

[6] Chen Y, Huang L, Xiao X, Yao B, Yuan L, Li T, Hu Z, Wang B, Wan J, and Zhou J, *Nano Energy*, **2015**, *15*, 66.

[7] Ma X, Ning G, Kan Y, Ma Y, Qi C, Chen B, Li Y, Lan X, and Gao J, *Electrochim. Acta*, **2014**, *150*, 108.

[8] Li Y, Liu Y, Wang M, Xu X, Lu T, Sun CQ, and Pan L, *Carbon*, **2018**, *130*, 377.

[9] Tian X, Zhao N, Song Y, Wang K, Xu D, Li X, Guo Q, and Liu L, *Electrochim. Acta*, **2015**,*185*, 40.

[10] Hsu YH, Lai CC, Ho CL, and Lo CT, *Electrochim. Acta*, **2014**, *127*, 369.

[11] Yang J, Wang Y, Luo J, and Chen L, *ACS Omega***, 2018**, *3*, 4647.

[12] Miao F, Shao C, Li X, Lu Na, Wang K, Zhan X, and Li Y, *Electrochim. Acta*, **2015**, *176*, 293.

[13] Liang J, Su S, Fang X, Wang D, and Xu S, *Mater. Sci. Eng. B.*, **2016**, *211*, 61.

[14] Chee WK, Lim HN, Andou Y, Zaina Z, Hamra AAB, Harrison I, Altarawneh M, Jian ZT, and Huang NM, *J. Energy Chem.*, **2017**, *26*, 790.

[15] Ke Q and Wang J, *J. Materiomics*, **2016**, *2*, 37.

[16] Li Z, Gadipeli S, Yang Y, He G, Guo J, Li J, Lu Y, Howard CA, Brett DJL, Parkin IP, Li F, and Guo Z, *Energy Storage Mater.*, **2019**, *17*, 12.

[17] Wang X, Sun G, Routh P, Kim DH, Huang W, and Chen P, *Chem. Soc. Rev.*, **2014**,*43*, 7067.

[18] Wang D, Min Y, Yu Y, and Peng B, *J. Colloid Interface Sci.*, **2014**, *417*, 270

[19] Yang J, Jo MR, Kang M, Huh YS, Jung H, and Kang YM, *Carbon*, **2014**, *3*, 106.

[20] Xing LB, Hou SF, Zhou J, Zhang JL, Si W, Dong Y, and Zhou S, *J. Solid State Chem.*,**2015**, 230, 224

[21] Liu D, Fu C, Zhang N, Zhou H, and Kuang Y, *Electrochim. Acta*, **2016**, *213*, 291.

[22] Tang L, Yang Z, Duan F, and Chen M, *Colloids Surf. A Physicochem. Eng. Asp.*, **2017**, *520*, 184.

[23] Nooshabadi MS and Zahedi F, *Electrochim. Acta*, **2017**, *245*, 575.

[24] Li J, Hao C, Zhou S, Huang C, and Wang X, *Electrochim. Acta*, **2018**, *283*, 467.

[25] Yang Z, Tian J, Yin Z, Cui C, Qian W, and Wei F, *Carbon*, **2019**, *141*, 467.

[26] John AR and Arumugan P, *J. Power sources*, **2015**, *277*, 387

[27] He X, Liu G, Yan B, Suo H, and Zhao C, *Eur. Polym. J.*, **2016**, *83*, 53.

[28] Malik R, Zhang L, McConnell C, Schott M Hsieh YY, Noga R, Alvarez NT, and Shanov V, *Carbon*, **2017**, *116*, 579

[29] Zhang M, Jia Y, Li H, and Wang J, *Synth. Met.*, **2017**, *232*, 66.

[30] Avasthi P, Kumar A, and Balakrishnan V, *ACS Appl. Nano Mater.*, **2019**, *2*, 1484.

[31] Abdah MAAM, Razali NSM, Lim PT, Kulandaivaly S, and Sulaiman Y, *Mater. Chem. Phys.*, **2018**, *219*, 120.

[32] Liang JY, Wang CC, and Lu SY, *J. Mater. Chem. A*, **2015**, *3*, 24453.

[33] Tang J, Salunkhe RR, Liu J, Torad NL, Imura M, Furukawa S and Yamauchi Y, *J. Am. Chem. Soc.*, **2015**, *137*, 1572.

[34] Khan IA, Badshah A, Khan I, Zhao D, and Nadeem MA, *Micropore. Mesopor. Mat.*, **2017**, *253*, 169.

[35] Zhang J, Chen G, Zhang Q, Kang F, and You B, *ACS Appl. Mater. Interfaces*, **2015**, 7, 12760.

[36] Wei X, Wan S, and Gao S, *Nano Energy*, **2016**, *28*, 206.

[37] Xu Y, Ren B, Wang S, Zhang L, and Liun Z, J. *Colloid Interface Sci.*, **2018**, *527*, 25.

[38] Zeng FY, Sui ZY, ShanLiu, Liang HP, Zhan HH, and Han BH, *Mater. Today Commun.*, **2018**, *16*, 1.

[39] Yang I, Kwon D, Kim MS, and Jung JC, *Carbon*, **2018**, *132*, 503.

[40] Azwar E, Mahari WAW, Chuah JH, Vo DVN, Ma NL, Lam WH, and Lam SS, *Int. J. Hydrogen Energy*, **2018**, *43*, 20811.

[41] Wang K, Yan R, Zhao N, Tian X, Li X, Lei S, Song Y, Guo Q, and Liu L, *Mater. Lett.*, **2016**, *174*, 249

[42] Zhao YQ, Lu M, Tao PY, Zhang YJ, Gong XT, Yang Z Zhang GQ, and LI HL, *J. Power Sources*, **2016**, *307*, 391

[43] Liew RK, Azwar E, Yek PNY, Lim XY, Cheng CK, Ng JH, Jusoh A, Lam WH, Ibrahim MD, Ma NL, and Lam SS, *Bioresour. Technol.*, **2018**, *266*, 1.

[44] Ibeh PO, Mateos FJG, Rosas RR, Rosas JM, Mirasol JR and Cordero T, *Materials*, **2019**, *12*, 2394

[45] Wang R, Wang P, Yan X, Lang J, Peng C, and Xue Q, *ACS Appl. Mater. Interfaces*, **2012**, *4*, 5800.

[46] Wu MB, Li LY, Liu J, Li Y, Ai PP, Wu WT, and Zheng JT, *New Carbon Mater*., **2015**, *30*, 471

[47] Misnon II, Zain NKM, Aziz RA, Vidyadharan B, and Jose R, *Electrochim. Acta*, **2015**, 174, 78

[48] Manyala N, Barzegar ABF, Khaleed AA, Momodu DY, and Dangbegnon JK, *Mate. Chem. Phys.*, **2016**, *182*, 139

[49] Liang C, Bao J, Li C, Huang H, Chen C, Lou Y, Lu H, Lin H, Shi Z, and Feng S, *Micropor. Mesopor. Mat.*, **2017**, *251*, 77

[50] Rawal S, Joshi B, and Kumar Y, *J. Energy Storage*, **2018**,*20*, 418

[51] Kurniawan A, Effendi C, Ong LK, Kurniawan F, Lin CX, Angkawijaya AE, Ju UH, Ismadki S, and Zhao XS, *Electrochim. Acta*, **2013**, *111*, 99

[52] Fan Y, Yang X, Zhu B, Liu PF, and Lu HT, *J. Power Sources*, **2014**, *268*, 284

[53] Puthusseri D, Aravindan V, Anothumakkool B, Kurungot S, Madhavi S, and Ogale S, *Small*, **2014**, *10*, 4395

[54] Ruibin Q, Zhongai H, Yuying Y, Zhimin L, Ning A, Xiaoying R, Haixiong H, and Hongying W, *Electrochim. Acta*, **2015**, *167*, 303

[55] Kurniawan F, Wongso M, Ayucitra A, Soetaredjo FE, Angkawijaya AE, Ju J, and Ismadji S, *J. Taiwan Inst. Chem. E.*, **2015**, *47*, 197

[56] Tian W, Gao Q, Tan Y, Yang K, Zhi L , Yang C, and Zhang H, *J. Mater. Chem.A*, **2015**, *3*, 5656.

[57] Hao P, Zhao Z, Tian J, Li H, Sang Y, Yu G, Cai H, Liu H, Wong CP, and Ahmad U, *Nanoscale*, **2014**, *6*, 12120.

[58] Hu Y, Tong X, Zhuo H, Zhong L, Peng X, Wang S, and Sun R, *RSC Adv.*, 2016, *6*, **15788**.

[59] Zhuo H, Hu Y, Tong X, Zhong L, Peng X, and Sun R, *Ind. Crop. Prod.*, **2016**, *87*, 229.

[60] Tian X. Zhu S, Peng J, Zuo Y, Wang G, Guo X, Zhao N, Ma Y, and Ma L, *Electrochim. Acta*, **2017**, *241*, 170.

[61] Yang X, Fei B, Ma J, Liu X, Yang S, Tian G, and Jiang Z, *Carbohydr. Polym.*,**2018**, *180*, 385.

[62] Xu J, Zhou X, Chen M, Shi S, and Cao Y, *Micropore. Mesopor.Mat.*, **2018**, *265*, *258*.

[63] Pal B, Yang S, Ramesh S, Thangadurai V, and Jose R, *Nanoscale Adv.*, **2019**, *1*,3807.

[64] Zhong C, Deng Y, Hu W, Qiao J, Zhang L, and Zhang J, *Chem. Soc. Rev.*, **2015**,*44*, 7484.

[65] Zhang Q, Rong J, Ma D, and Wei B, *Energy Environ. Sci.*, **2011**, *4*, 2152.

[66] Shi M, Kou S, and Yan X, *Chem. Sus. Chem.*, **2014**, *7*, 3053

[67] Kurig H, Vestli M, Tonurist K, Janes A, and Lust E, *J. Electrochem. Soc.*, **2012**, *159*, 7.

[68] Largeot C, Portet C, Chmiola J, Taberna PL, Gogotsi Y, and Simon P, *J. Am. Chem. Soc.*,**2008**, *130*, 2730.

[69] Bissett MA, Kinloch IA, and Dryfe RAW, *ACS Appl. Mater. Interfaces*, **2015**, *7*, 31, 17388.

[70] http://www.hohsen.co.jp/en/products/detail.php?id=107

[71] Bhattacharjya D, Kim MS, Bae TS, and Yu JS, *J. Power Sources*, **2013**,*244*, 799.

[72] Lal MS, Lavanya T, and Ramaprabhu S, *Beilstein J. Nanotechnol.*,**2019**, *10*, 781.

[73] Lecoeur C, Daffos B, Lin R, Divay L, Barney PL, Thi MP, Taberna PL, and Simon P, *Mater. Renew. Sustain. Energy*, **2013**, *2*, 13

[74] Meryl D. Stoller and Rodney S. Ruoff, *Energy Environ. Sci.*, ***2010***, 3, 1294

CHAPTER 3

EXPERIMENTAL TECHNIQUES

&

CHARACTERIZATION

This chapter gives the details of the methods of synthesis and fabrication adopted for the preparation of micro-structural carbons from agricultural wastes. The physical and electrochemical characterization techniques that are employed in this work have been detailed in this chapter. The method of fabrication of electrodes and assembly of cells is also discussed in brief.

3.1 Reagents and Apparatus

The chemicals and raw material used during this research, along with their purities and sources are listed in **Table 3.1**. These chemicals are used as such without any further purification.

Table 3.1 Chemicals and raw materials used for micro-structural carbon synthesis

Chemicals	**Purity**	**Grade / Supplier**
Potassium hydroxide (KOH)	84%	Emplura®/ Merck
Sodium hydroxide (NaOH)	97%	Emplura®/ Merck
Urea	99-100%	Emparta®/Merck
Acetone	99%	Emplura®/ Merck
Isopropyl alcohol (IPA)	99%	Emplura®/ Merck
Polytetrafluoroethylene (PTFE) solution	66 wt%	Hindustan Fluorocarbon Ltd.
Polyvinylidene fluoride (PVDF)	99%	Alfa Aesar
N, N Dimethyl formamide (DMF)	99%	Emplura®/ Merck
Nylon filter paper	Pore size - 0.45 μ, Diameter – 47 mm	Riviera Glass Pvt. Ltd
1-butyl 3-methyl immidazolium bistriflurosulfonylimide (BmIm-TFSI)	100%	Received from JAIST, Japan
Tamarind seeds	-	Local vendor

Jute fibres	-	Local vendor

3.2 Synthesis of Porous Carbon Microstructures

3.2.1 Preparation of Activated Carbon Fibres

Jute fibres are procured from the local market in Chennai, India. Jute fibres are thoroughly washed with isopropyl alcohol (IPA) at 50 ˚C followed by washing with deionized water. The washed samples are dried at 100 ˚C for 24 h. The dried jute fibres were carbonized at 700 ˚C under continuous flow of Ar gas (100 ml min^{-1}) and were labeled as JCF71. The powdered JCF71 is mixed with chemical activating agent at different weight ratios (C/KOH-1:1, 1:3 & 1:5) in 20 ml of deionized (DI) water and stirred for 8 h at room temperature, then dried at 100 ˚C overnight and chemically activated at 700 ˚C under continuous flow of Ar gas (100 ml min^{-1}) [1]. The resultant samples are cooled down to room temperature and washed with water until neutral pH. These samples are dried at 100 ˚C for 24 h. The samples are designated as JACF1, JACF3, and JACF5 with respect to the proportion of activating agent respectively (**Figure 3.1**).

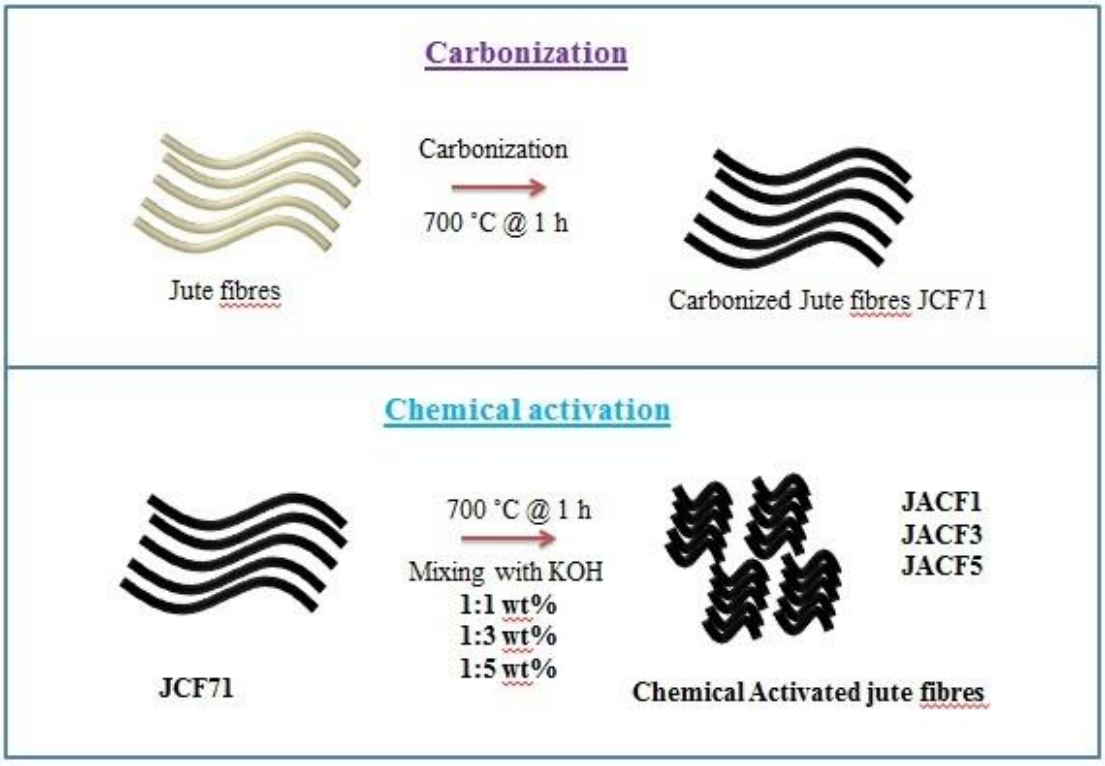

Figure 3. 1 Schematic of activated carbon fibres synthesized from jute.

3.2.2 Preparation of Porous Carbon Micro-spheres

2 g of tamarind seed kernel powder is mixed with 60 ml water and stirred for 3 h. The mixture is transferred to Teflon lined stainless steel vessel of 200 ml capacity. Further, it is heated up to 250 ˚C and kept for 12 h. The solid residue was collected and washed several times with IPA and DI water, labeled as MS-250. 1 g of MS-250 is mixed in a solution containing 1 g of KOH (20 ml DI water) and stirred for 3 h. The mixture is transferred to an alumina boat and placed inside a tubular furnace for chemical activation. The activation process is carried out at 800 ˚C for 2 h in an inert atmosphere (200 ml of N_2). The resultant product was continuously washed with DI water to remove unreacted KOH and trace impurities. The final carbon powder is dried at 100 ˚C for overnight and labeled as PSMC-800. The synthesis process of the porous carbon microspheres is shown in **Figure 3.2**.

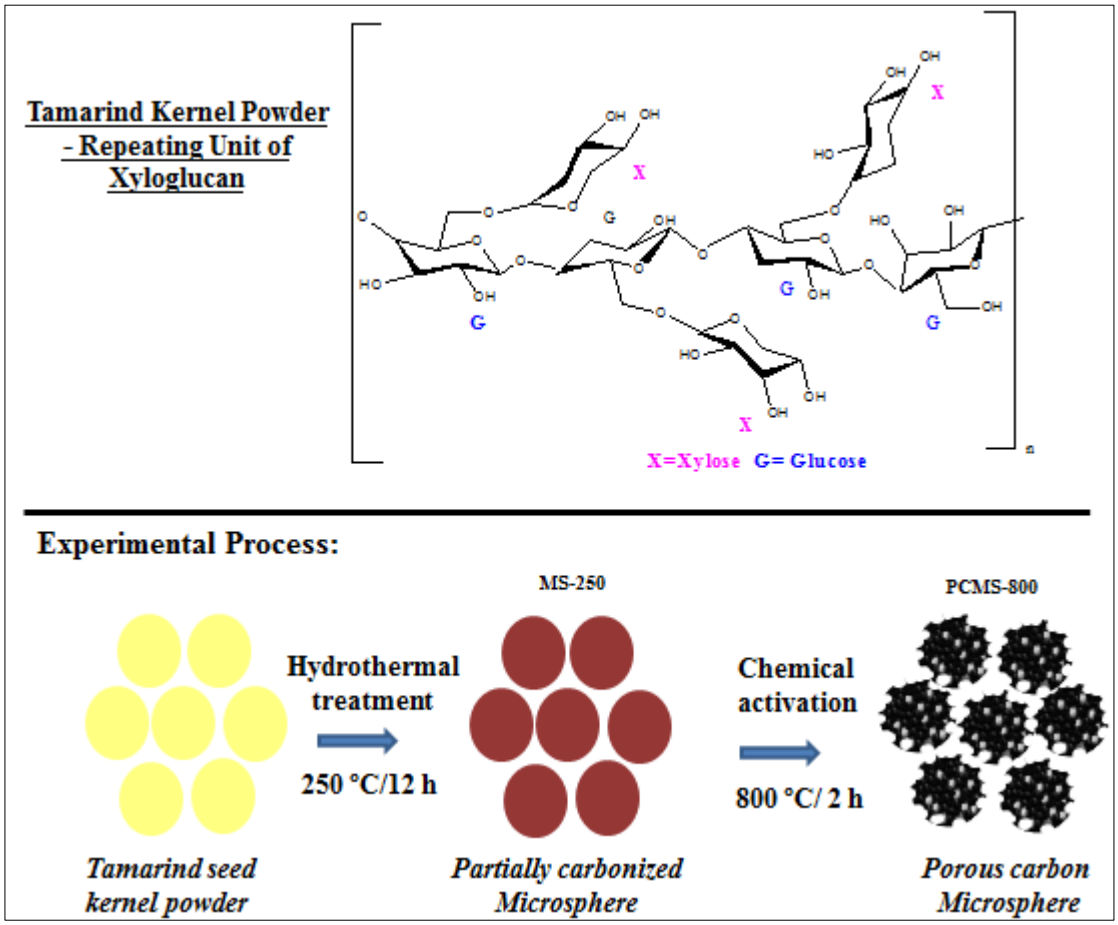

Figure 3.2 Schematic of porous carbon microspheres synthesized from tamarind seed kernel.

3.2.3 Preparation of Porous Carbon Microfibres

Tamarind seeds are purchased from local market in Chennai, India. The tamarind seeds are washed with DI water several times until it is clear of the residual water. Tamarind seeds are then subjected to a preparatory method as described elsewhere [2]. 2 g of seed coat powder dispersed in 60 ml of DI water is hydrothermally carbonized at 250 ˚C. Later, it is subjected to high-temperature carbonization to obtain carbon microfibres. The carbonized fibre is activated using a facile scheme, wherein, the carbonized fibre is mixed with KOH in the weight ratio of 1:1, 1:2, and 1:3 in deionized water and stirred continuously. The resultant mixture was dried at 100 ˚C and then activated at 800 ˚C for 1 h in the flow of Ar at a heating rate of 5 ˚C min^{-1}. The final product was washed with DI water several times and dried at 100 ˚C. The chemically activated sample is labeled as PCMF-x (porous carbon microfibres), where x is the KOH weight ratio. The synthesis process of the hierarchical porous carbon micro-fibres is shown in **Figure 3.3**.

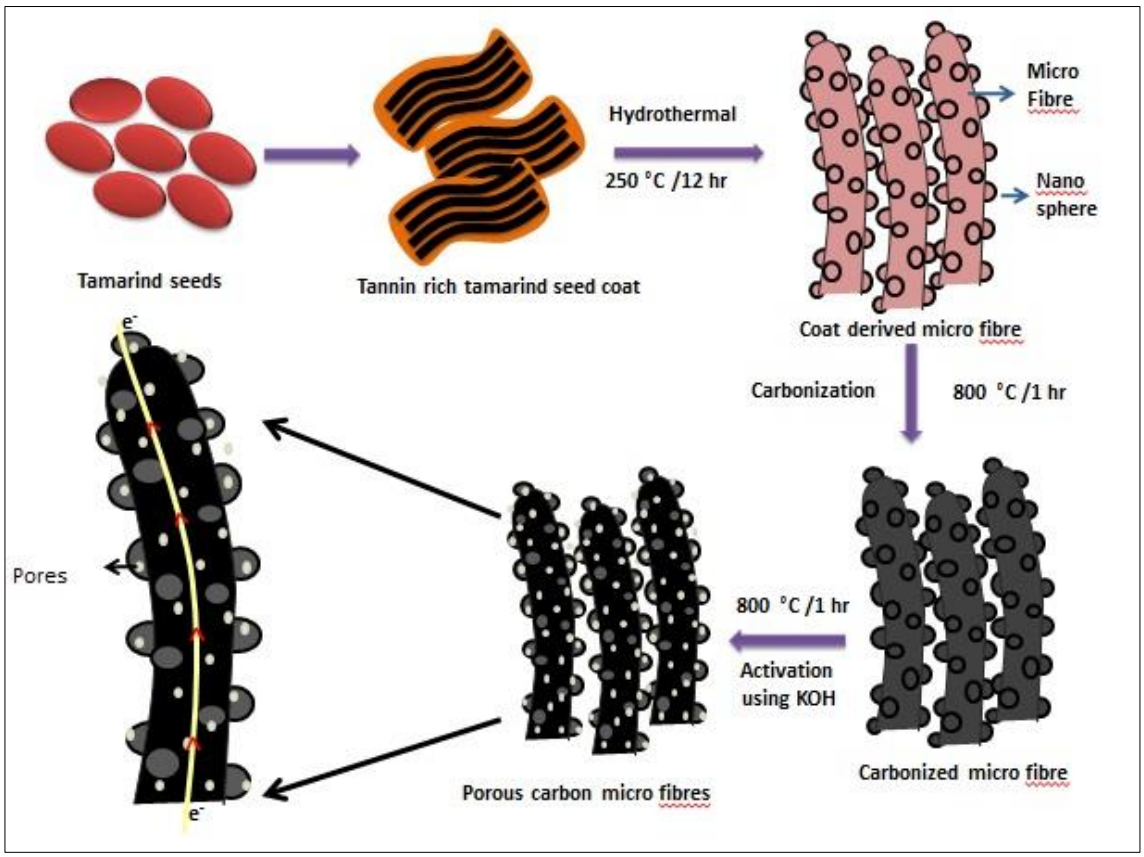

Figure 3.3 Schematic of hierarchical porous carbon micro-fibres synthesized from the tamarind seed coat.

3.2.4 Preparation of Porous Carbon Aerogel

The schematic of carbon aerogel synthesis is shown in **Figure 3.4**. The aerogel is prepared by dissolving 2 g of tamarind seed kernel powder in a mixture containing 6 g NaOH and 3.5 g urea dissolved in 40 ml DI water. The mixture is placed in an oven for 24 h at 50 °C to obtain a brown colour gel. The gel is dried at 70 °C for 48 h to form aerogel and was further carbonized under nitrogen atmosphere at various temperatures ranges from 500 °C to 800 °C with a heating rate of 5 °C min^{-1}. The samples are held for 2 h at respective temperatures before bringing down the temperature to the ambient. The powder obtained is extensively washed with DI water to remove excess NaOH to attain a pH value of 7. Subsequently, the samples were dried at 100 °C for 12 h and denoted as CAG-xxx, where xxx represents the carbonization temperature (500 °C, 600 °C, 700 °C and 800 °C).

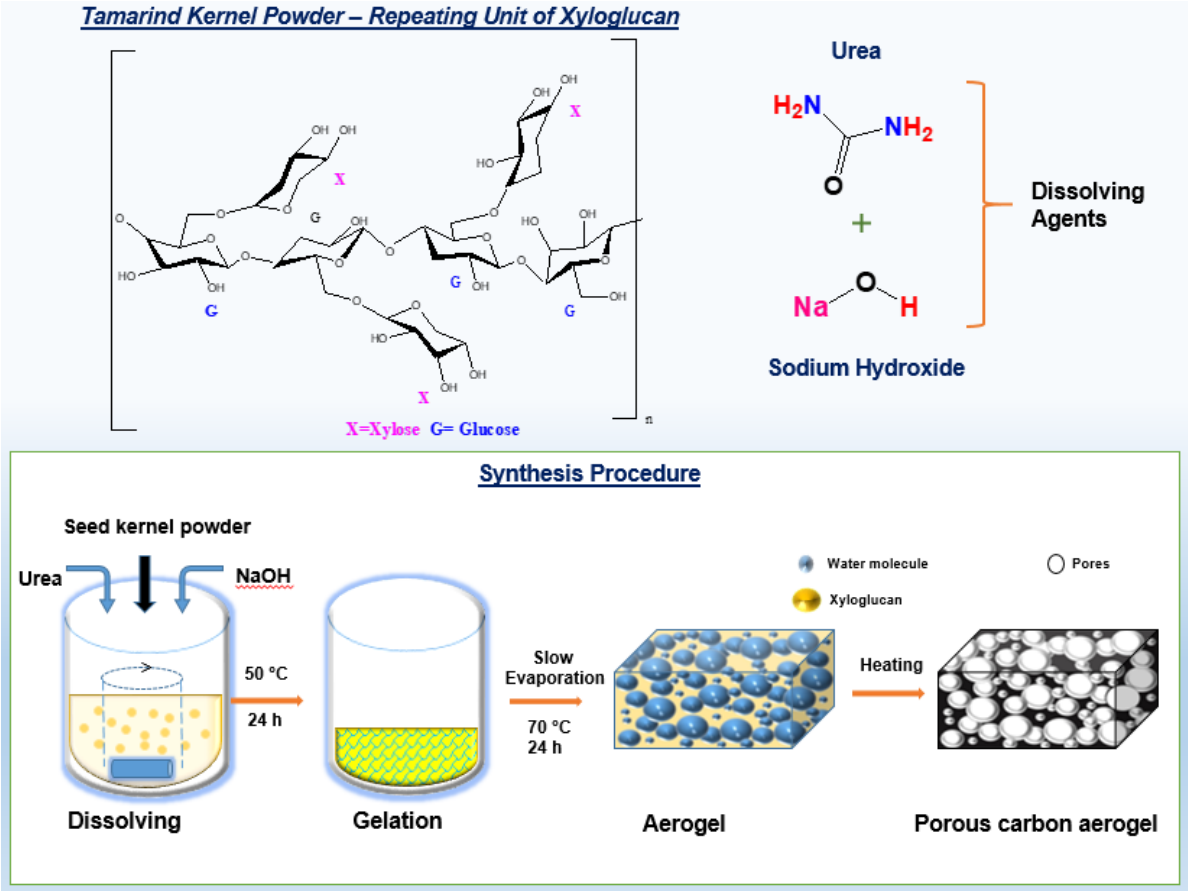

Figure 3.4 Schematic of porous carbon aerogel preparation from tamarind seed kernel.

3.3 Characterization

3.3.1 Scanning Electron Microscopy

Scanning Electron Microscope (SEM) provides a 3D image of the sample morphology and structure. A SEM is a type of electron microscope that produces images of a sample by scanning it with a focused beam of electrons. A thermionic type electron gun is used to produce the stream of electron stream via filament heating, which is directed vertically towards the sample specimen by a set of electromagnetic lenses. The electron interactions with the sample produce secondary and backscattered electrons which provide information about the morphology and structure of the samples [3-5]. In this thesis, SEM images of the prepared carbon samples are recorded using the HITACHI SU1510 instrument. For the imaging purpose, a few mg of the sample is dispersed in Acetone and drop cast on conducting adhesive tape fixed on Aluminium metal stub.

3.3.2 Field Emission Electron Microscopy

Field Emission Electron Microscopy (FESEM) is generally used to get morphology of both conducting and non-conducting samples. For the imaging purpose, a thin layer of gold and palladium is sputtered on the non-conducting sample. In FESEM, electrons emitted from a field emission gun are focused towards the sample with the help of an electromagnetic lens system. Secondary electrons emitted from the sample are detected and the signals are resolved to obtain the morphology of the sample [6-7]. The sample preparation process is similar to that of the SEM. In this work, the FESEM instrument JEOL-7000 was used to characterize the morphology of the samples.

3.3.3 Transmission Electron Microscopy

Transmission Electron Microscopy (TEM) is a microscopy technique wherein a beam of electrons is transmitted through an ultra-thin specimen, interacting with the specimen as it passes through. An image is formed from the interaction of the electrons transmitted through the specimen, and the image is magnified and focused onto an imaging device [8]. A JEOL model JEM 2100 EX instrument TEM operated at an acceleration voltage of 200 kV was used to reveal the internal structure of the materials. The sample specimen for TEM analysis was prepared by the drop casting method. Initially, powdered carbon samples (1 mg) are dispersed in acetone to obtain agglomerate-free particles by ultra-sonication for 30 min. 2 µl of the prepared solution is drop cast on the carbon coated Cu grid (400 mesh).

3.3.4 X-ray Diffraction

X-ray Diffraction (XRD) is used to identify the crystallographic information about the material. In this technique, a beam of monochromatic X-rays was irradiated on the sample over a wide range of angles and measured the corresponding intensity of diffracted X-rays by the detector. The crystal structure of the materials can be identified by Bragg's law, given by the following equation (3.1):

$$\sin\theta = n\lambda/2d \qquad (3.1)$$

Where n is an integer (n=1, 2, 3, etc) and λ is the wavelength of incident X-ray (λ= 1.5406 Å). The crystal structure can be determined by the phenomenon of diffraction [9-11]. In the present work, XRD (Smartlab, Rigaku) is used to find the dual nature of prepared porous carbon materials. The powdered carbon samples are closely packed on the quartz plate (0.5 mm depth).

3.3.5 Fourier Transform Infrared spectroscopy

Fourier Transform Infrared spectroscopy (FTIR) is commonly employed to identify the presence of chemical functional groups. A single beam of IR is irradiated on the sample at different frequencies and the absorbance intensity is measured. Each functional group has its own absorption characteristics based on its chemical bonding. Thus, the presence of chemical functional groups can be determined from the recorded absorption spectrum [12-13]. In this work, FTIR spectra were recorded on a Varian 3100 FTIR instrument with the KBr pellet technique.

3.3.6 Surface Area Analysis

The surface area and pore size distribution of the prepared samples are measured using nitrogen (N_2) adsorption/desorption analysis [14]. The samples are filled inside the glass tube, which is subjected to degassing at a particular temperature (200 – 300 ˚C) for several hours (12-24 h) in order to remove surface adsorbed contaminations. The weight of the sample is recorded after cooling down to room temperature (approximately ~ 250 mg). After degassing, the sample was subjected to N_2 gas at variable pressures and isothermal temperature (generally at -196 ˚C). The amount of nitrogen gas adsorption/desorption with an increase/decrease in applied pressure is measured [15-16].

The specific or total surface area (S_{tot}) of the samples is calculated from N_2 adsorption/desorption by multiple-point Brunauer-Emmett-Teller (BET) model within the relative pressure ranges from 0.05 to 0.25 [14]. The micropore surface area and micropore

volume are calculated using the t-plot method. The total pore volume of the materials is calculated at a relative pressure value of 0.99. The t-plot is used to calculate the micropore surface area (S_{mic}) and micropore volume (V_{mic}) [17-18]. The difference between S_{tot} and S_{mic} gives the external surface are which consists of mesopores and macropores. The density functional theory (DFT) model was used to identify the pore size distribution of the material [19]. The N_2 sorption/desorption has been carried out using a Micromeritics ASAP2020 analyzer.

3.4 Electrochemical Characterization

A two-electrode symmetric cell system is used for evaluating the electrochemical performance of the prepared carbon materials. Different electrolyte solutions are used as the electrolytes including 6 M KOH and 1-butyl 3-methyl imidazolium bistriflurosulfonyloimde (BmIm-TFSI).

3.4.1 Electrode Fabrication and Cell Assembly

The electrode for aqueous (6 M KOH) electrolyte solution was prepared using active material, conducting carbon, and binder. Typically, 20 mg of carbon sample and 2 mg of acetylene black are dispersed in 200 µl of IPA, and 2 µl solution containing PTFE (66 wt%) is added to the dispersion. The slurry containing the active carbon and binder was allowed to form a paste, which was pressed on a nickel mesh (1 x 1 cm^2) and dried at 100 °C for 12 h. The mass loading of the electrode materials was maintained approximately at 24 mg. The electrodes and separator were immersed in 6 M KOH electrolyte prior to assembly. The cell was assembled using two identical electrodes and a separator, which is clipped between two poly (ethylene terephthalate) plates [20].

The electrode for ionic liquid electrolyte (BmIm-TFSI) was prepared using active material, conducting carbon, and binder. Typically, 20 mg of carbon sample, 2 mg of acetylene black, and 2 mg of PVDF are dispersed in 1 ml of dimethylformamide (DMF) by sonication for 30 min. The slurry is spray coated on the aluminium current collector (1 cm^2) and a 2 mg mass loading was maintained, approximately, and dried at 100 °C for 12 h. The cell was assembled using two identical electrodes separated by a polypropylene separator soaked in the BmIm-TFSI electrolyte in an HS-type cell [21].

The most commonly used electrochemical techniques are cyclic voltammetry, galvanostatic charge-discharge, and electrochemical impedance spectroscopy are employed to

evaluate the electrochemical performance of the assembled cell. These experiments were carried out using Solartron (Model-1400) and Biologic (VmP3) at room temperature.

3.4.2 Cyclic Voltammetry

Cyclic voltammetry (CV) technique is a simple and effective electrochemical characterization tool used to identify the faradaic/non-faradaic reaction at the interface of electrode and electrolyte as a function of applied voltage (V). In this technique, the voltage is applied between the two electrodes of the cell at a constant scan rate (mV s^{-1}) within the specified voltage range, in both forward and reverse directions. The corresponding current (i) response is measured and plotted against the applied voltage. Generally, a non-faradaic charge formation occurs at the electrode/electrolyte interface for carbon based supercapacitor system, which is known as electric double layer capacitance (EDLC). The capacitance of an EDLC is given by the following equation (3.2) [20,22]

$$C = 2\,\frac{i}{\frac{dV}{dt}.m} \qquad (3.2)$$

Where i is the current (A), $\frac{dV}{dt}$ is the scan rate (mV s^{-1}) and m is the mass of each electrode (g).

3.4.3 Galvanostatic charge-discharge

Galvanostatic charge-discharge (GCD) is one of the most reliable methods for estimating the capacitive behavior of the cell under constant current. This approach varies from CV because a constant current is applied and the changing voltage across the cell is measured. This method is often referred to as chrono-potentiometry and provides valuable information about capacitance, internal resistance, and cyclability of the cell. The specific capacitance of the cell can be calculated using the following equation, [20, 23]

$$C = 2\frac{i.t}{m.\Delta V} \qquad (3.3)$$

where, i the specific current density (A g^{-1}), t is the discharge time (s) after iR drop, m is the mass of each electrode (g) and ΔV is discharge voltage (V). The cyclic stability of the cell is measured by conducting GCD continuously over a large number of cycles.

3.4.4 Electrochemical impedance spectroscopy

The electrochemical impedance spectroscopy (EIS) is used to identify the interaction of charge or ion with the electrode surface at a stationary condition. It can provide information on valuable parameters like cell resistance, double layer capacitance and charge transfer resistance

[24]. These parameters are the deciding factors for the performance of an electrochemical system. In this method, an AC sinusoidal voltage is applied to perturb the system and its corresponding AC sinusoidal current is measured. The AC perturbation is applied over a wide range of frequencies, typically from very high frequency (1 M Hz) to very low frequency (0.01 Hz). The ratio and phase-angle between AC voltage and current measured provides complex impedance Z, which consists of real (Resistor) and imaginary components (Capacitor and Inductor). The complex impedance plots are usually represented by Nyquist and Bode plot [25-26].

In this work, the EIS study was conducted using PESI mode by Biologic. The measurement is performed at AC perturbation voltage of 10 mV_{rms} with in the frequency range of 1 MHz to 0.1 Hz.

3.4.5 Dynamic electrochemical impedance spectroscopy

Dynamic Electrochemical Impedance Spectroscopy (DEIS) was used to find the charge transfer reaction at a non-stationary or dynamic condition of an electrochemical system. DEIS is well explored in corrosion inhibition, Li-ion batteries, and Fuel Cell evaluation. In this technique, an AC perturbation signal is applied at each potential within the allowed voltage window of the electrochemical system, and reaction mechanism is measured with respect to cell potential. In this work, the DEIS measurements are carried out from 0 to 1 V at intervals of 20 mV in the frequency range from 100 kHz to 0.01 Hz with 10 points per frequency decade and applying AC amplitude of 10 mV_{rms}. The experiment was performed with Biologic (VmP3) potentiostat.

References

[1] Ramesh T, Rajalakshmi N, and Dhathathreyan KS, *Renew. Energy Environ. Sustain.*, **2017**, *2*, 4.

[2] Sahu S. R, Devi D. P, Phanikumar V. V. N, Ramesh T, Rajalakshmi N, Praveena G, Prakash R, Das B, and Gopalan R, *Ionics*, **2018**, *24*, 3413.

[3] Kane PF and Larrabee GB, *Characterization of Solid Surfaces*, **1974**, 1st Edition, Plenum press (Chap 5).

[4] Patrick Echlin, Handbook of sample preparation for scanning electron microscopy and X-Ray microanalysis, **2009**, 2nd Edition, Springer (Chap 1).

[5] Hodnik N, Dehm G, and Mayrhofer KJJ, *Acc. Chem. Res.*, **2016**, *49*, 2015.

[6] Bonard JM, Dean KA, Coll BF, and Klinke C, *Phys. Rev. Lett.*, **2002**, *89*, 19.

[7] Chalmers GR, Bustin RM, and Power IM, *AAPG Bulletin*, **2012**, 96, 1099.

[8] Ayache J, Beaunier L, Boumendil J, Ehret G, and Laub D, Sample preparation handbook for transmission electron microscopy, **2009**, 4th Edition, Springer (Chap 4).

[9] Pope CG, *J. Chemical Education*, **1997**, *74*, 1.

[10] Whitfield P, *Int. J. NanoSci.*, **2004**, *3*, 757.

[11] Ravi Sharma, Bisen DP, Usha S ,and Sharma BG, *Recent Res. Sci. Technol.*,**2012**, *4*, 77.

[12] Bhargava R, Wang S, and Koenig JL, *Adv. Polym. Sci.*, **2003**, *163*, 137.

[13] Sammon C, Mura C, Yarwood J, Everall N, Swart R, and David Hodge, *J. Phys. Chem. B*, **1998**, *102*, 3402.

[14] Sing KSW, Everett DH, Haul RAW, Moscou L, Pierotti RA, Rouguerol J, and Siemieniewska T, *Pure Appl. Chem.*, **1985**, *57*,603.

[15] Cai J, Niu H, Li Z, Du Y, Cizek P, Xie Z, Xiong H, and LinT, *ACS Appl. Mater. Interfaces*, **2015**, *7*, 14946.

[16] Dong Y, Lin H, Zhou D, Niu H, Jin Q, and Qu F, *Electrochim. Acta*, **2015**, *159*, 116.

[17] Demiral H and Demiral I, *Surf. Interface Anal.*, **2008**, *40*, 612.

[18] Galarneau A, Villemot F, Rodriguez J, Fajula F, and Coasne B, *Langmuir*, **2014**, 30, *44*, 13266.

[19] Jagiello J and Thommes M, *Carbon*, **2004**, *42*, 1227.

[20] Ramesh T, Jafri RI, Reddy NP, Raveendra NV, Rajalakshmi N, Dhathathreyan KS, Tamilarasan P, and Ramaprabhu S, *Adv. Porous Mater.*, **2018**, *6*, 8.

[21] Bhattacharjya D, Kim MK, Bae TS, and Yu JS, *J. Power Sources*, **2013**, *244*, 799

[22] Ferrero GA, Sevilla M, and Fuertes AB, *Carbon*, **2015**, *88*, 239

[23] Qian W, Sun F, Xu Y, Qiu L, Liu C, Wang S, and Yan F, *Energy Environ. Sci.*, **2014**, *7*, 370.

[24] Ghosh S, Santhosh R, Jeniffer S, Raghavan V, Jacob G, Nanji K, Kollu P, Jeong SK, and Grace AN, *Sci. Rep.*, **2019**, *9*, 4746.

[25] Misnon II, Zain NKM, Aziz RA, Vidyadharan B, and Jose R, *Electrochim. Acta*, **2015**, *174*, 78

[26] Abdulhakeem B, Farshad B, Damilola M, Fatemeh T, Mopeli F, Julien D, and Ncholu M, *RSC Adv.*, **2014**, *4*, 39066.

CHAPTER 4

ACTIVATED CARBON FIBRES DERIVED FROM JUTE FOR HIGH PERFORMANCE SUPERCAPACITOR

4.1 Introduction

Energy fulfillment and environmental sustainability are the key challenges encountered by renewable energy storage technologies. Supercapacitor technology is one of the energy storage technologies which can satisfy both energy requirements and environmental sustainability [1]. Fascinating properties such as high specific capacitance, high power density, long cyclic life, and safe handling make them suitable for consumer electronics and transport applications [2-4]. The electrochemical performance of supercapacitors mainly depends on the electrode materials and the electrolyte medium [5-7].

Generally, carbon materials of different structures have been extensively used as electrode material for supercapacitor application because of their very high surface area, wide pore size distribution, and electrical conductivity [8, 9]. Among the various carbon forms, activated carbon fibres have drawn much attention due to its very high surface area and long-range fibrous structure which is expected to facilitate fast ion and electron transfer [10, 11]. Typically, activated carbon fibres are widely synthesized using organic precursors such as poly-acrylonitrile, poly-benzimidazole, and petroleum-based isotropic pitch by the electro-spinning method [12-15]. However, the high temperature carbonization of organic precursors releases highly toxic substances which are not environmentally benign. It, therefore, necessitates an alternative method to synthesize activated carbon fibres from sustainable and environmental friendly precursor materials.

Recently, activated carbon fibres derived from biomass have attracted great attention owing to its ability to act as both template and precursor [16-20]. The intense exploration to substitute supercapacitor electrodes with natural carbon fibres is due to the high surface area, electrically conductive nature, stability in the electrochemical environment, and low cost. So far, the natural fibres such as cotton [21], jute [22-23], coconut shell [24], cellulose fibre [25], banana fibres [26], and human hair [27] have been used as precursors. However, the resultant structural and textural properties of carbon fibres mainly depend on the physical and chemical properties of the natural fibre used.

Jute is the second largest available natural fibre, mostly used in the textile and packing industry due to its high mechanical and tensile strength [28]. Interestingly, the jute has high lumen or lacunas, which are empty spaces, available in the fibres [29-30]. The lumens do not play any significant role in physical properties of the fibres. Only sporadic reports on utilizing the jute derived carbons for supercapacitor and the importance of the lumen are found in the literature. For instance, Kasinath Ojha et al. prepared a graphene-like porous carbon from jute

fibres by dehydration and chemical activation process [22]. The resultant porous carbon presented a very high specific capacitance of 476 F g^{-1} at very low current density of 0.2 A g^{-1} in a three electrode set-up using 0.5 M H_2SO_4 electrolyte. Further, Zequine et al. followed a high temperature carbonization process to prepare carbon from recycled jute fibre [23]. The carbonized jute fibres exhibited a specific capacitance value of 408 F g^{-1} at a low scan rate of 1 mV s^{-1} in a three electrode configuration using 3 M KOH electrolyte. However, the assembled supercapacitor device presented only 51 F g^{-1} at a scan rate of 5 mV s^{-1}. Both the reports have claimed appealing capacitance value at very low scanning conditions in three electrode configuration. But, both the approaches yield very low specific capacitance in the two electrode configuration which is essential and mimics the real time supercapacitor device.

The primary objective of this work is to develop a hollow micro-fibrous carbon material from the jute leveraging on its lumen structure. Further, the textural properties of the jute based carbon fibres have been modified by the chemical activation method. A symmetric supercapacitor cell was fabricated to evaluate its electrochemical performance.

4.2 Results and Discussion

The morphology of the carbonized and chemically activated jute fibres was studied by Scanning Electron Microscopy (SEM). The SEM image, shown in **Figure 4.1a** shows the retention of fibrous structure for the carbonized jute fibre at 700 ˚C. The different sizes of opening in the cross-sectional view seen in the figure are attributed to the intrinsic hollow lumen micro-structure [29-30]. **Figure 4.1 (b-d)** shows that the fibrous structure of the chemically activated carbonized fibres is retained with shortened lengths. It can also be clearly observed in Figure 4.1d that chemical activation of carbonized fibres has led to the deepening of through pores forming a micro-tubular structure [28].

The structural characteristics of the prepared samples were examined by XRD. **Figure 4.2** shows the XRD patterns of the carbonized and chemical activated jute fibres. The patterns show two broad peaks at about 22˚ and 43˚, corresponding to the diffraction of graphitic planes (002) and (100), respectively [28, 31]. It has been observed that the peak intensity of chemically activated jute fibres is reduced compared to that of carbonized jute fibre due to the destruction of graphitic planes, especially with the KOH weight ratio of 3 (JACF3). The collapse in the graphitic phase can be attributed to the strong and vigorous reaction between carbon lattice and KOH at high temperature (≥700 ˚C) resulting in the enhancement of porosity [28, 31].

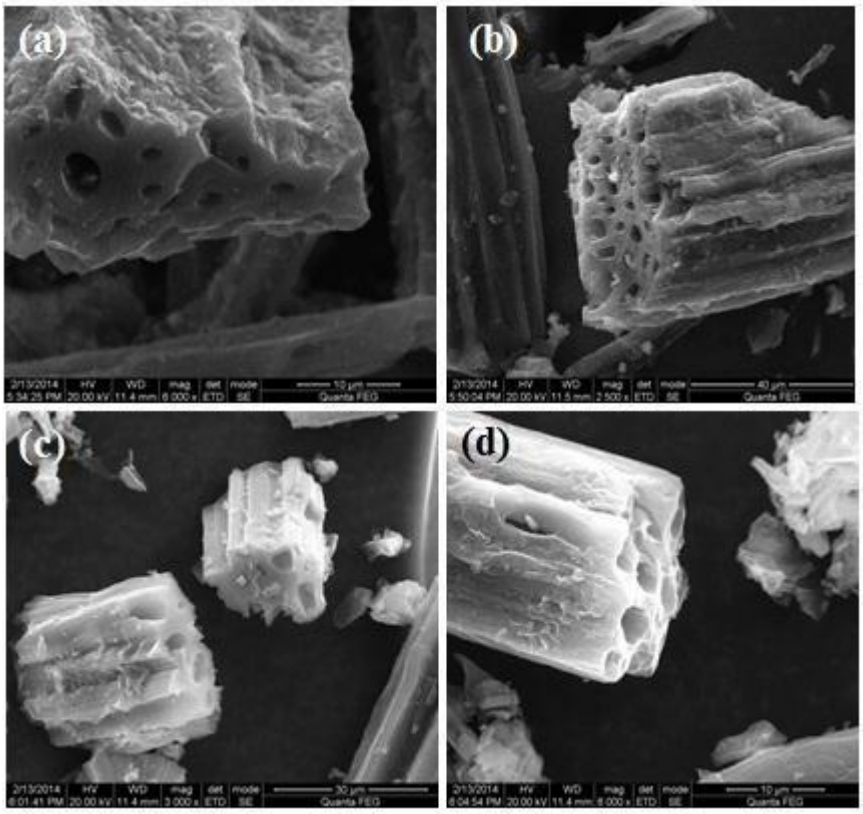

Figure 4.1 SEM images of activated carbon fibre samples. Scale (a) 50 µm (b) 40 µm (c) 30 µm and (d) 10 µm

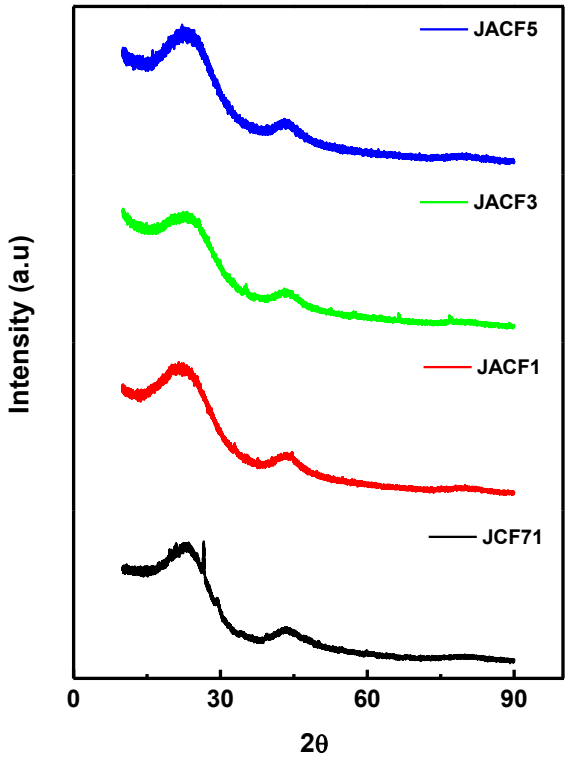

Figure 4.2 XRD patterns of activated carbon fibre samples.

The textural properties of the samples are measured by the N_2 adsorption/desorption isotherms, and the results are shown in **Figure 4.3a**. The isotherms of chemically activated jute fibres show the Type-I isotherm with H4-type hysteresis loop suggesting that it contains both micropores and mesopores, in accordance with IUPAC classification [32]. The JACF samples showed a significant increase in N_2 uptake at a relative pressure (P/P_0) above 0.4, clearly indicating the formation of mesopores.

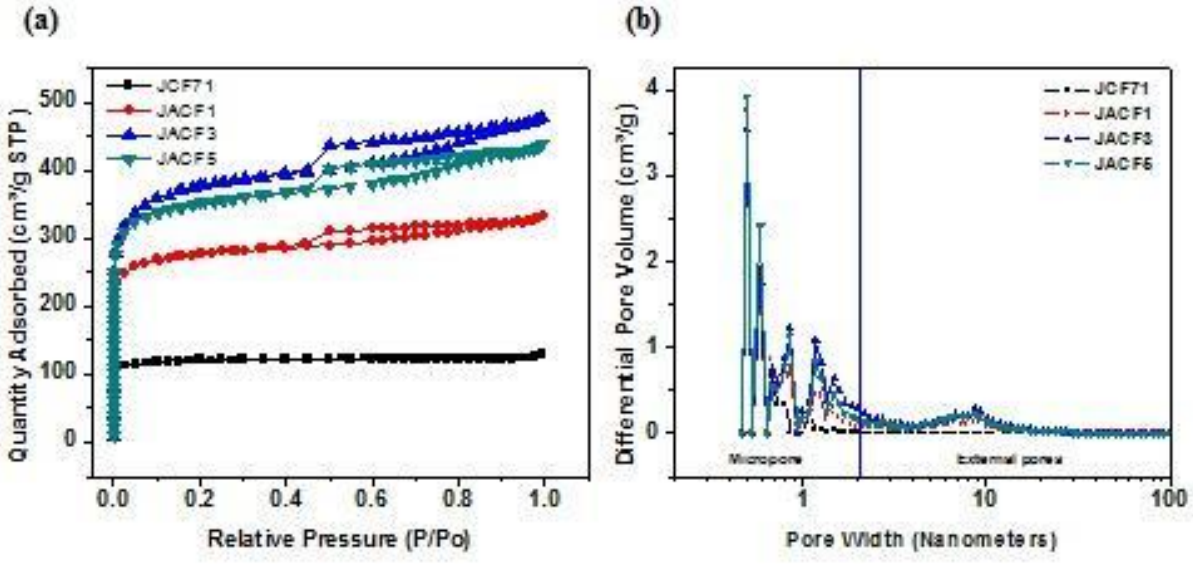

Figure 4. 3 Nitrogen adsorption/desorption isotherm of the activated carbon fibre samples.

The surface area and pore volume of the samples have increased with increase in the KOH weight ratio up to 3 and reached the maximum value of 1224 $m^2\ g^{-1}$ and 0.74 $cm^3\ g^{-1}$, respectively. Further increase in the ratio of KOH reduced the surface area and total pore volume to 1141 $m^2\ g^{-1}$ and 0.67 $cm^3\ g^{-1}$. The pore size distribution curves reveal that most of the pores lie below 2 nm for all the samples (**Figure 4.3b**). However, the JACF samples have exhibited an additional pore size distribution in the range between 4-12 nm. It is well understood that the presence of micropores on activated carbon fibres enhances the diffusion and transportation of electrolyte ions deeper into the electrode which boosts the specific capacitance [33].

The FTIR spectrums of all the samples are shown in **Figure 4.4**, which provides information on the chemical structure of the materials. It can be observed from the **Figure 4.4** that all the samples showed a similar pattern revealing the O–H, C–H, and C–C bond stretching. The band at around 3400–3450 cm^{-1} represents the O–H stretching vibration mode of hydroxyl functional groups, while the band at around 2921 cm^{-1} represents the C–H symmetric and

asymmetric vibration modes. The band around 1630–1640 cm^{-1} is attributed to C═C stretching vibration mode of olefinic C═C bonds, which is also reported by Yang et al. [34].

Table 4.1 Textural properties of jute derived activated carbon fibres.

Sample	Total Surface area ($m^2 g^{-1}$)	Micropore Surface Area ($m^2 g^{-1}$)	External Surface area ($m^2 g^{-1}$)	Total Pore Volume ($cm^3 g^{-1}$)	Micropore Volume ($cm^3 g^{-1}$)
JCF71	382	340	42	0.19	0.16
JACF1	894	724	170	0.51	0.35
JACF3	1224	888	336	0.74	0.43
JACF5	1141	873	268	0.67	0.42

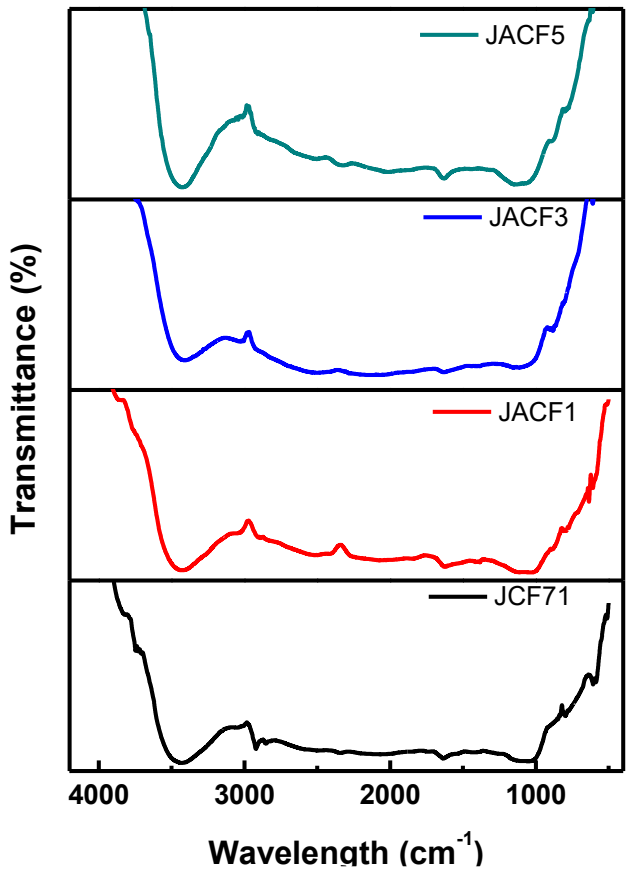

Figure 4.4 FTIR spectra of the activated carbon fibre samples.

Cyclic voltammetry (CV) and galvanostatic charge-discharge (GCD) measurements were carried out at ambient conditions to investigate the electrochemical performance of JACFs. **Figure 4.5a** shows the CV plots for the JACF electrodes measured at various scan rates of 20 mV s^{-1}, 50 mV s^{-1}, and 100 mV s^{-1}. The voltammograms represented a typical rectangular plot confirming the double-layer charge formations at the electrode/electrolyte interface which is a characteristic feature of the supercapacitor [22-23]. The specific capacitance remained high up to a relatively high scan rate of 50 mV $s^{-1}$for all the electrode materials, as shown in **Figure 4.5b**. At a higher scan rate of 100 mV s^{-1}, the deformation of rectangular shape was observed, resulting in reduced capacitance indicating the deterioration of the double layer nature of charge storage. Among all the four samples, JACF3 has exhibited the highest rectangular area with a maximum specific capacitance value of 114 F g^{-1} at 20 mV s^{-1}. The high specific capacitance of JACF3 is attributed to the combined effect of the hollow fibrous structure and high surface area associated with a large volume of micropores.

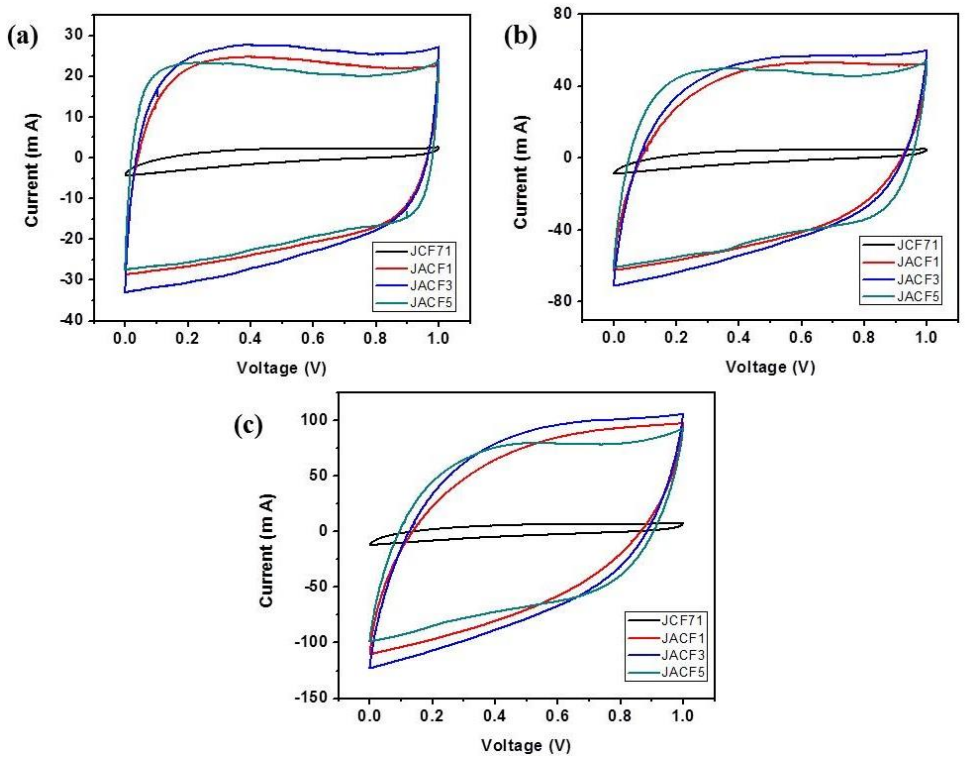

Figure 4.5 Cyclic voltammogram of all samples measured at different scan rates. (a) 20 mV s^{-1}, (b) 50 mV s^{-1}, and (c) 100 mV s^{-1}.

The GCD curves of the activated carbon fibres at different current densities are plotted in **Figure 4.6**. The symmetric cells prepared with the JCF71 sample did not exhibit any meaningful charge-discharge behavior due to its low surface area. The activated carbon fibre (JACFs) samples exhibited the typical triangular shape with high reversibility indicating the

formation of double-layer charge formation [22-23]. The calculated specific capacitance values are 84, 97, and 83 F g^{-1} at a current density of 1 A g^{-1} in 6 M KOH solution for JACF1, JACF3, and JACF5, respectively.

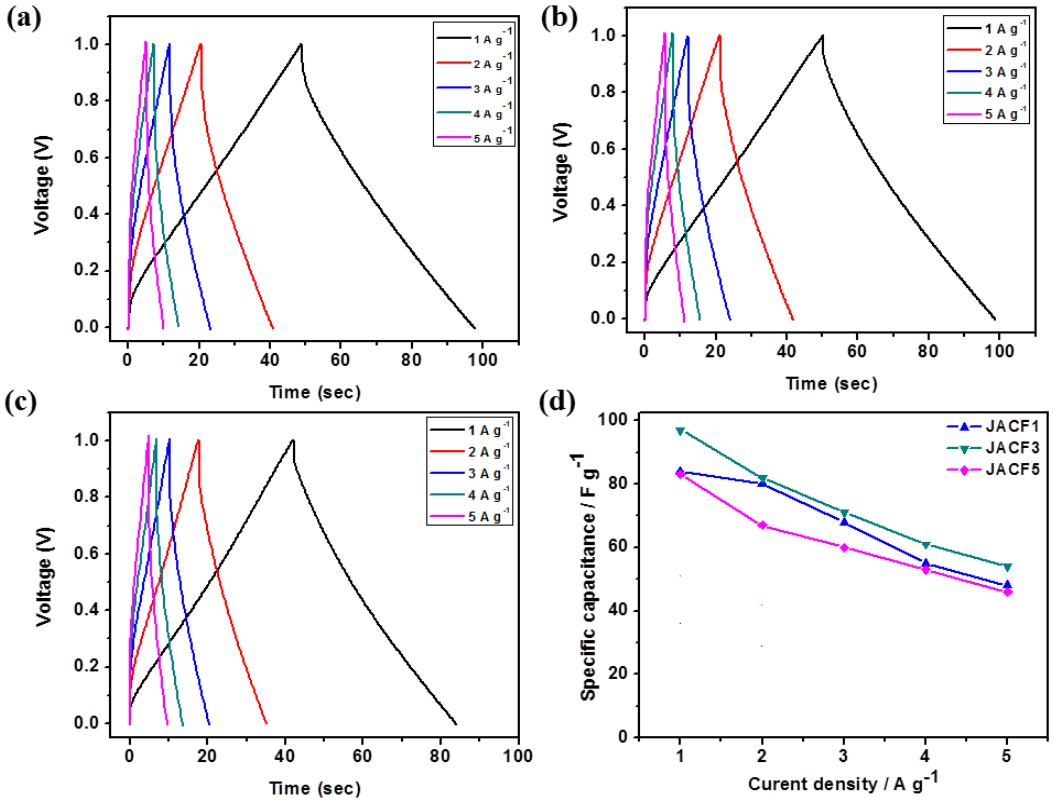

Figure 4.6 GCD pattern of (a) JACF1, (b) JACF3, and (c) JACF5 (d) rate capability of JACFs electrode at different current densities.

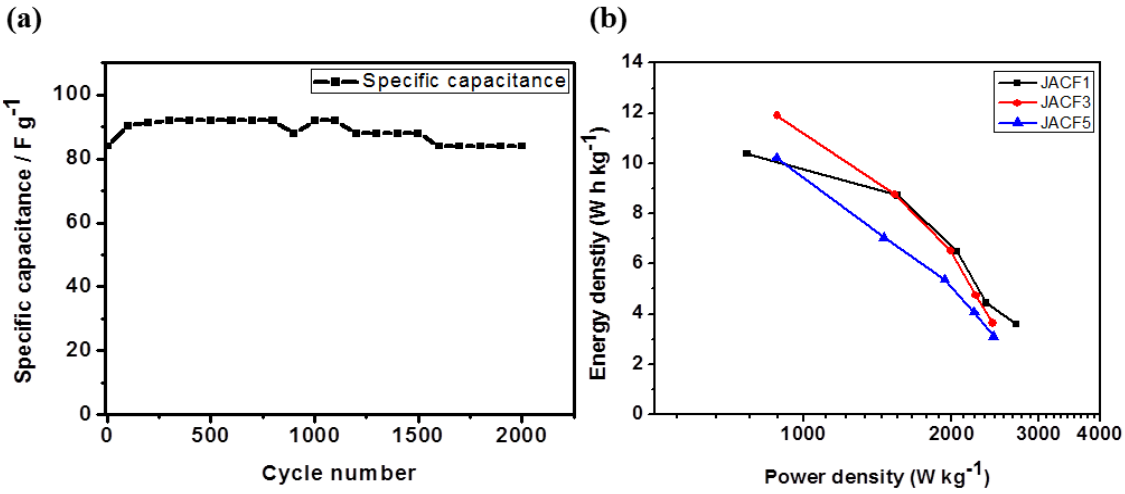

Figure 4.7 (a) Cyclic stability of JACF3 at 2 A g^{-1} for 2000 cycles and (b) Ragone plot of JACFs.

The reported values of specific capacitance obtained from various biomass derived carbon fibres are summarized in **Table 4.2** for the purpose of comparison. Firstly, the electrochemical performance of the jute derived activated carbon fibres are matched well with the other biomass derived carbons. Secondly, the performance of JACF3 (present work) is significantly better compared to other jute derived carbons.

Table 4.2 Comparison of specific capacitance of jute derived carbon fibres with other biomass-derived carbons.

Material	Specific surface area ($m^2\ g^{-1}$)	Specific capacitance ($F\ g^{-1}$)		Test conditions		Electrode system	Reference
		C.D	S.R	C.D ($A\ g^{-1}$)	S. R ($mV\ s^{-1)}$		
Rice husk	1493	112	n.a	1.0	-	2 electrode	[35]
Cotton stalk	1481	114	n.a	0.5	-	2 electrode	[36]
Oil palm kernel shell	727	123	n.a	0.5	-	2 electrode	[37]
Bagasse	1892	142	n.a	0.5		2 electrode	[38]
Natural Jute	825	476	n.a	0.5	-	3 electrode	[22]
Recycled Jute	1769	n.a	51	-	5	2 electrode	[23]
Jute fibres	**1224**	**97**	**114**	**1.0**	**20**	**2 electrode**	**This work**

C.D- Charge/discharge **S.R- Scan rate** **n.a – Not available**

The cyclic stability of the electrode materials for supercapacitors is an essential factor for practical applications. **Figure 4.7a** shows the results of cycling stability tests for over 2000 cycles for the JACF3 sample, at a current density of 2 $A\ g^{-1}$. JACF3 exhibited good cycling stability with retaining 96% of its initial capacitance even after 2000 cycles. The highest

capacitance of JACF3 results from its unique fibrous structure, high specific surface area, and optimal pore size distribution.

The energy and power characteristics of JACF samples are shown in **Figure 4.7b**. A maximum energy density of 11.8 Wh kg^{-1} was achieved for the JACF3 electrode. However, the energy density of the JACF3 electrode has declined from 11.8 to 3.6 Wh kg^{-1} as the power density increased from 0.88 to 2.42 kW kg^{-1}, by considering the scale factor of 4 for practical device applications [39]. The energy density and power density of the electrode prepared with JACF3 is found to be 2.88 Wh kg^{-1} and 0.25 kW kg^{-1}.

4.3 Conclusions

Chemical activation of the carbonized jute fibres is effective in enhancing the specific surface area and optimizes the ratio of micro-to-mesopore. A maximum specific capacitance of 114 F g^{-1} at 20 mV s^{-1} is achieved for JACF3 sample which has a combination of high specific surface area and optimal pore size distribution. Further, the JACF3 has exhibited superior capacitance retention at 96% over 2000 cycles. The enhanced electrochemical performance of JACFs is attributed to the combination of hollow fibrous structure and high surface area with large micro- to mesoporous ratio. The cost-effective and facile route adopted for the synthesis of hollow carbon fibres from natural jute is amenable for the large scale production for the commercial application.

References

[1] Gao YP, Zhai ZB, Huang KJ, and Zhang YY, *New J. Chem.*, **2017**, *41*, 11456.

[2] Rajagopal RR, Aravinda LS, Rajarao R, Bhat BR, and Sahajwalla, *Electrochim. Acta*, **2016**, *211*, 488.

[3] Konikkara N, Kennedy LJ, and Vijaya J, *J. Hazard. Mater.*, **2016**, *318*, 173

[4] Karnan M, Subramani K, Srividhya PK, and Sathish M, *Electrochim. Acta*, **2017**, *228*, 586

[5] Faraji S and Ani FN, *Renew. Sust. Energ. Rev.*, **2015**, *42*, 823.

[6] Mini V and Devendrappa H, *Mater. Today Proce.*, **2018**, *5*, 23148.

[7] Mangisetti SR, Kamaraj M, and Ramaprabhu S, *Electrochim. Acta*, **2019**, *305*, 264.

[8] Borenstein A, Hanna O, Attias R, Luski S, Brousse T, and Aurbach D, *J. Mater. Chem. A*, **2017**,*5*, 12653.

[9] Chen X, Paul R, and Dai L, *Natl. Sci. Rev.*, **2017**, *4*, 453.

[10] Vijayakumar M, Santhosh R, Adduru J, Rao TN, and Karthik M, *Carbon*, **2018**, *140*, 465.

[11] Wen Y, Qin T, Wang Z, Jiang X, Peng S, Zhang J, Hou J, Huang F, He D, and Cao G, *J. Alloys Compd.*, **2017**, *699*, 126.

[12] Kim C, Ngoc BTN., Yang KS, Kojima M, Kim YA, Kim YJ, Endo M, and Yang SC, *Adv. Mater.*, **2007**, *19*, 2341.

[13] Kim C and Yang KS, *Appl. Phys. Lett.*, **2003**, *83*, 1216.

[14] Kim C, Park SH, Lee WJ, and Yang KS, *Electrochim. Acta*, **2004**, *50*, 877.

[15] Park SH, Kim C, and Yang KS, *Synth. Met.*, **2004**, *143*, 175.

[16] Sodtipinta J, Leosakulrat C, Poonyayant N, Kidkhunthod P, Chanlek N, Amornsakchai T, and Pakawatpanuru P, *Ind. Crop. Prod.*, **2017**, *104*, 13.

[17] Dai C, Wan J, Shao J, and Ma F, *Mater. Lett.*, **2017**, *193*, 279.

[18] Su XL, Li SH, Jiang S, Peng ZK, Guan XX, and Zheng XC, *Adv. Powder Technol.*, **2018**, *29*, 2097

[19] Azwar E, Mahari WAW, Chuah JH, Vo DVN, Ma NL, Lam WH, and Lam SS, *Int. J. Hydrogen Energy*, **2018**, *43*, 20811.

[20] Sun J, Li W, Lei E, Xu Z, Ma C, Wu Z, and Liu S, *J. Power Sources*, **2019**, *438*, 227030.

[21] Ramesh T, Jafri RI, Reddy NP, Raveendra NV, Rajalakshmi N, Dhathathreyan KS, Tamilarasan P, and Ramaprabhu S, *Adv. Porous Mater.*, **2018**, *6*, 8.

[22] Ojha K, Kumar B, and Ganguli AK, *J. Chem. Sci.*, **2017**, *129*, 397.

[23] Zequine C, Ranaweera CK, Wang Z, Dvornic PR, Kaho PK, Singh S, Tripathi P, Srivastava ON, Singh S, Gupta BK, Gupta G , and Gupta RK, *Sci. Rep.*, **2017**, *7*, 1174.

[24] Mi J, X.R. Wang, FanRJ, QuWH, and LiWC, *Energy Fuels*, **2012**, *26*, 5321.

[25] Deng L, Young RJ, Kinloch IA, Abdelkader AM, Holmes SM, De Haro-Del Rio DA, and Eichhorn SJ, *ACS Appl. Mater. Interfaces*, **2013**, *5*, 9983.

[26] Chaitra K, Vinny RT, Sivaraman P, Reddy N, Hu C, Venkatesh K, Vivek CS, Nagaraju N, and Kathyayini N, *J. Energy Chem.*, **2017**, *26*, 56..

[27] Qian W, SunF, Xu Y, Qiu L, Liu C, Wang S, and Yan F, *Energy Environ. Sci.*, **2013**, *7*, 379.

[28] Ramesh T, Rajalakshmi N, and Dhathathreyan KS, *Renew. Energy Environ. Sustain.*, **2017**, *2*, 4

[29] Hossain MR, Islam MA, Vuure AV, and Verpoest I, *Procedia Engineering*, **2014**, *90*, 52.

[30] Phan NH, Rio S, Faur C, Coq LL, Cloirec PL, and Nguyen TH, *Carbon*, **2006,** *44*, 2569.

[31] Dong Y, Lin H, Zhou D, Niu H, Jin Q, and Qu F, *Electrochim. Acta*, **2015**, *159*, 116.

[32] He X, Ling P, Yu M, Wang M, Zhang X, and Zheng M, *Electrochim. Acta*, **2013**, *105*, 635.

[33] Ma C, Yu Y, Li YJ, Shi JL, Song Y, and Liu L, *J. Electrochemical Society*, **2014**, *161*, A1.

[34] Yang K, Peng J, Srinivasakannan C, Zhang L, Xia H, and Duan X, *Bioresour. Technol.*, **2010**, *101*, 6163.

[35] Ganesan A, Mukherjee R, Raj J, and Shaijumon M, *J. Porous Mater*., **2014**, *21*, 839

[36] Chen M, Kang X, Wumaier T, Dou J, Gao B, Han Y, Xu G, Liu Z, and Zhang L, J. *Solid State Electrochem.*, **2013**, *17*, 1005.

[37] Misnon II, Zain NKM, Aziz RA, Vidyadharan B, and Jose R,*Electrochim. Acta*, **2015**, *174*, 78.

[38] Hao P, Zhao Z, Tian J, Li H, Sang Y, Yu G, Cai H, Liu H, Wong C. P, and Umar A, *Nanoscale*, **2014**, *6*, 12120.

[39] Park DW, Cañas NA, Schwan M, Milow B, Ratke L, and Friedrich KA, *Curr. Appl. Phys.*, **2016**, *16*, 658.

CHAPTER 5

MICRO AND MESOPORE DECORATED CARBON MICROSPHERES DERIVED FROM TAMARIND SEED KERNEL FOR SUPERCAPACITOR APPLICATION

5.1 Introduction

Carbon has **attracted** immense attention as an electrode material for supercapacitor. Recently, carbon microspheres, an exoticform of carbon, has been extensively explored as the electrode material for supercapacitors owing to its interconnected pores, very high surface to volume ratio, high packing density, and excellent electrical conductivity [1-3]. Intense efforts to produce carbon microspheres by various experimental techniques and cost effective precursor materials are underway globally [4]. The low cost agricultural biomass wastes and their by-products are being recently explored to produce the carbon microspheres.

Most of the synthesis procedures employ multiple experimental procedures or used highly refined derivatives (cellulose, glucose, fructose, xylose, carrageenan, starch, etc) to prepare carbon microspheres from biomass wastes. For example, Kurniawan et al. (2015) followed a two-step process to convert the water hyacinth into porous carbon microspheres using dilute H_2SO_4 as a catalyst. The resulting porous carbon microspheres presented a maximum surface area of 1010 $m^2 g^{-1}$ for the KOH impregnation ratio of 1 and exhibited a high capacitance value of 179 F g^{-1} at a 1 A g^{-1} in three electrode systems [3]. Most of the reports reveal that the biomass precursors are converted to polysaccharides for the synthesis of carbon microspheres. The process of producing microspheres from biomass is a highly attractive research area and is gathering momentum. However, currently there is only sporadic reporting owing to its infancy.

Direct use of biomass without adapting the extraction process or catalysts can be an effective way to prepare carbon microspheres also minimizes the production cost. Tamarind seed kernel, rich in polysaccharide has been selected as the precursor for the synthesis of carbon microspheres. The other advantage with tamarind seed kernel powder is that it doesn't require any specific extraction process and use of a catalyst (H_2SO_4, KOH). The tamarind seed kernel is subject to hydrothermal treatment followed by chemical activation using KOH. These resultant porous carbon microspheres have been used as electrodes for supercapacitors and showed excellent electrochemical performance.

5.2 Result and discussion

Polysaccharides in tamarind seed kernel can easily be dissolved in water which makes them suitable for the synthesis of carbon spheres. The synthesis strategy for carbon microspheres from tamarind seed kernel is shown in **Figure 3.2**. The surface morphology of the samples is analyzed using SEM, both before and after the chemical activation. The SEM

image (**Figure 5.1a)** shows that the MS-250 sample consists of a large volume of spherical shaped particles in micrometer size (4-8 μm) with a smooth surface. **Figure 5.1b** shows that the spherical morphology is retained in PCMS-800 after chemical activation and the pores are created on the surface of the spheres due to vigorous reaction with KOH.

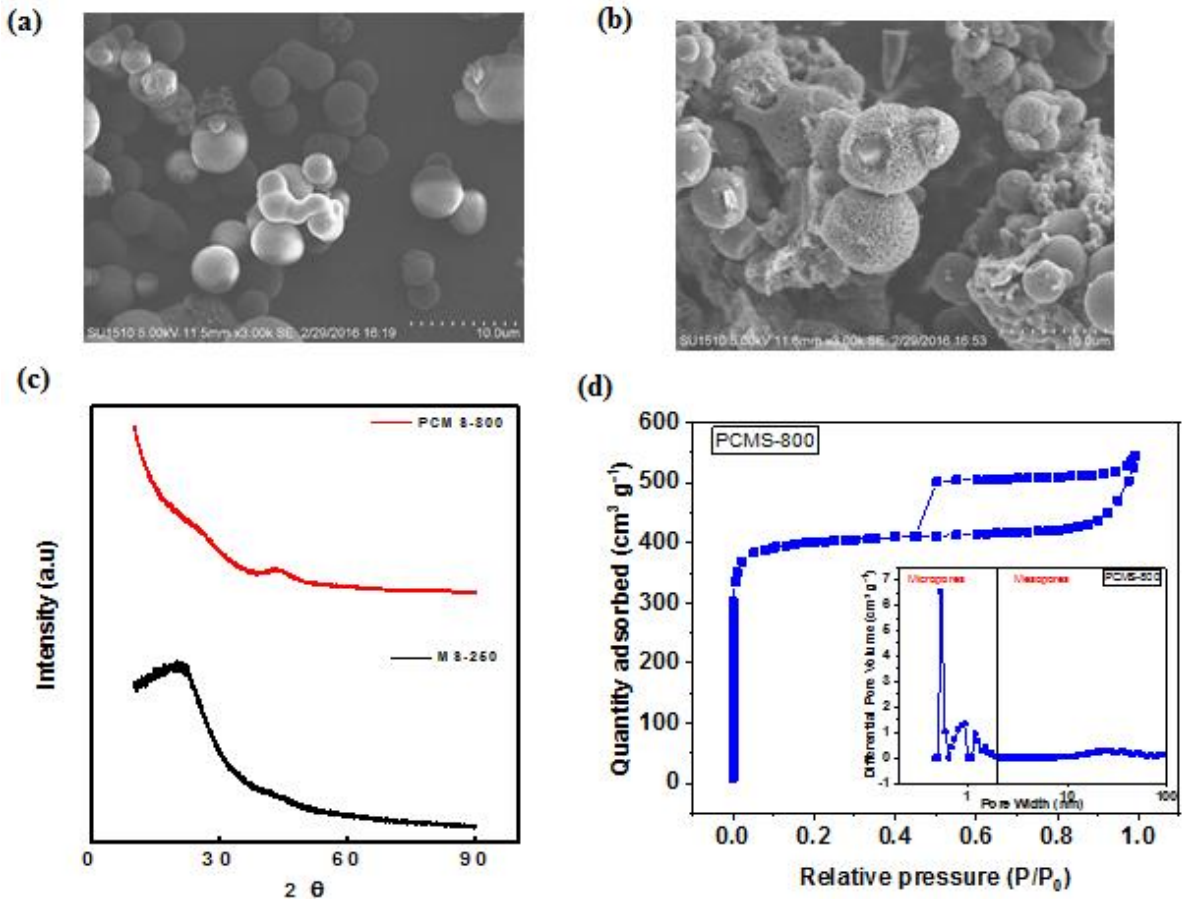

Figure 5.1 SEM images of (a) MS-250 (scale 10 μm), (b) PCMS-800 (scale 10 μm), (c) XRD patterns of all samples, and (d) Nitrogen adsorption/desorption isotherm of PCMS-800.

The XRD patterns of the MS-250 and PCMS-800 samples are shown in **Figure 5.1c**. The MS-250 exhibits a broad peak centered at 22° typical of amorphous carbon, corresponding to the (002) plane of graphite [1]. The intensity of peak at 22° was drastically decreased in PCMS-800, due to the vigorous reaction of KOH with the hexagonal lattice carbon at high temperature. The peak centered at 43º corresponds to the (100) plane evincing the graphitic phase [6]. **Figure 5.1d** depicts the type I isotherm of PCMS-800 with an H4 hysteresis loop, which indicates the presence of a large volume of micropores and minimal volume of mesopores. The pore size distribution curve reveals that the majority of pore volume lies within the pore size range below 2 nm (inset **Figure 5.1d**). The specific surface area of PCMS-800 is found to be as high as 1284 m^2 g^{-1}, deeming it suitable for supercapacitor application.

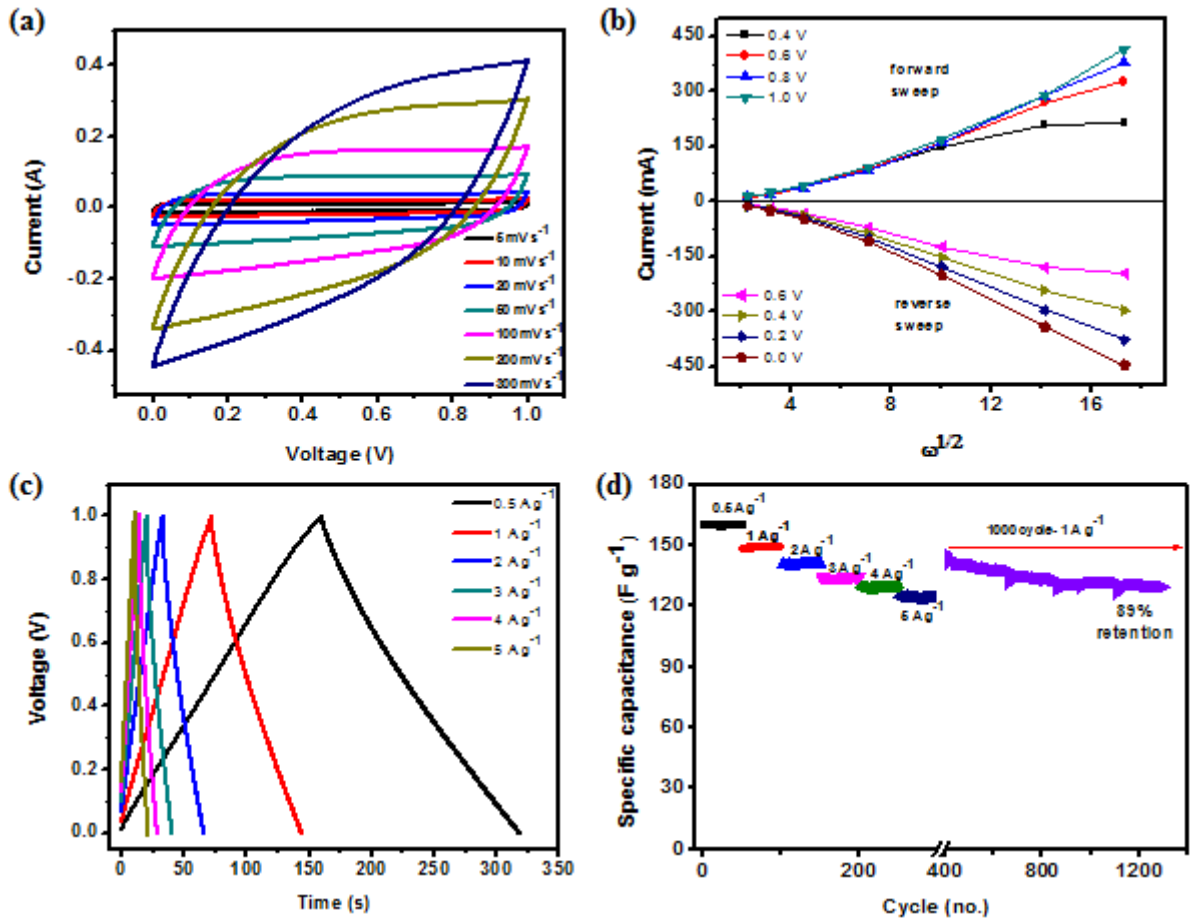

Figure 5.2 Electrochemical performance of PCMS-800 in the symmetrical system: (a) Cyclic voltammogram measured at different scan rates, (b) the measured current vs. square root of scan rate, (c) GCD profiles measured at various current densities, and (d) the cyclic stability at different current densities.

Further, the electrochemical characteristics were studied using cyclic voltammetry (CV) at different scan rates to understand the double layer formation and its kinetics in the potential range between 0 to 1 V. **Figure 5.2a** shows a perfect rectangular voltammogram for PCMS-800 electrode, at a scan rate of 5 mV s^{-1}. This typical shape indicates the formation of a good electrochemical double layer at the electrode/electrolyte interface. The retention of rectangular voltammogram at a fast scan rate of 100 mV s^{-1} indicates efficient and fast ion transport at the electrode/electrolyte interface. The double-layer formation kinetics and reversibility calculated from the CV are shown in **Figure5.2b**. It can be seen that the measured current values linearly increase with increasing scan rate, indicating the rapid double layer charge formation at the electrode/electrode interface and confirms the highly reversible nature of the electrodes [5].

The galvanostatic charge-discharge method is employed to evaluate the real time charge/discharge characteristics. **Figure5.2c** shows the GCD profiles measured at various

current densities ranging from 0.5 A g^{-1} to 5 A g^{-1} and shows triangular shaped curves indicating the formation of a reversible double layer. The specific capacitance values calculated from the discharge curves, leaving the voltage drop for different current densities presented in **Figure 5.2d**. A maximum capacitance yield was 160 F g^{-1} at 0.5 A g^{-1}. The retention of capacitance was 77% at 5 A g^{-1}. After 1,000 cycles of successive charge/discharge, the PCMS-800 electrode retained 89% of initial capacitance and it compares well with the other carbon spheres electrode materials [3,4] **(Figure5.2d)**.

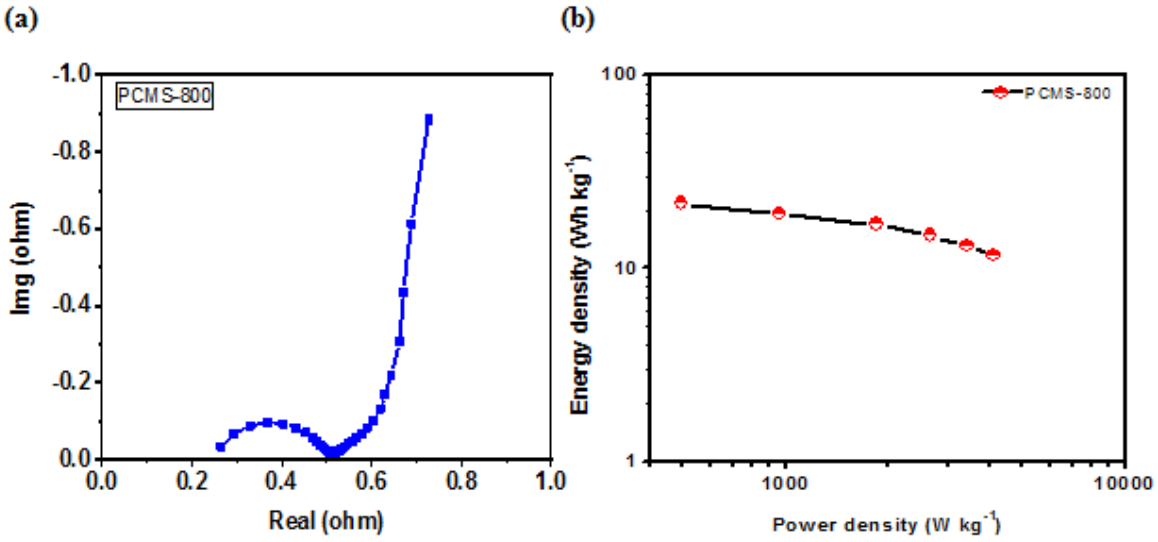

Figure 5.3 (a) Nyquist plot and (b) Ragone plot for the PCMS-800 electrode.

The impedance measurements confirmed the superior properties of PCMS-800 electrode, as shown in **Figure 5.3a**. The internal resistance of the PCMS-800 electrode was low at 0.26 Ω owing to the faster ion transport in the open porous structure. **Figure 5.3b** shows the energy characteristics of the PCMS-800 electrode. It is clearly seen that the symmetric supercapacitor system delivers an extremely high energy density of 21.5 Wh kg^{-1} at a power density of 0.493 kW kg^{-1}, and retains 53% of its energy density at maximum power density of 4.1 kW kg^{-1}. The energy characteristics of tamarind seed kernel derived carbon microspheres are comparable to that of other biomass derived carbon materials like potato starch (21.5 Wh kg^{-1}@ 0.75 kW kg^{-1}) [1], the bamboo by-product (6.1 Wh kg^{-1} @ 26 kW kg^{-1}) [7] and tamarind seed coat (21.1 Wh kg^{-1} @ 0.491 kW kg^{-1}) [8].

The carbon microspheres derived from tamarind seed kernel has exhibited a reasonable specific capacitance of 160 F g^{-1} at 0.5 A g^{-1}, in a two electrode system, due to its unique spherical structure and high specific surface area with plentiful open pores when compared with the carbons derived from various agricultural biomass and its derivatives (**Table 5.1)**. These

results indicate the tamarind seed kernel derived carbon microspheres are promising electrode material for supercapacitor device application.

Table 5.1 Comparison of electrochemical properties of porous carbons derived from various agricultural biomass precursors by hydrothermal method.

Precursor	Total surface area ($m^2\ g^{-1}$)	Calculated specific capacitance ($F\ g^{-1}$)	Discharge Current density ($A\ g^{-1}$)	Electrode / Conc. of Electrolyte	Reference
Potato starch	456	68	1.0	2 / 1 M KOH	[1]
Carrageenan	2502	261	0.5	3 / 6 M KOH	[2]
Water hyacinth	1010	179	1.0	3 / 6 N KOH	[3]
Bamboo byproduct	1472	301	0.1	2 / 6 M KOH	[7]
Tamarind seed coat	1702	157	0.5	2 / 6 M KOH	[8]
Tamarind seed kernel	**1284**	**160**	**0.5**	**2 / 6 M KOH**	**This work**

5.3 Conclusions

Novel carbon microspheres with micro- and mesopore combination have been successfully synthesized from tamarind seed kernel for supercapacitor application. The direct use of seed kernel for the synthesis of carbon spheres has eliminates the involvement of catalysts and an additional extraction process. This process is very simple and viable for the production of carbon microspheres in bulk. In terms of specific capacitance, rate capacity, and cyclic stability, the PCMS-800 electrode has exhibited excellent electrochemical performance owing to its superior morphological and textural properties. The results compared well with other biomass derived materials. The tamarind seed kernel holds great promise for further exploration of supercapacitor application.

References

[1] Ruibin Q, Zhongai H, Yuying Y, Zhimin L, Ning A, Xiaoying R, Haixiong H, and Hongying W, *Electrochim. Acta*, **2015**, *167*, 303.

[2] Fan Y, Yang X, Zhu B, Liu PF, and Lu T, *J. Power Sources*, **2014**, *268*, 584.

[3] Kurniawan F, Wongso M, Ayucitra A, Soetaredjo FE, Angkawijaya AE, Ju YH, and Ismadji S, J. *Taiwan Inst. Chem. E*, **2015**, *47*, 197.

[4] Zheng MT, Liu YL, Xiao Y, Zhu Y, Guan Q, Yuan DS, and Zhang JX, J. *Phys. Chem. C*, **2009**, *113*, 8455.

[5] Ramesh T, Vedarajan R, Rajalakshmi N, and Reddy LRG, *J. Mater. Sci.: Mater. Electron.*, **2020**, *31*, 1681.

[6] Quach NKN, Yang WD, Chung ZJ, and Tran HL, Adv. Mater. Sci. Eng., **2017**, 1-9.

[7] Tian W, Gao Q, Tan Y, Yang K, Zhu L, Yang C, and Zhang H, *J. Mater. Chem. A*, **2015**, *3*, 5656.

[8] Ramesh T, Rajalakshmi N, Dhathathreyan KS, and Reddy LRG, *ACS Omega*, **2018**, *3*, 12832.

CHAPTER 6

HIERARCHICAL POROUS CARBON MICRO-FIBRES DERIVED FROM TAMARIND SEED COAT FOR HIGH ENERGY SUPERCAPACITOR APPLICATION

6.1 Introduction

High surface area carbons with excellent electrical conductivity are usually employed as the supercapacitors electrode materials. These materials exhibited high electrochemical capacitance but poor rate capability owing to inadequate ionic diffusion and charge transfer resistance inside the tortuous pores. Therefore, the quest to achieve high capacitance with novel porous carbon materials with modified and improved morphology is ongoing and high power density with capacity retention has not been punctuated to date.

Paving the way to novel morphologies was the advent of hierarchical porous carbon, considered to be one of the ideal electrode materials for supercapacitor due to their three-dimensional (3D) porous channels with well-balanced micro, meso and macroporous structure [1]. Hierarchical porous carbons are widely synthesized from resorcinol-formaldehyde [2], polystyrene [3], polypyrrole [4], sucrose [5], fructose [6], glucose [7], and cellulose [8] by template method. Furthermore, the existing template methods mostly employ expensive, synthetic, and non-green route precursor materials along with surfactants that are non-renewable.

To circumvent these issues, biomass and it's derivatives such as cotton [9], metaplexis japonica [10], cyclosorus interrupts [11], cotton, hardwood, softwood, bamboo [12], rice straw, soybean stalk, wheat straw, corn stalk, rice straw, cotton stalk, peanut shell [13] were introduced as a precursor for the hierarchical porous carbon. Exemplary synthesis strategies have been reported with these types of biomass precursors in order to achieve the desired morphology and well-defined porosity. All the aforementioned carbon materials have been reported to possess the high capacity in electrochemical devices owing to the microporous and mesoporous tuning [9-15].

To highlight a few such materials with high capacity, Tian et al. developed a hierarchical porous carbon derived from bamboo by hydrothermal method, and the optimized sample exhibited a maximum surface area of 1472 $m^2\ g^{-1}$ and capacitance of 148 F g^{-1} at a current density of 0.1 A g^{-1} in 6 M KOH [16]. An interconnected channel like hierarchical porous carbon aerogel obtained from bagasse by freeze drying method, has a maximum surface area of 1892 $m^2\ g^{-1}$ and exhibits a high capacitance of 142 F g^{-1} at current density of 0.5 A g^{-1} [1]. Later, Peng et al. developed a loose porous structure carbon with well-developed porosity derived from mixture of sewage sludge (SS) and coconut shell (SS) as precursor materials by hydrothermal method to obtain super-hierarchical porous carbon, which had a surface area of

3003 $m^2 g^{-1}$, presenting a capacitance value of 62 F g^{-1} at a current density of 0.5 A g^{-1} in a 6 M KOH [17]. Recently, Fierro et al. reported an application of tannin related polyphenol derived hierarchical porous carbon as a supercapacitor electrode material with excellent capacitance performance (277 F g^{-1} at 0.5 mV s^{-1} in the 3-electrode system), demonstrating good feasibility to utilize tannin polyphenols to synthesize carbon materials with high electrochemical activity [18]. It should be emphasized here that a hard template route employing SBA-15 was adopted in Fierro eta al. work. Though this material exhibits high surface area and good specific capacitance, its synthesis requires regress route which makes these methods inconvenient for commercialization.

The efficiency of polyphenols as a precursor in achieving a hierarchical porous carbon (HPC) is evident from the number of reports [19-23. Hence, natural biomass rich in polyphenols with an inherent template was hypothesized to lead to a HPC. Tannin rich tamarind seed (*Tamarindus Indica L*) largely available in India, Thailand, Indonesia, Myanmar, and the Philippines emerges as a candidate material [24]. The tamarind seed comprises of carbon (~51.7%), nitrogen (~35.5%) and oxygen (~12.4%) [24]. The Whole tamarind seed contains 70% of kernel (white colour) and 30% seed coat or testa (brown) [25]. The seed kernel consists of protein and polysaccharides widely employed in pet food, textile, mining, and pharmaceutical industry. The seed coat consists of a high portion of fibres, tannin (30-40%), and dyeing matter which are unsuitable for the food industry. Large quantities of seed coat obtained from the food industry during the separation process are discarded as bio-waste.

These, generally discarded seed coat possess two salient features making it unique as a precursor. Firstly, the tannin contains polyphenolic compounds (phloroglucinol, gallic acid, and catechin) of high molecular weight (about 500–3000) and is soluble in water which becomes the source of carbon [24]. Secondly, the crude fibre contains a lignocellulose highly stable till 300 ˚C under hydrothermal conditions [25]. Therefore, the fibrous structure is expected to be retained even after the hydrothermal process allowing it to act as a self-template for the formation of microfibres. The specific chemical composition and microstructure of tamarind seed coat can be utilized to form a hierarchical porous carbon microfibre by hydrothermal method without using any template and catalyst. Herein, we demonstrated the preparation of hierarchical porous carbon micro fibre using tamarind seed by hydrothermal method. The synthesis strategy to form hierarchical porous carbon microfibres from seed coat is schematically illustrated in **Figure3.3**. This process of making HPC microfibres is simple,

economical, and can be easily scaled up. The tuning of micro and mesopores on the mechanically stable microfibres is crucial for the electrode application.

6.2 Results and discussion

The macroscopic image of an untreated tamarind seed coat is shown in **Figure 6.1a**. The seed coat covers the kernel protecting it from any mechanical damage and the brown colored seed coat evinces the tannin rich surface. In **Figure 6.1b**, an electron microscopic view of the cross section of the seed coat reinforced with numerous interconnected fibres is shown. These fibres possess high amount of lignocellulose content after subjecting to hydrothermal treatment (MF-250), resulting in a morphology in **Figure 6.1c**, which clearly depicts the retainment of the fibrous nature. Further, a high temperature carbonization at 800 ℃ yielded distinct strands of fibres as shown in **Figure 6.1d** and labeled as CMF-800.

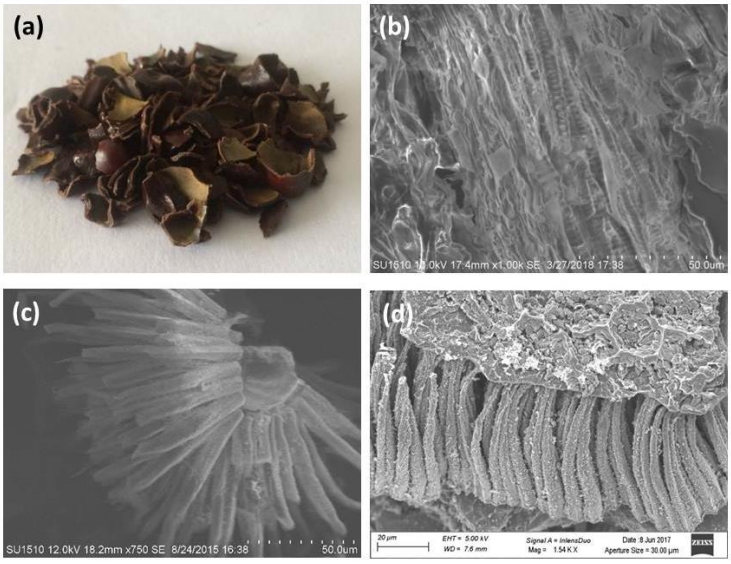

Figure 6.1 (a) Photograph of seed coat, (b) SEM cross section image of seed coat (scale 50 µm), SEM image of (c) MF-250 (scale 50 µm), and (d) FESEM images of CMF-800 (scale 50 µm).

The porosity can be tuned on the hierarchical structure by the chemical activation using KOH. The effect of KOH concentration on porosity was studied. In **Figure 6.2a–c**, the FESEM images of the carbon microfibres which were chemically activated are shown. The fibrous structure was retained after chemical activation indicating that the carbonized microfibres were thermally stable. Pores on the sphere surface were observed with an increase in KOH concentration. The chemically activated sample has been labeled as PCMF-x (porous carbon micro-fibres), where x is the KOH weight ratio respectively.

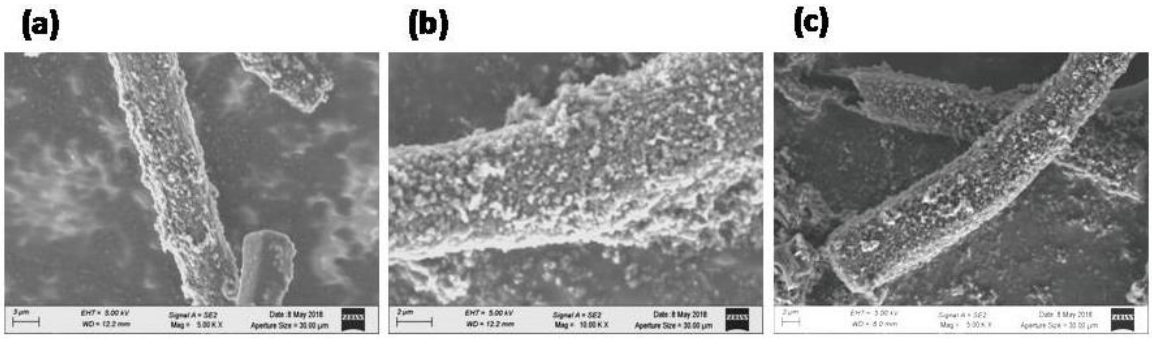

Figure 6.2 FESEM images of (a) PCMF-1, (b) PCMF-2, and (c) PCMF-3. (Scale 2 µm)

Samples MF-250 and CMF-800 were further characterized using TEM and SAED patterns as shown in **Figure 6.3**, to study the changes in morphology and crystallinity. The TEM analysis of both MF-250 (**Figure 6.3a & b**) and CMF-800 **(Figure 6.3 d & e**) revealed an interconnected network of polygonal nanograins [27, 28]. The average size of the grain was found to be ca. 50 nm. The grains are connected to form the fibre undulated with more such grains at irregular intervals in a 3D framework. The SEAD pattern of MF-250 (**Figure 6.3c**) was found to be typical of an amorphous material.

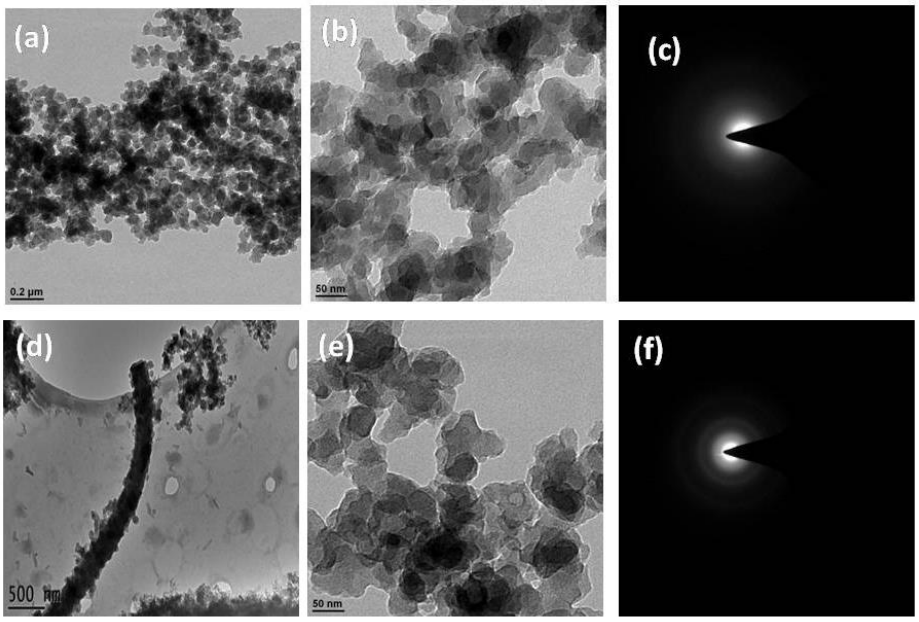

Figure 6.3 TEM images of MF-250 (a&b) and CMF-800 (d&e), SAED pattern of MF-250 (c) and CMF-800 (f).

However, careful observation for CMF-800 (**Figure 6.3f**) revealed three lean diffraction rings around a central bright zone. The SAED pattern evinced the presence of two phases, an ordered phase and a disordered phase, typical of a dual nature carbon [29].

XRD diffractograms revealed the amorphous structure in MF-250 with characteristic broad peaks at 2θ values of 15˚ and 22˚as presented in **Figure 6.4** [30]. The heat (carbonized) treated sample exhibited the presence of graphitic planes (002) at 23˚ and (100) at 43˚ evincing complete carbonization. The XRD results are in good coherence with the SAED pattern. These results indicated that prior to heat treatment the high lignocellulose content dominated the amorphous nature in the sample [31]. On treatment with Conc. KOH, the graphitic nature of the sample is reduced and the amorphous nature is pronounced as indicated by the broad peak at 23 ˚ in the diffractogram for PCMF-1 to PCMF-3 shown in **Figure 6.4**. The broadening of the peak increased with increased concentration of KOH. This could be attributed to the strong etching effect of KOH over carbon [31,32]. This etching can produce significant disorder over the graphitic phase thereby increasing the functionalities as well as the porous nature of the substrate.

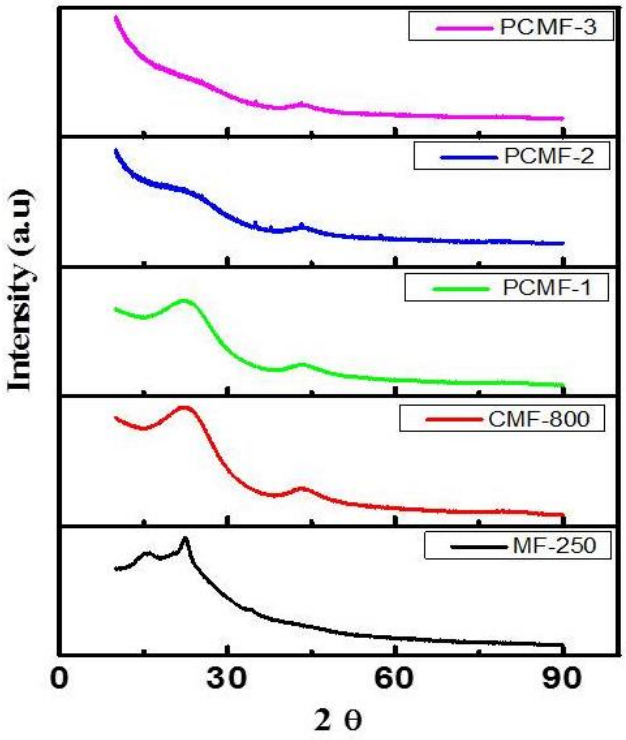

Figure 6.4 XRD patterns of porous carbon micro-fibres (PCMFs)

Nitrogen adsorption-desorption curves are used to study the pore characteristics of all the samples. For all of the PCMF samples, type IV isotherm exhibiting H3- type hysteresis loops indicate the presence of micro and mesoporous structure, as shown in **Figure 6.5a** [33]. Moreover, the presence of macropores is indicated as inferred from the sharp increase in the N_2 uptake from the isotherm at high relative pressures ($P/P_0 > 0.9$). For the samples treated with KOH, the adsorption studies revealed that surface area increases with an increase in KOH

concentrations (**Figure 6.6**). The carbonized fibres exhibited 26% of mesopores because of the space between interconnected polygonal nanograins. From **Figure 6.6**, the influence of chemical activation on the percentage of micro and mesopore was also studied. Increasing in the concentration of KOH increased the percentage of mesopores that are essential to achieve high specific capacitance.

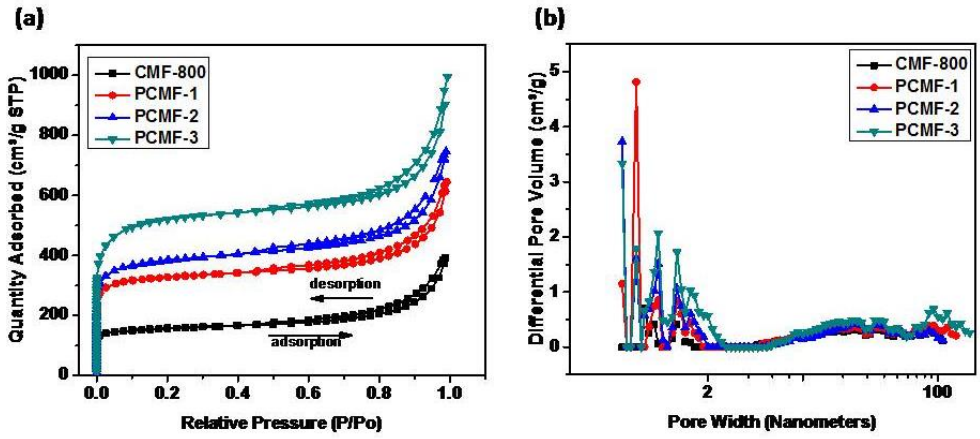

Figure 6.5 (a) Nitrogen adsorption-desorption isotherm and (b) pore size distribution.

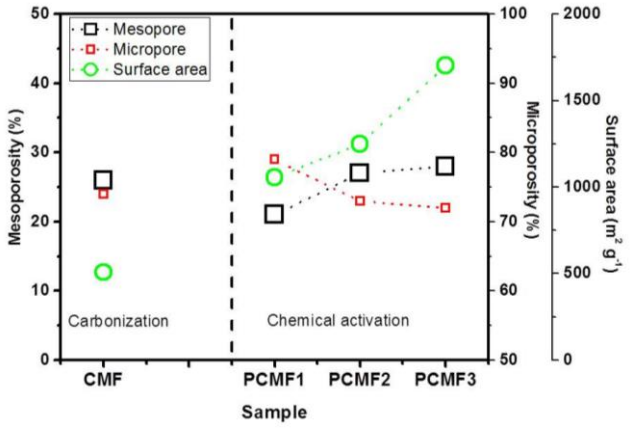

Figure 6.6 Influence of KOH concentration on surface area and percentage of micropores and mesopores.

The abundance of micropore and mesopore surface area is enhanced as a function of KOH concentration and is tabulated in **Table 6.1**. The PCMF-3 sample recorded the highest surface area of 1702 m^2 g^{-1} with 72% and 28% of micropore and mesopore, respectively. The optimization of mesopore and micropore is important for supercapacitor to achieve high specific capacitance and high capacity retention. The DFT method is used to analyze pore size distribution and is given in **Figure 6.5b**. From **Figure 6.5b**, large pore volume in the

microporous (about 1.7 nm) region and less pore volume in the mesoporous (about 2.3–10 nm) region was observed. The presence of micropores can effectively enhance the diffusion and mobility of electrolyte ions to interiors of electrode and increase the rate capability. While mesopores can accommodate more electrolytes which can effectively enhance the specific capacitance [33, 34].

Table 6.1 Pore parameters of porous carbon microfibres.

Sample	S_{BET} (m^2g^{-1})	S_{micro} ($m^2\ g^{-1}$)	S_{meso} ($m^2\ g^{-1}$)	V_{tot} ($cm^3\ g^{-1}$)	V_{micro} ($cm^3\ g^{-1}$)
CMF	508	377	131	0.61	0.18
PCMF-1	1056	843	213	0.99	0.41
PCMF-2	1250	924	326	1.15	0.44
PCMF-3	1702	1195	507	1.53	0.58

S_{BET}, specific surface area; S_{micro}, micropore surface area; S_{meso}, mesopore surface area; V_{tot}, total pore volume; V_{micro}, micropore volume. The values are calculated using the nitrogen adsorption/desorption isotherm data.

Electrochemical characterizations were performed in both aqueous and ionic liquid electrolytes to understand the influence of ion size on the pore size of the electrode. **Figure 6.7a** shows the cyclic voltammogram of the carbonized and chemically activated samples in 6 M KOH electrolyte. A characteristic rectangular voltammogram confirmed the EDLC capability of the samples. As anticipated from the surface area data the material with maximum surface area (PCMF-3; 1702 $m^2\ g^{-1}$) exhibited the highest capacitance. The order of capacitance followed the trend observed for the surface area. All the chemically activated samples showed higher capacitance than the only carbonized sample (CMF-800). Another significant observation was the marginal reduction in the stable potential window in the activated samples compared to CMF-800.

The effect of scan rate on the cycling as well as capacitive behavior of each sample is shown in **Figure 6.8**. The results were in line with the values reported by others. A comparative plot showing the effect of scan rate on each sample is given in **Figure 6.7b**. Typical to such

samples, a gradual drop in capacity was observed with increasing scan rate. However, a very high capacity of approximately 100 F g^{-1} at 200 mV s^{-1} was retained for PCMF-3.

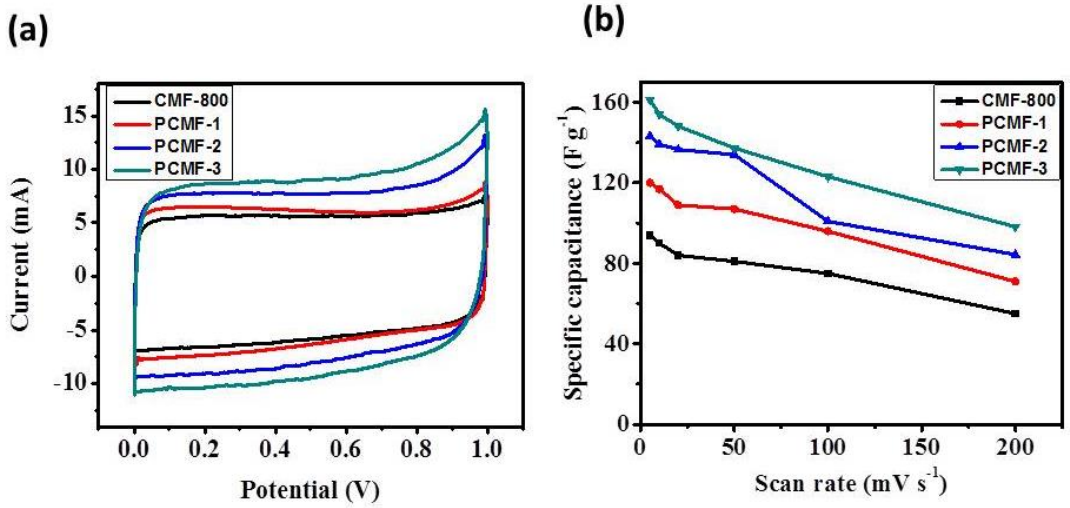

Figure 6.7 (a) CV curves of PCMF electrodes at the scan rate of 5 mV s^{-1} in 6 M KOH electrolyte, (b) specific capacitance of PCMFs at various scan rates.

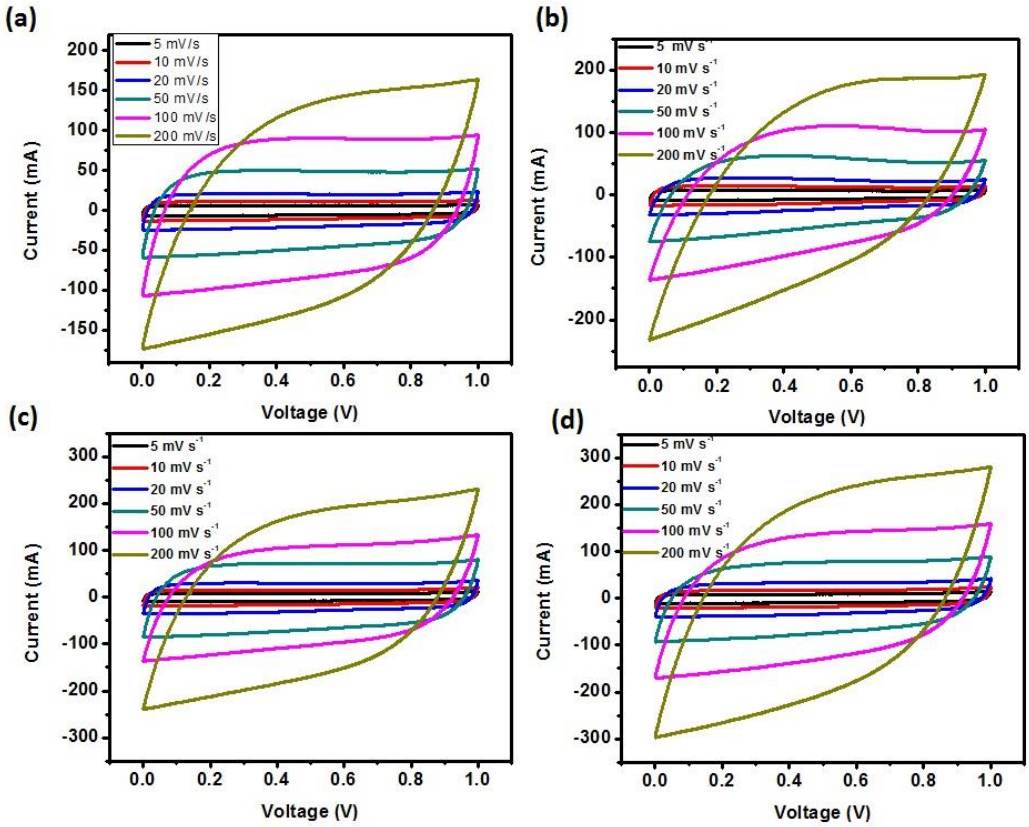

Figure 6.8. Cyclic voltammogram of (a) CMF-800, (b) PCMF-1, (c) PCMF-3 and (d) PCMF-3 samples in 6 M KOH at different scan rates.

Galvanostatic charge/discharge (GCD) studies of these PCMF electrodes in a symmetric cell further confirmed the high capacitive behavior. The charging and discharge was done in a potential window that is the same as that of the CV test as shown in **Figure 6.9**. The PCMFs electrode had nearly linear and symmetrical GCD curves, clearly indicating the superior electric double layer capacitance characteristic and electrochemical reversibility, as well as the fast charge/discharge behavior as shown in **Figure 6.9a**.

However, the chemically activated samples had an extended discharge time than the carbonized sample, indicating that chemical activation presents a much higher capacitance. The GCD curves of PCMF-3 electrode is shown in **Figure 6.9b**. The individual GCD curves of other PCMF electrodes were shown in **Figure 6.10**. The curves are almost linear and symmetrical showing perfect capacitive behavior. At a current density of 5 A g^{-1}, there's a negligible drop in cell voltage which can be ascribed to the presence of micropores on the one dimensional structure permitting quick electron and ion transfers, which is in agreement with the CV tests. The specific capacitance of the PMCFs has been measured at various current densities and is shown in **Figure 6.9c**.

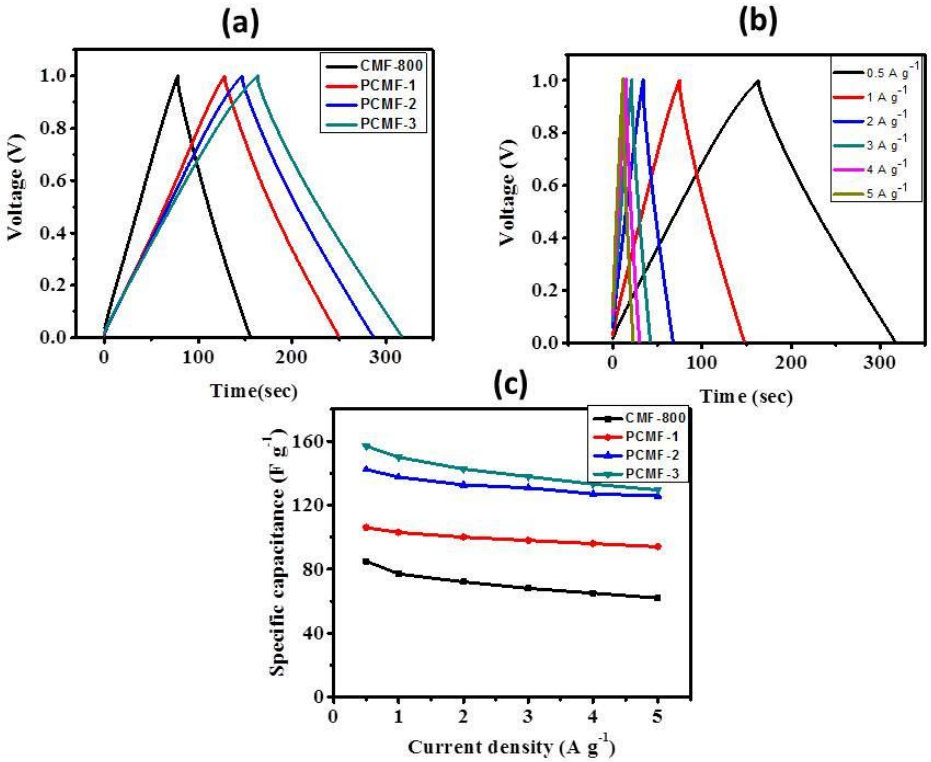

Figure 6.9(a) GCD curves of PCMF electrodes at a current density of 0.5 A g^{-1} in 6 M KOH electrolyte, (b) GCD curves of PCMF-3 at different current densities, (c) specific capacitance of PCMFs at different specific currents.

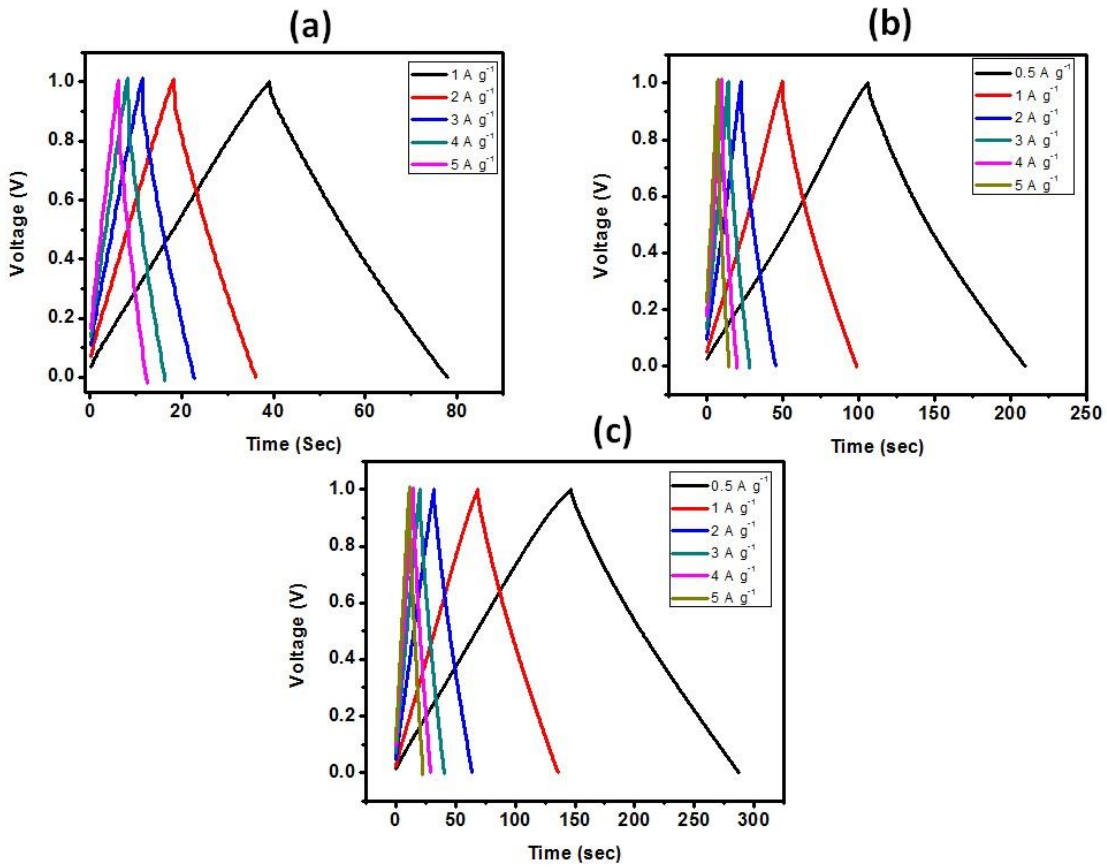

Figure 6.10 GCD curves of (a) CMF-800, (b) PCMF-1, and (c) PCMF-3 samples in 6 M KOH at different current densities.

Applications of aqueous electrolyte systems are restricted in terms of energy density as compared to batteries because of their narrow working voltage window (1V). The energy density of the system can be improved by the change of an aqueous electrolyte to an ionic liquid (IL) electrolyte, which has an operating potential of more than 3.5 V. The choice of IL as 1-butly 3-methyl imidazolium bistrifluorosulfonylimide (BmIm-TFSI) was based on its potential window range from 0 to 3.5 V. Also, selection of bulky anion in the electrolyte was to understand the influence of electrolyte ion size on the pore size of the electrode.

The cyclic voltammogram in IL electrolyte exhibited typical rectangular profiles for all the samples and are shown in **Figure 6.11**. However, the chemically modified electrode (PCMFs) showed a pronounced increase in pore size evincing increased capacitance. As expected, with increment in surface area the specific capacitance also increased. However, the increase in capacitance value between PCMF-2 and PCMF-3 was significantly high.

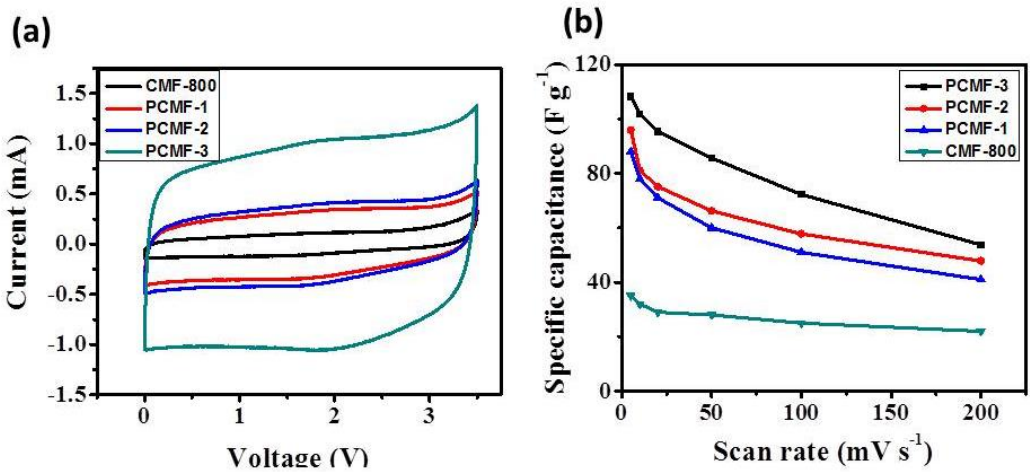

Figure 6.11(a) CV curves of PCMF electrodes at the scan rate of 5 mV s^{-1} in IL electrolyte, (b) specific capacitance of PCMFs at various scan rates

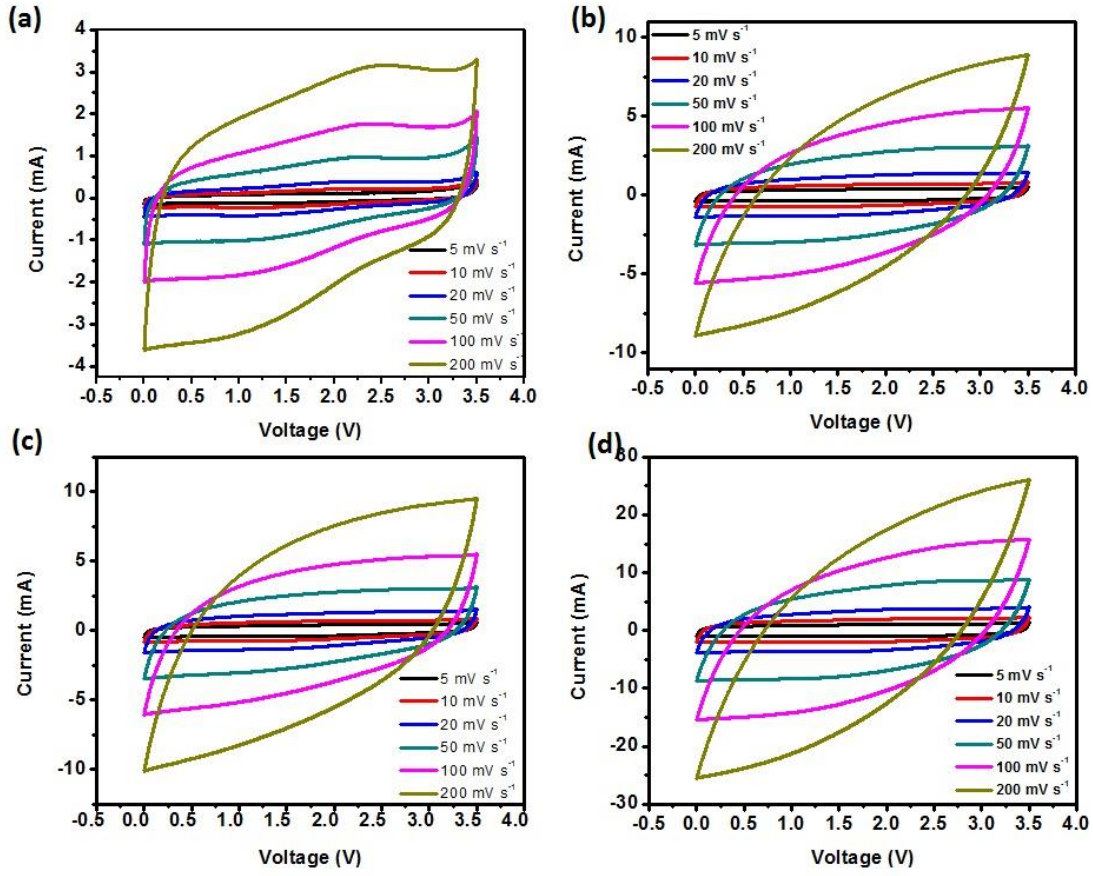

Figure 6.12 Cyclic voltammogram of (a) CMF-800, (b) PCMF-1, (c) PCMF-2, and (d) PCMF-3 samples in ionic liquid (BmIm-TFSI) at different scan rates.

The effect of scan rate on the cycling as well as capacitive behavior of each sample is provided in **Figure 6.12**. At higher scan rates the voltammogram reflected a psuedo capacitance behaviour. Also, one significant attribute of the voltammogram in

IL was its lower current density compared to the aqueous counterpart, which can be attributed to the lower conductivity of IL especially with TFSI anions.

The GCD was conducted at various current densities of 0.5 - 5 A g^{-1} to evaluate the retention capacity, and is shown in **Figure 6.13**. The electrodes exhibited a linear voltage response with respect to time while charging and discharging. The specific capacitance (**Figure 6.13b**) of PCMF-3 was calculated to be 76 F g^{-1} at 0.5 A g^{-1} and the retention ratio was about 78% for a scan rate of 5 A g^{-1} which are listed in **Table 6.2**. The GCD curves for the other samples were shown in **Figure 6.14**. From **Figure. 6.13c**, it was observed that the specific capacitance of PCMF-3 to be higher than other samples and agrees well with CV results. The specific capacitance value of tamarind seed coat derived HPC is comparable with the other biomass derived carbon electrodes as can be seen in **Table 6.3**.

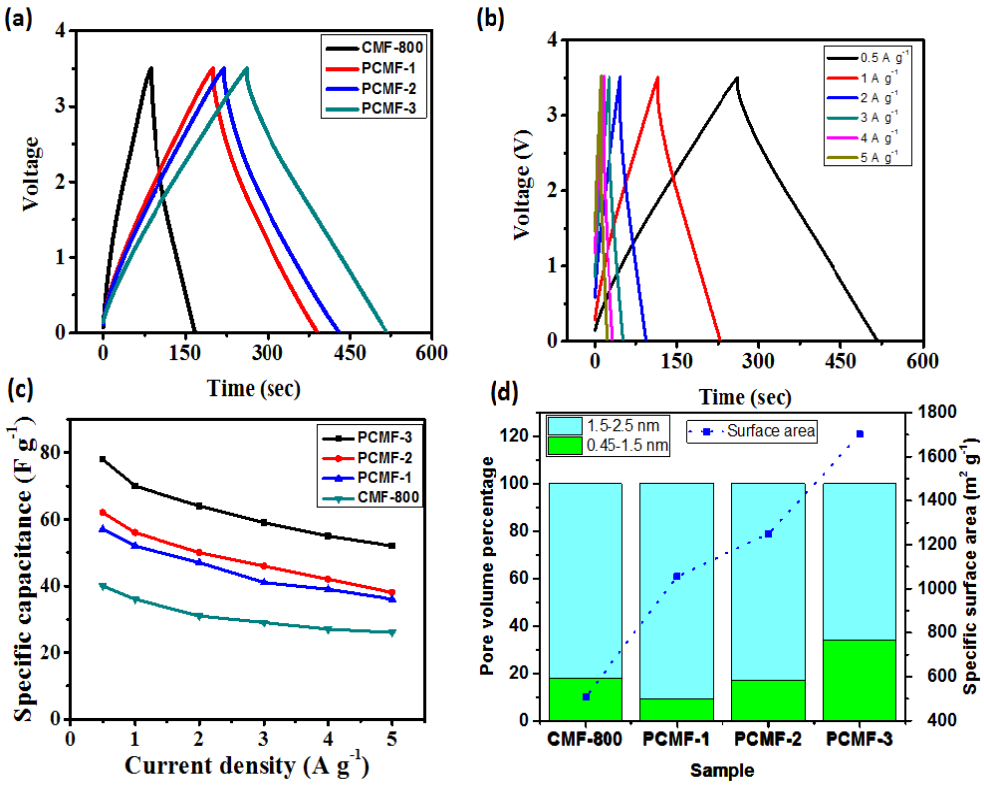

Figure 6.13 (a) GCD curves of PCMF electrodes at a current density of 0.5 A g^{-1} in BmIm-TFSI electrolyte, (b) GCD curves of PCMF-3 at various current densities, (c) specific capacitance of PCMFs at different specific current, and (d) percentage of micropore volume vs samples.

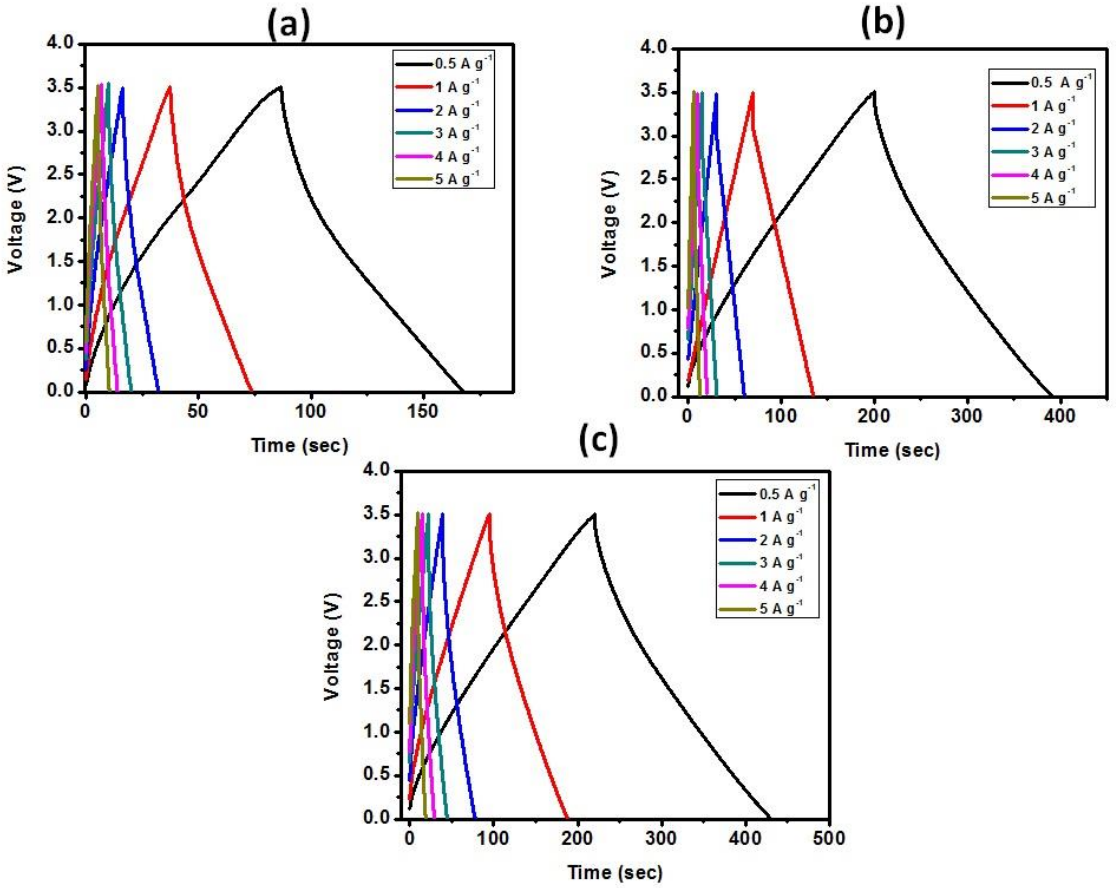

Figure 6.14 GCD curves of (a) CMF-800, (b) PCMF-1, and (c) PCMF-3 samples in ionic liquid (BmIm-TFSI) at different current densities.

Table 6.2 Specific capacitance of PCMFs under different current densities.

Sample	Specific capacitance (F g^{-1})			
	6 M KOH		BMIM-TFSI	
	0.5 A g^{-1}	5.0 A g^{-1}	0.5 A g^{-1}	5.0 A g^{-1}
CMF	82	68	40	26
PCMF-1	124	94	57	36
PCMF-2	142	125	62	38
PCMF-3	157	129	78	52

Considering the capacitance of PCMF-3 in aqueous electrolyte, it was evident that the surface area was the only parameter controlling the specific capacitance. However, in the case of IL based systems, the anomalous behavior observed between PCMF-2 and PCMF-3 could be reasoned based on the ionic size of the electrolyte. For instance, in the case of the BmIm-TFSI, the ionic size was calculated to be around 0.74

nm. The huge ionic size requires larger pores for higher capacitance. The pores with size in the range of 0.5 - 1.5 nm does not provide free access for the ions into the interior portion of the electrode. A pore size of more than 1.5 nm is essential for free access of the ionic liquid. PCMF-3 which has 34% of its micropores in the range of 1.5-2.5 nm becomes highly suitable for ionic liquid electrolyte. The other samples exhibit lower capacitance not only because of lower surface area but also due to the lack of sufficient pores with the size in the range of 1.5 - 2.5 nm.

Table 6.3 Comparison of specific capacitance of the HPC derived from tamarind seed coat with other biomass derived carbon.

Raw material	Surface area ($m^2\ g^{-1}$)	Specific capacitance ($F\ g^{-1}$)	Electrolyte/ Cell system	Current density ($A\ g^{-1}$)	Reference
Coconut shell+ sewage sludge	3003	62	6 M KOH/ 2electrode	0.5	[17]
Corncob	1210	120	6 M KOH	1	[36]
Bagasse	1892	142	6 M KOH/ 2 electrode	0.5	[1]
Bamboo-industrial waste	1472	148	6 M KOH/ 2 electrode	0.1	[16]
Potato starch	456	245	1 M KOH/ 3 electrode	1	[38]
Carrageenan	2502	261	6 M KOH/ 3 electrode	0.5	[31]
Tannin-polyphenol	1006	~196	1 M H_2SO_4/ 3 electrode	0.1	[18]
Tamarind seed coat	**1702**	**157**	**6 M KOH/ 2 electrode**	**0.5**	**Present Study**

The cyclic stability is one of the key factors for the supercapacitor device application. The cyclic stability of PCMF-3 electrode has been performed in both 6 M KOH and BmIm-TFSI electrolyte over up to 1000 cycles. After 1000 cycles of consecutive charge-discharge at 2 A g^{-1} (Figure 6.15a), the specific capacitance of PCMF-3 electrode was maintained at 136 F g^{-1} for the 6 M KOH and 59 F g^{-1} for the BmIm-TFSI, which corresponds to 96% and 93% of its initial value. The PCMF-3 electrode shows good cyclic stability in both the electrolytes.

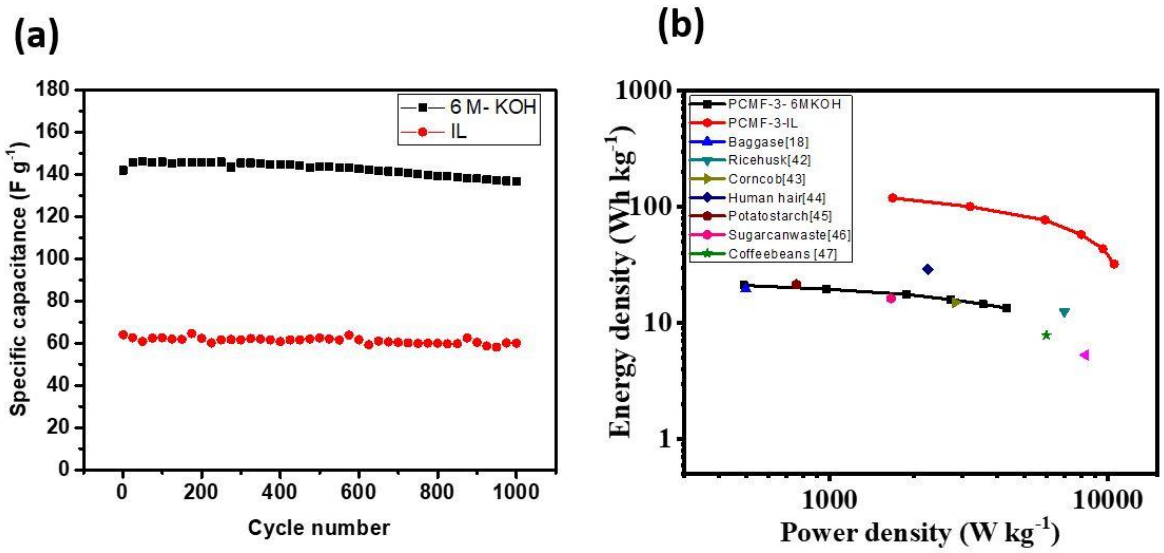

Figure 6.15 (a) Long term cyclic stability test of PCMF-3 electrode at a current density of 2 A g^{-1} in both 6 M KOH and BmIm-TFSI, (b) Power characteristics of PCMF-3 in comparison with other report samples.

The PCMF based symmetric supercapacitors were calculated for its energy density and power density. The calculated values were plotted in comparison with other notable reported biomass derived carbons and are shown in **Figure 6.15b**. In aqueous system, the energy density of PCMFs ranged from 10.7 Wh kg^{-1} to 21.1 Wh kg^{-1} at 0.5 A g^{-1}. PCMF-3 electrode still retains an energy density of 13.4 Wh kg^{-1} with a high-power density of 4.3 W kg^{-1}. The achieved energy density values are similar to the reported values for HPC derived from bagasse[1], rice husk [35],corn cob [36], human hair [37], potato starch [38], sugarcane waste [39], coffee ground [40].The maximum energy density was found for PCMF-3 electrode in BmIm-TFSI is 119.2 Wh kg^{-1} at a power density of 1680 W kg^{-1}, much greater than 6 M KOH (21.1 W h kg^{-1} at 491 W kg^{-1}). These results show that PCMFs derived from tamarind seed coat are favorable material for a high-performance supercapacitor with large power and energy density.

The superior properties can of PCMFs be attributed to the material structure and composition increasing the mechanical stability as well as electronic conductivity

through their fibrous pathway. The 3-dimensional fibrous like structure seen from electron microscopic results show interconnected polygonal particles which can provide low resistance pathway for the electron transfer. Further, the void space between polygonal particles allows more volume for the electrolyte which can lower the ion transfer resistance. This combination of hierarchical porous structure with partial graphitic nature, identified by XRD, in corroboration with the micro-mesopores is favorable for a supercapacitor electrode application. The high rate capability makes this material suitable for high power supercapacitor applications.

6.3 Conclusions

The synthesis of hierarchical porous carbon micro-fibres was reported. Raw materials chosen for HPC are easily available, and the process for making is amenable for large scale production. The criteria for choosing these materials are their higher polyphenol content. Tamarind seed coats are used as the carbon precursor which forms the natural template to facilitate the formation of well-structured carbon micro-fibres, without any expensive surfactants. The effect of chemical activating agent concentration on specific surface area and porosity was carefully studied. The highest surface area was obtained for the sample which is treated with a concentration of 3 (KOH) at 800 ˚C. The synthesized PCMF-3 possesses superior capacitance in both 6 M KOH and BmIm-TFSI electrolytes with excellent cyclic stability. High specific capacitances of 157 F g^{-1} in the 6 M KOH and 76 F g^{-1} in the BmIm-TSFI at a current density of 0.5 A g^{-1} are achieved. With the large voltage offered by the ionic liquid electrolyte, the PCMF-3 electrode could store/release the maximum energy of 119.2 Wh kg^{-1} at a power density of 1.68 kW kg^{-1}. These findings suggest that the pore size between 1.5-2.5 nm is essential to obtain high specific capacitance in an ionic liquid electrolyte which has bulky anion like TFSI. The well-developed porous structure on the carbon microfibres was found to be the key factor for enhancement in the supercapacitor performance. Mere increase in micro-porosity would not contribute to the increase in capacitance and its retention. The work reported here provides an attractive route for the production of microstructural carbon material through the transformation of low cost, renewable, and abundantly available biomass for supercapacitor electrode application.

References

[1] Hao P, Zhao Z, Tian J, Li H, Sang Y, Yu G, Cai H, Liu H, Wong C. P, and Umar A, *Nanoscale*, **2014**, *6*, 12120.

[2] Balach J, Tamborini L, Sapag K, Acevedo D. F, and Barbero C. A, *Colloids Surfaces A Physicochem. Eng. Asp.*, **2012**, *415*, 343.

[3] Xu F, Cai R, Zeng Q, Zou C, Wu D, Li F, Lu X, Liang Y, and Fu R, *J. Mater. Chem.*, **2011**, *21*, 1970.

[4] Yang C. M, Weidenthaler, C, Spliethoff B, Mayanna M, and Schüth F, *Chem. Mater.*, **2005**, *17*, 355.

[5] Zhang B, Wu Y, Meng F, Xu T, Zhu J, and Sun M, *Procedia Eng.*, **2012**, *27*, 762.

[6] Luo H. M, Yang Y. F, Sun Y. X, Zhao X, and Zhang J. Q,*J Solid State Electrochem*, **2015**, *19*, 1491.

[7] Shi J, Li W and Li D,*Colloids Surfaces A Physicochem. Eng. Asp.*, **2015**, 485, 11.

[8] Dutta S, Huang S. Y, Chen C, Hou C.H, and Wu K. C. W, *ACS Sustainable Chem. Eng.* **2016**, *4*, 1885.

[9] Liu Y, Shi Z, Gao Y, An W, Cao Z, and Liu J, *ACS Appl. Mater. Interfaces*, **2016**, 8, 28283.

[10] Liang C, Bao J, Li C, Huang H, Chen C, Lou Y, Lu H, Lin H, Shi Z, and Feng V, *Microporous Mesoporous Mater.*, **2017**, *251*, 77.

[11] You X. L, Liu L. J, Zhang M. Y, Walle M. D, Li Y, and Liu Y. N, *Mater. Lett.*, **2018**, *217*, 167.

[12] Chen L, Ji T, Mu L, Shi Y, Wang H, and Zhu J,*J. Environ. Manage.*, **2017**, *196*, 168.

[13] Chen J, Zhou X, Mei C, Xu J, Zhou S, and Wong C. P, *J. Power Sources*, **2017**, *342*, 48.

[14] Chen L, Ji T, Mu L, and Zhu J, *Carbon*, **2017**, *111*, 839.

[15] Dutta S, Bhaumik A, and Wu K. C. W, *Energy Environ. Sci.*, **2014**, *7*, 3574.

[16] Tian W, Gao Q, Tan Y, Yang K, Zhu L, Yang C, and Zhang H, *J. Mater. Chem. A*, **2015**, *3*, 5656.

[17] Peng L, Liang Y, Dong H, Hu H, Zhao X, Cai Y, Xiao Y, Liu Y, and Zheng M, *J. Power Sources*, **2018**, *377*, 151.

[18] Sanchez A. S, Izquierdo M. T, Ghanbaja J, Medjahdi G, Mathieu S, Celzard A, and Fierro V, *J. Power Sources*, **2017**, *344*, 15.

[19] Mayes R. T, Tsouris C, Kiggans Jr J. O, Mahurin S. M, DePaoli D. W, and Dai S, *J. Mater. Chem.*, **2010**, *20*, 8674.

[20] Szczurek A, Fierro V, Pizzi A, Stauber M, and Celzard A, *Carbon*, **2013**, *65*, 214.

[21] Szczurek A, Fierro V, Pizzi A, and Celzard A.*Carbon*, **2014**, *74*, 352.

[22] Bai C. X, Shen F, and Qi X. H, *Chinese Chem. Lett.*, **2017**, *28*, 960.

[23] Saha D, Warren K. E, and Naskar A. K, *Carbon*, **2014**, *71*, 47.

[24] Ramesh T, Rajalakshmi N, and Dhathathreyan K. S, *J. Energy Storage*, **2015**, *4*, 89.

[25] Prabhu K. H and Teli M. D, *J. Saudi Chem. Soc.*, **2014**, *18*, 864.

[26] Kang S, Li X, Fan J, and Chang J, *Bioresour. Technol.*, **2008**, *99*, 3424.

[27] Falco C, Baccile N, and Titirici M. M, *Green Chem.*, **2011**, *13*, 3273.

[28] Kang S, Li X, Fan J,, and Chan J, *Ind. Eng. Chem. Res.*, **2012**, *51*, 9023.

[29] Cheng K. K, Hsu T. C, and Kao L. H, *J. Mater. Sci.*, **2011**, *46*, 3914.

[30] Guo S, Dong X, Wu T, Shi F, and Zhu C, *J. Anal. Appl. Pyrolysis*, **2015**, *116*, 1.

[31] Fan Y, Yang X, Zhu B, Liu P. F, and Lu H. T, *J. Power Sources*, **2014**, *268*, 584.

[32] Zhang M, He C, Liu E, Zhu S, Shi C, Li J, Li Q, and Zhao N, *J. Phys. Chem. C*, **2015**, *119*, 21810.

[33] Dong Y, Lin H, Zhou D, Niu H, Jin Q, and Qu F, *Electrochim. Acta,*, **2015**, *159*, 116.

[34] Cai J, Niu H, Li Z, Du Y, Cizek P, Xie Z, Xiong H, and Lin T, *ACS Appl. Mater. Interfaces*, **2015**, *7*, 14946.

[35] Ganesan A, Mukherjee R, Raj J, and Shaijumon M. M, *J. Porous Mater.*, **2014**, *21*, 839.

[36] Qu W. H, Xu Y. Y, Lu A. H, Zhang X. Q, Li, and W.C, *Bioresour. Technol.*, **2015**, *189*, 285.

[37] Qian W, SunF, Xu Y, Qiu L, Liu C, Wang S, and Yan F, *Energy Environ. Sci.*, **2013**, *7*, 379.

[38] Ruibin Q, Zhongai H, Yuying Y, Zhimin L, Ning A, Xiaoying R, Haixiong H, and Hongying W, *Electrochim. Acta*, **2015**, *167*, 303.

[39] Jain A and Tripathik S. K, *J. Energy Storage*, **2015**, *4*, 121.

[40] Rufford T. E, Hulicova-jurcakova D, Zhu Z, and Lu G. Q, *Electrochem. Comm.*, **2008**, *10*, 1594.

CHAPTER 7

DYNAMIC ELECTROCHEMICAL IMPEDANCE SPECTROSCOPY AS A RAPID SCREENING TOOL FOR SUPERCAPACITOR ELECTRODE MATERIALS

7.1 Introduction

Design and development of advanced materials for supercapacitor is crucial to achieve superior electrochemical performance. Concurrently, developments in characterization methods to evaluate the performance of such material precisely under limited time boundary would synergistically hasten the material development. Various porous carbon materials are used as electrode materials in supercapacitors, specifically called as an electrochemical double layer capacitor [1-2]. Numerous strategies have been employed to improve the electrochemical performance by modifying structure and increasing the surface area of the electrode materials [3-8].

Novel carbon materials derived from numerous precursors have exhibited superior gravimetric capacitance values in the range of 141-195 F g^{-1} due to its structural and textural properties. They also present excellent retention capacity and high current density. Generally, the capacitive behavior of newly developed materials is evaluated using standard electrochemical techniques such as cyclic voltammetry (CV), galvanostatic charge-discharge (GCD), and electrochemical impedance spectroscopy (EIS) [9-12]. It was well established that the charge accumulation on the electrode/electrolyte interface mainly depends on the surface area, pore size distribution, and electrical conductivity. Many results have suggested that the improved capacitance performance can be achieved by increasing the surface area with a nominal decrease in electrical conductivity. However, the rate capability has been a key factor which mainly depends on the compatibility of the electrolyte ion size with pore size distribution [13].

The complexity between surface area and pore size distribution has been fairly understood in terms of achieving high capacitance and capacity retention. In particular, to understand the fundamental relation between textural property (surface area and pore size distribution) and electrochemical performance (high capacitance and retention), a series of CV and GCD experiments is required. But, the process involved takes a lot of experimentation and analysis time which impedes the optimization of new novel materials. A standalone characterization and diagnosis tool has been a long time requirement to effectively evaluate the electrode material with least waste of time and effort.

Recently, numerous researchers have utilized EIS technique to understand the charge storage mechanism of the supercapacitor device by both experimental and theoretical approaches [14-18]. Khang et al. conducted EIS study on a cell fabricated using aqueous and

organic electrolyte solution at different potentials [19]. They reported that the charge transfer resistance (R_{ct}) decreased and double layer capacitance (C_{dl}) increased with increasing applied potential. Also, the change in R_{ct} and C_{dl} was found to be more prominent in the organic electrolyte compared to the aqueous electrolyte because of its low ionic mobility [19]. Zhang et al. demonstrated that the impedance of a 3, 000 F commercial supercapacitor cell varied the state-of-charge and temperature [20]. As compared with state-of-charge, the change in temperature showed a significant change in impedance of a cell, owing to the temperature dependent ionic conductivity of the electrolyte [20]. However, the aforementioned reports proved that the impedance of the cell majorly varied either with the state-of-charge or temperature. To date, no report has provided the dependency of electrode material property majorly influencing the capacitive performance of the supercapacitor. It is imperative to recognize the dependency of the textural properties of the electrode materials on the electrochemical performance for betterment of materials development and EIS would be the best method to achieve it.

For the first time, we introduced DEIS technique to evaluate the electrochemical performance of newly developed carbon materials. The electrode materials were subjected to DEIS measurement within acceptable potential limits of the electrolyte. The CV and GCD experiments were also performed in order to validate the use of DEIS in supercapacitor study. Previously, our group and few other groups have used the tamarind seed as the precursor material due to its proven ability in various energy applications [21-23]. In the present work, the seed kernel was specifically opted because of its innate chemical properties [24-25]. The seed kernel contains glucose, xylose, and galactose which is readily soluble in water. The aerogel was formed by dissolving kernel powder in a mixture of KOH and Urea followed by gelation and ambient drying process. The aerogel was carbonized at various temperatures to optimize surface area and pore size distribution. Dependency of textural properties on electrochemical performance is studied extensively using the DEIS.

7.2 Results and Discussion

It has been understood that the selection of material for supercapacitor electrodes, based primarily on surface area may not yield the expected capacitance and capacity retention. Proven over the years, material with graded porosity has shown superior capacitive behavior. Carbon aerogels, in the recent years have satisfactorily exhibited both high surface area and graded hierarchical porosity [26-29]. The synthesis process of biomass derived carbon aerogel was shown in **Figure 3.4**. Biomass based aerogel is prepared by treatment of kernel from tamarind

seeds with aqueous NaOH and 0.5 M Urea. This was followed with a carbonization process. The effect of temperature on the carbonization as well as order of porosity was investigated at 500 °C, 600 °C, 700 °C, and 800 °C. The surface morphology of the prepared samples is studied using FESEM and the results are presented in **Figure7.1**. The sample carbonized at 500 °C showed poor porosity with irregular pore and texture. With increase in carbonization temperature to 600 °C, the morphology portrayed a highly inter-connected, matured, and randomly shaped porous surface. Further increase in carbonization temperature to 700 °C, the morphology developed into a highly porous and volumous with uniform macropores (approximately ca. 0.5 μm) this could be attributed to the strong reaction between NaOH and the precursor at an elevated temperature.

Increase in carbonization temperature to 800 °C, exhibited a collapse in the pore structure leading to widening of macropores. The morphological studies clearly indicated the crucial role played by carbonization temperature in improving and optimizing the porosity of the carbon aerogels. The nitrogen adsorption-desorption experiments have been carried out to investigate in detail of the textural properties of the samples.

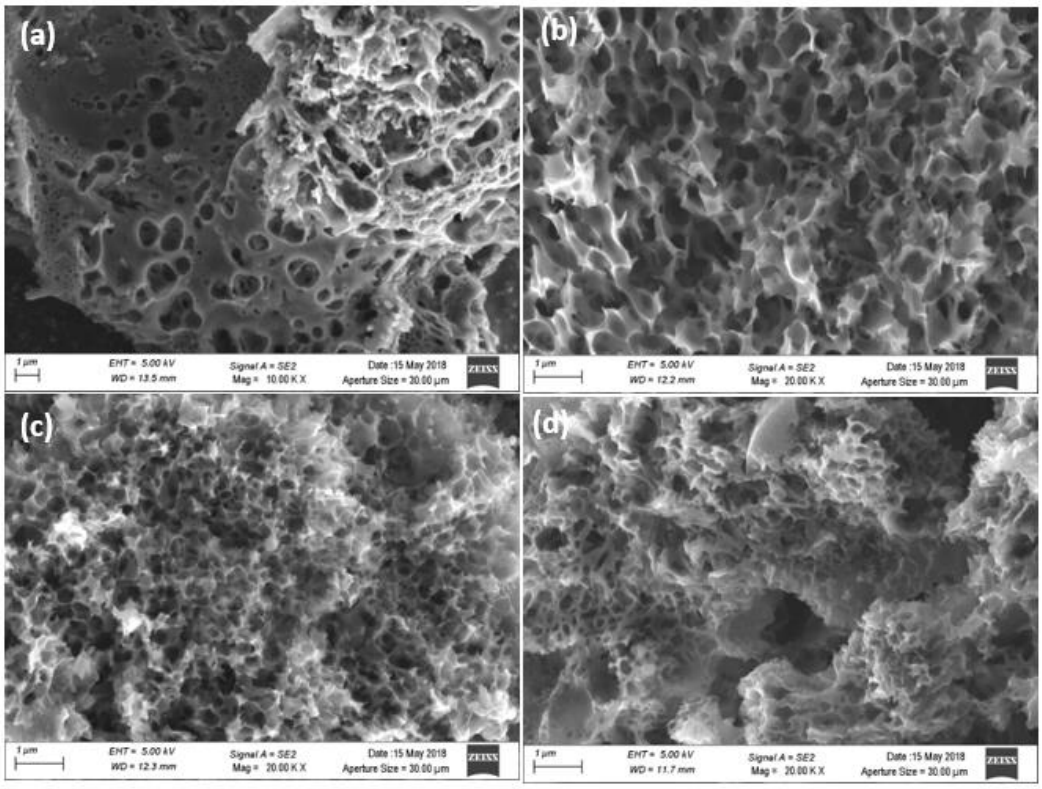

Figure 7.1 FESEM images of (a) CAG-500, (b) CAG-600, (c) CAG-700, and (d) CAG-800. (Scale 1 μm)

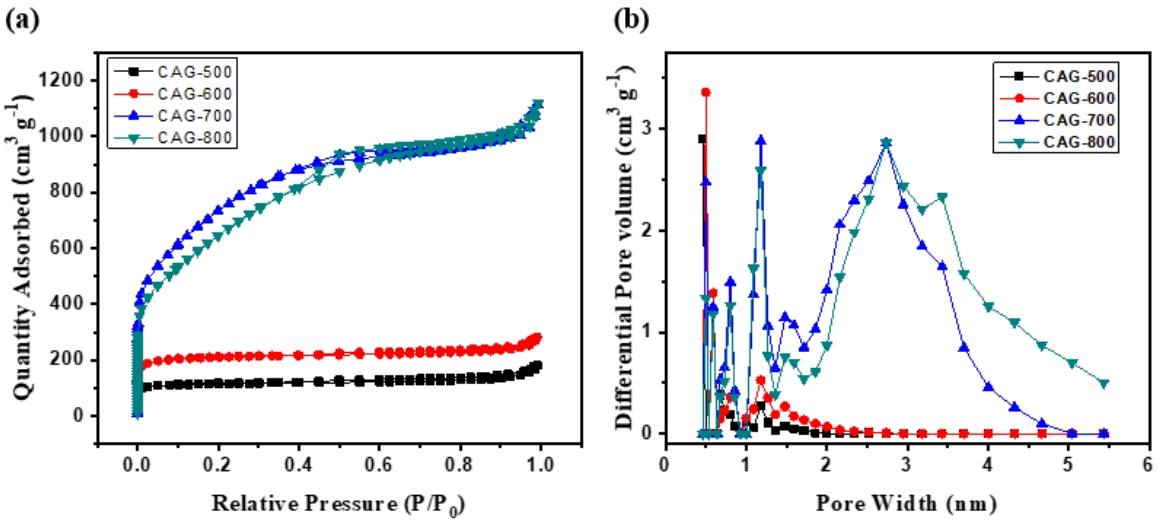

Figure 7.2 (a) Nitrogen adsorption-desorption isotherms and (b) pore size distribution of all the carbon aerogel samples.

The recorded adsorption isotherms for all the samples are presented in **Figure7.2a**. The adsorption isotherm exhibited a Type-I and Type-IV with H4 for carbon aerogel material indicating the presence of micropores and mesopores [9, 30]. The samples carbonized below 600 °C predominantly exhibited a Type-I isotherm indicating the existence of micropores [9]. Further, increase in carbonization temperature above 700 °C, the isotherm deviated from Type-I, and increase in adsorption was found in the relative pressure range of 0.1-0.6 indicating the presence of mesopores [30].

The pore size distribution curves for all the carbon aerogel samples are shown in **Figure 7.2b**. The pore size of the samples carbonized at 500 °C and 600 °C were determined to be below 2 nm, classified in the micropore range indicating large volume. The pore size distribution of the sample carbonized at 700 °C was determined to be between 2-5 nm. Further increase in temperature to 800 °C resulted in the broadening of pore size distribution in the range of 2-8 nm due to destruction of pore walls at high temperature, which can be corroborated with the FESEM morphological results.

The effect of temperature on the growth of pores can be justified based on the formation and decomposition of Na_2CO_3 initiating and propagating the growth of mesopores. At lower temperatures, the decomposition was not profound while at 800 °C, the high temperature creates undue pore wall thinning leading to collapse of the pore structure. Adsorption measurements

indicate the presence of micropores and mesopores underneath the macropores, as revealed in FESEM images. The availability of micropores can be considered as a valuable attribute required for the retention of electrolyte and it can potentially enhance the ion diffusion pathways. The CAG-700 sample was found to possess the highest pore volume and the greatest specific surface area with 1.72 $cm^3\ g^{-1}$ and 2645 $m^2\ g^{-1}$, respectively. The textural properties of the carbon aerogel samples are summarized in **Table 7.1**.

Table 7.1 Textural properties of the prepared carbon aerogels.

Carbon aerogel	S_{total}[a] ($m^2\ g^{-1}$)	S_{micro}[b] ($m^2\ g^{-1}$)	S_{meso}[c] ($m^2\ g^{-1}$)	V_{total}[d] ($cm^3\ g^{-1}$)	V_{micro}[e] ($cm^3\ g^{-1}$)
CAG-500	371	303	68 (18%)	0.27	0.14
CAG-600	680	564	116 (17%)	0.43	0.27
CAG-700	2645	1289	1356 (51%)	1.72	0.61
CAG-800	2346	981	1365 (58%)	1.72	0.46

a) S_{total} - Total Surface area ($m^2\ g^{-1}$)
b) S_{micro} - Micropore surface area ($m^2\ g^{-1}$)
c) S_{meso} - Mesopore surface ($m^2\ g^{-1}$)
d) V_{total} - Total pore volume ($cm^3\ g^{-1}$)
e) V_{micro} - Micropore volume ($cm^3\ g^{-1}$)

Physicochemical properties of the materials alone cannot be sufficient to understand the electrode performance. A series of electrochemical experiments are necessary to evaluate the performance parameters of the electrode materials, such as specific capacitance and rate capability. In addition to the conventional electrochemical measurements, an advanced technique of dynamic electrochemical impedance spectroscopy (DEIS) was used in this study.

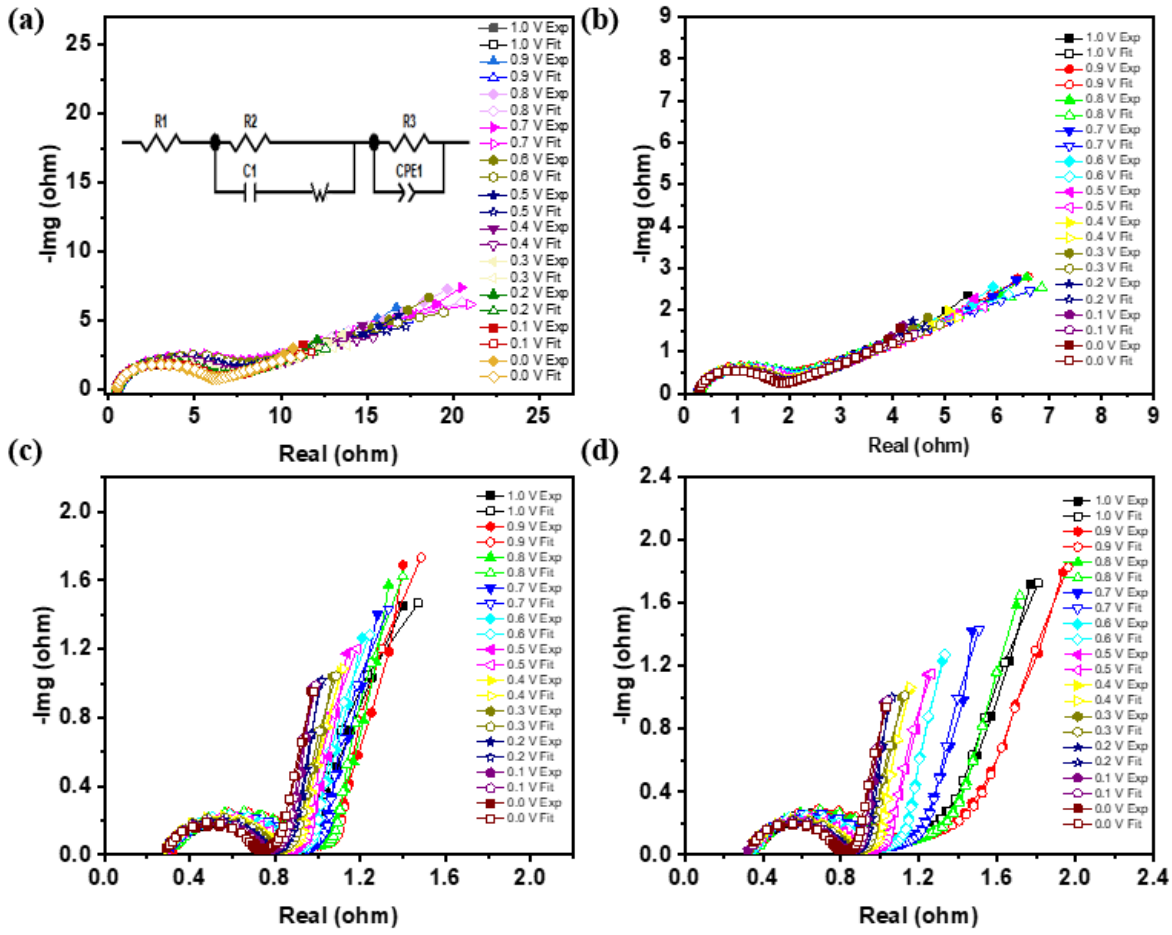

Figure 7.3 Nyquist plot of all samples during reverse sweep of DEIS study. (a) CAG-500, (b) CAG-600, (c) CAG-700, and (d) CAG-800.

Representative Nyquist plots of the carbon aerogel electrodes obtained using DEIS, under discharging potential condition, are shown in **Figure7.3**. The Nyquist plots obtained for the carbon aerogel electrodes are similar to a typical porous carbon electrode. The Nyquist plot describes the intrinsic property of electrode materials in three major segments viz., high, mid and low frequency regions. The high frequency region describes combination of resistance (R_s) offered by electrolyte, separator and current collector. The mid frequency region semicircle gives details of charge transfer and double layer capacitance i.e. rate capability of the cell. The low frequency region can be attributed to diffusion of ions on the electrode surface indicating the capacitive behavior. The values of R_s for the four systems under test were found to be almost same, which confirms that measurements were made under similar electrolytic condition (6M KOH), as R_s was predominantly associated with the electrolyte behavior. The insignificant variation in R_s can be associated with change in applied potential due to small difference in the migratory ions. For the samples CAG-500 and CAG-600, the low frequency capacitive tail with slope tending towards 30° indicates a bad capacitive behavior.

Whereas, CAG-700 and CAG-800, the capacitive tail with slope value above 80˚, nearly parallel to imaginary axis evinces the relatively superior capacitive behavior in these samples. Finally, the mid frequency charge transfer resistance of CAG-500 and CAG-600 were found to be higher compared to CAG-700 and CAG-800.

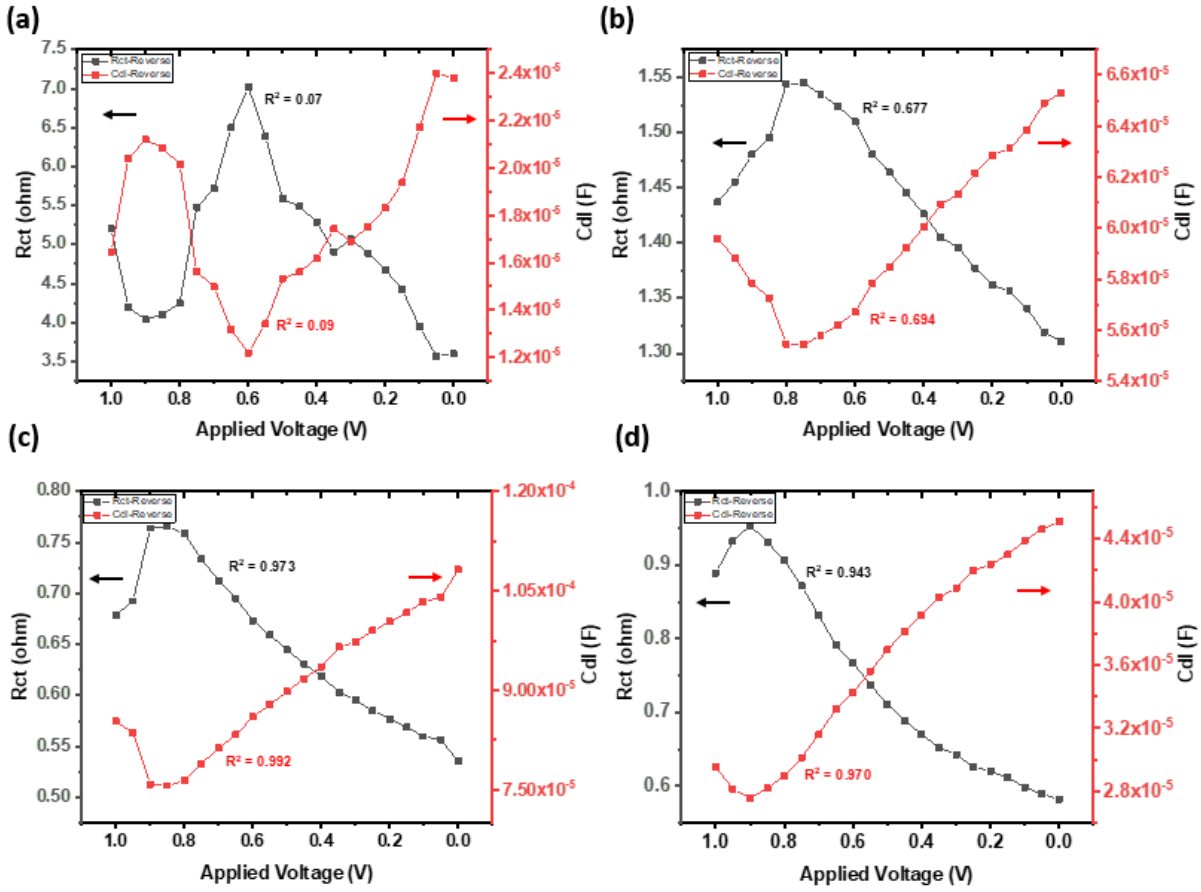

Figure 7.4 Plots showing charge resistance and double layer capacitance: (a) CAG-500, (b) CAG-600, (c) CAG-700 and (d) CAG-800.

Figure 7.4 (a-d) shows the dependency of the charge transfer resistance (R_{ct}) and the double layer capacitance (C_{dl}) on the applied voltage for all the electrode materials, determined from equivalent circuit fitting. The non-linear R_{ct} behavior of CAG-500 and CAG-600 can be attributed to the low surface area and non-uniform pore structure with lack of mesoporosity. Whereas, the CAG-700 and CAG-800 showed a linear increase in charge transfer resistance with increase in applied potential owing to its high surface area with thecombination of micropores and mesopores which helps in reducing the ion diffusion resistance and can increase ion transfer.

The typical behavior of an ideal capacitor is increase in C_{dl} and decrease in R_{ct} with applied voltage, which explicitly reveals the electrochemical performance of the material such as specific capacitance and rate capability. However, the samples, CAG-500 and CAG-600, though at initially followed an ideal capacitor trend, exhibited downward behavior at higher applied voltage, showing high and low values of R_{ct} and C_{dl}, respectively. At higher voltages, the mobility of the electrolyte ions to the inner surface of the electrode was restricted by the random shaped pore which limits double layer formation. Interestingly, the electrodes CAG-700 and CAG-800 present linear increase and decrease in C_{dl} and R_{ct} with increase in applied potential. The CAG-700 depicted a very high C_{dl} compared to all other electrode materials and the small linear change in R_{ct} value indicates the superior electrochemical property of the material owing to its high surface with graded micropores beneath the mesopores.

The change in C_{dl} and R_{ct} values are a direct measure of specific capacitance and capacitance retention of the newly developed material. The fit results of CAG-700 showed a high linear regression (R^2) value of 0.992 and 0.973 for C_{dl} and R_{ct}, respectively. From the DEIS results, it was expected that the sample, CAG-700 can present a very high specific capacitance and capacitance retention compared to other carbon aerogel electrodes. In order to validate the DEIS result, cyclic voltammetry, and galvanostatic charge-discharge experiments were conducted.

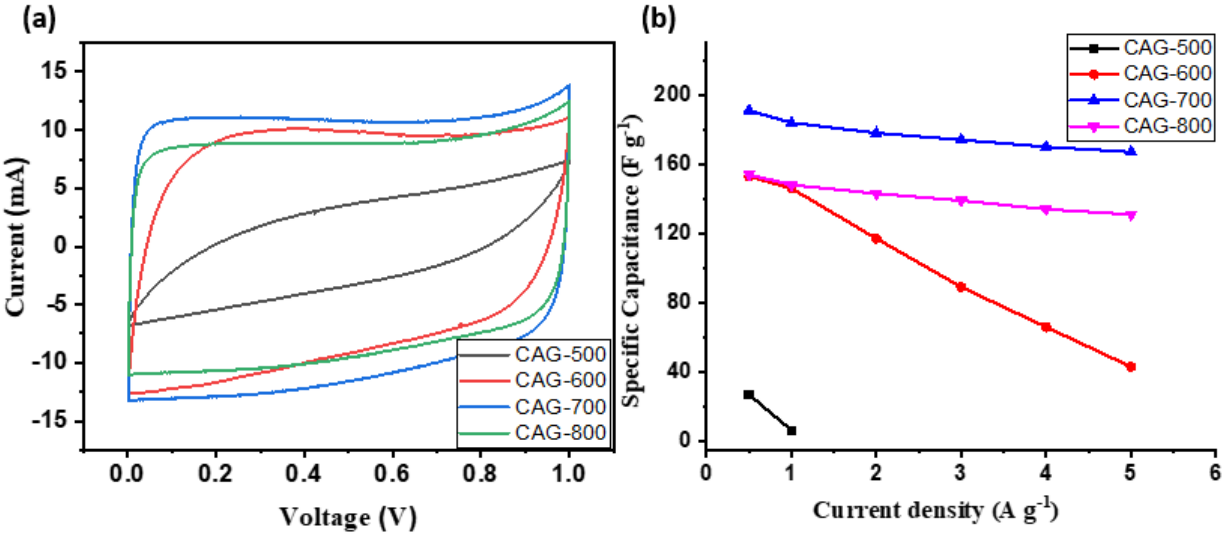

Figure 7.5 (a) Cyclic voltammogram of all samples at 5 mV s^{-1}, (b) specific capacitance vs. current density.

The voltammograms from CV of the samples presented a rectangular shape curve typical of capacitive materials, except for CAG-500, at a scan rate of 5 mV s^{-1}, as displayed in

Figure. 7.5a. Both CAG-600 and CAG-800 present nearly same loop under the potential window, CAG-600 is also exhibited as a pseudocapacitance behavior due to nitrogen functionalities. The CAG-700 exhibited large loop under the potential window indicating the high double layer capacitance formation and the result was in good agreement with mid frequency region of DEIS results in terms of C_{dl} formation at the electrode/electrolyte interface. The CV voltammogram curve of each sample at different sweep rate is shown in **Figure 7.6**.

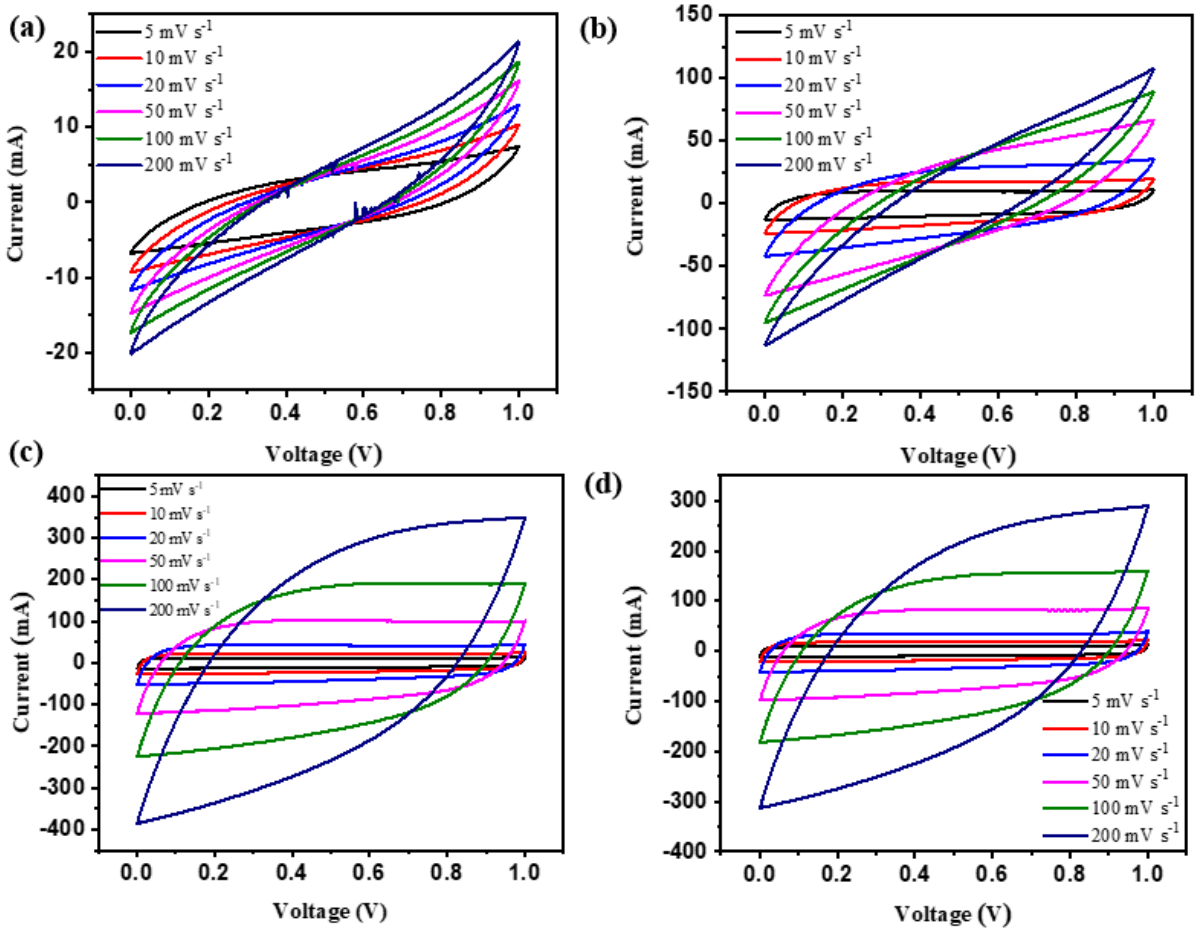

Figure 7.6 CV curves of all the carbon aerogel samples. CAG-500 (a), CAG-600 (b), CAG-700 (c), and CAG-800 (d)

The current response against different scan rates are plotted to understand the double layer formation and reversibility and are shown in **Figure 7.7**. Comparing the scan rate profile at 1 V, the maximum linearity has been obtained for the CAG-700 (R^2 = 0.998) and CAG-800 (R^2 = 0.997) samples, indicating the ability of high double layer formation and reversibility [31].

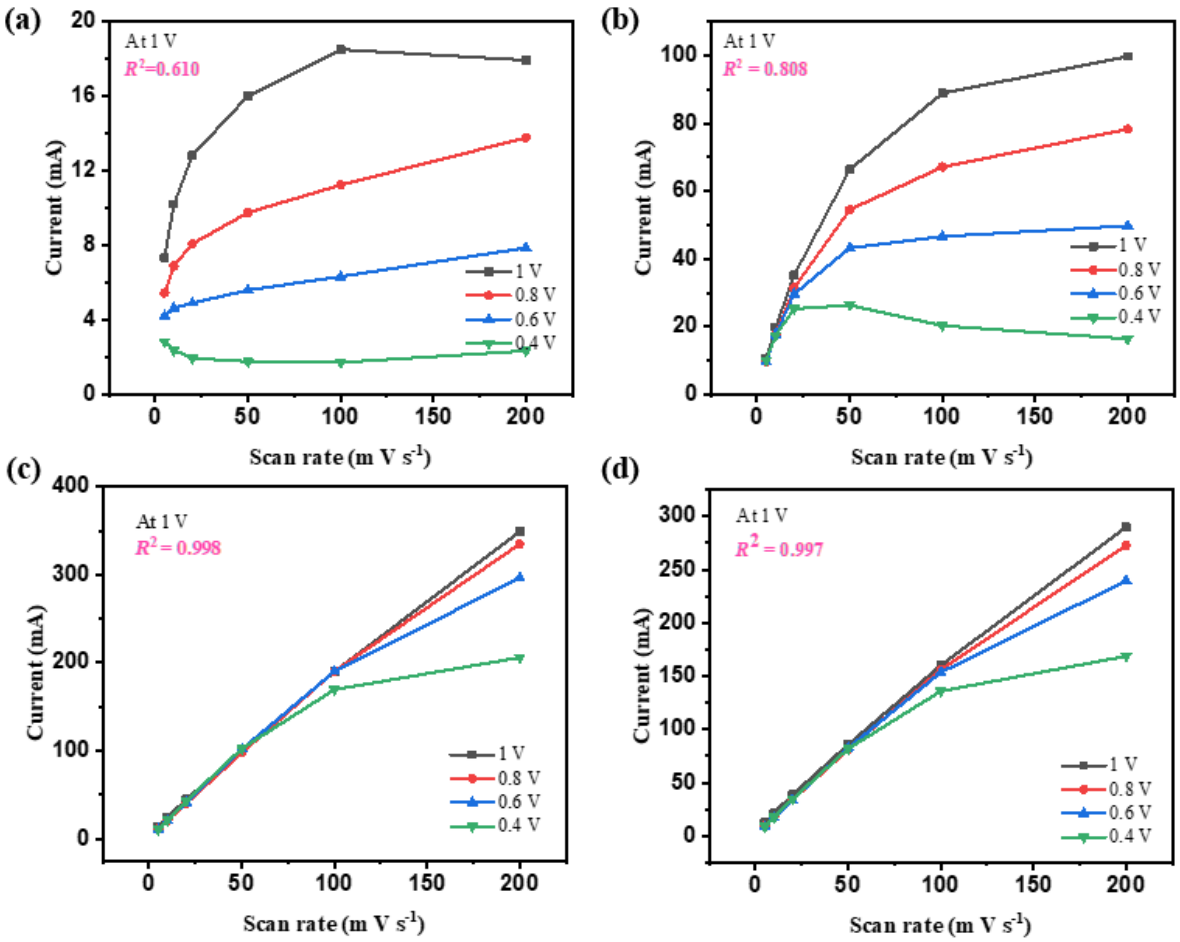

Figure 7.7 Dependency pattern of current versus scan rate for all the carbon aerogel electrodes.

The charge-discharge ability of the carbon aerogel electrodes was performed at various current densities, and the charge-discharge profile of each carbon aerogel electrodes are given in **Figure 7.8**. The calculated specific capacitance values versus current density are shown in **Figure 7.5b**. At a low current density of 0.5 A g^{-1} the sample CAG-700 presents a very large specific capacitance value of 191 F g^{-1} and capacitance retention was found to be 87% at high current density of 5 A g^{-1}. Both the samples CAG-500 and CAG-600 samples were unable to retain the capacitance above 1 A g^{-1} due to low surface area and lack of mesoporosity.

The samples CAG-600 and CAG-800 presented nearly the same capacitance value at low current density, while with an increase in current density CAG-800 retains the specific capacitance value owing to its large volume of mesopores. Comparing the GCD results with DIES, it can be clearly understood that the rate capability of the electrode material at high current density can be directly correlated to the change in charge transfer resistance with applied potential. The current density (**Figure 7.5 b**) and the charge transfer resistance (**Figure 7.4**),

randomly varies with applied potential, charge transfer resistance value of CAG-600 exhibited random behavior while the CAG-800 presented a linear change with applied potential.

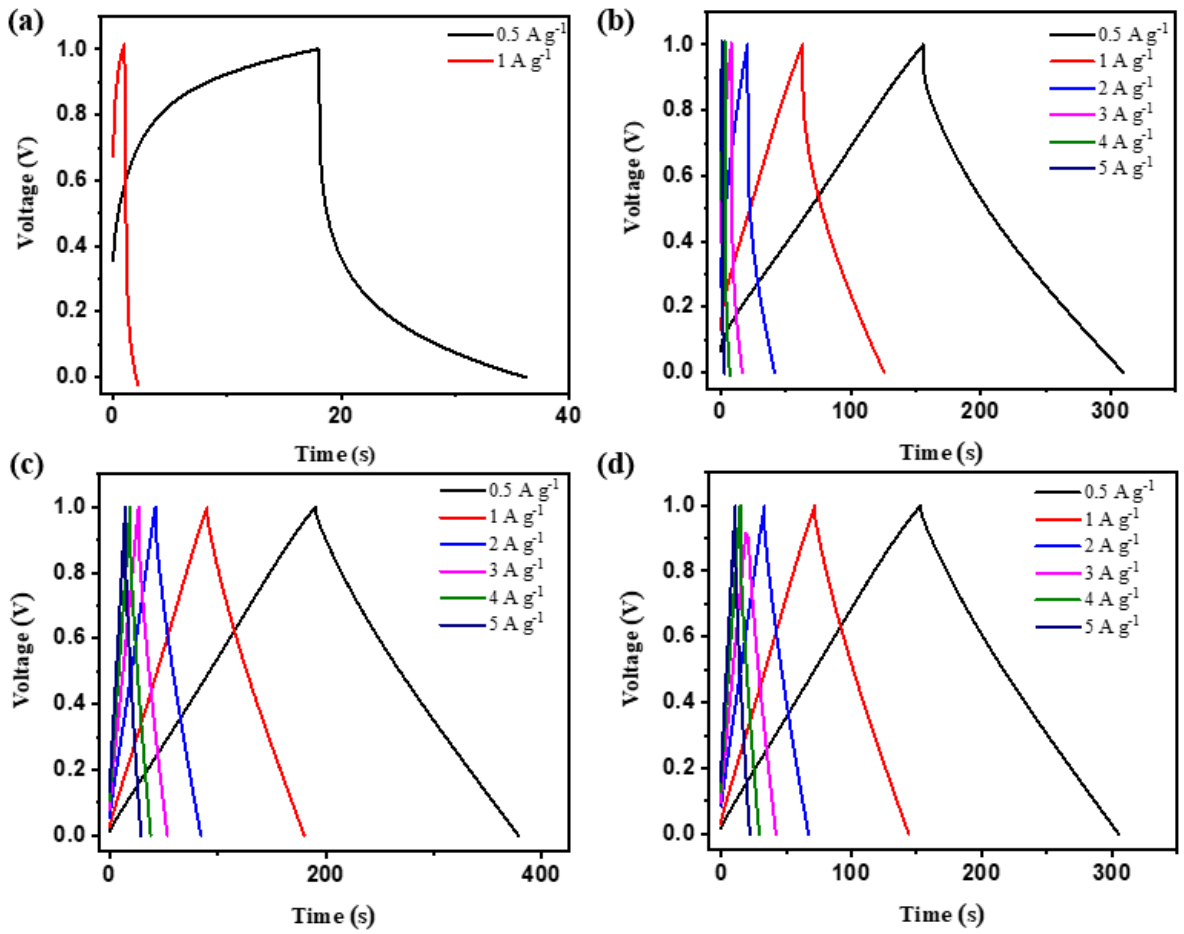

Figure 7.8 GCD curves of all the carbon aerogel samples, CAG-500 (a), CAG-600 (b), CAG-700 (c) and CAG-800 (d).

In conclusion, it is clearly evident that the samples have a plentiful volume of mesopores which can minimize ion diffusion resistance that helps in retaining the specific capacitance at high current densities. Moreover, the CAG-700 presents excellent electrochemical properties because of its high surface area and tuned pore size distribution. Both CV and GCD results are in concordance with the DEIS result. In comparison with the recently reported carbon aerogel electrode which were synthesized from biomass and other precursors (**Table 7.2**), the tamarind seed kernel derived carbon aerogel show the highest surface area and a highly competitive capacitance of 191 F g^{-1} at 0.5 A g^{-1}.

Table 7.2 Comparison of electrochemical properties of porous carbon electrodes derived from various precursors for supercapacitor reported in recent papers.

Carbon source	Specific capacitance ($F\ g^{-1}$)	Specific Current ($A\ g^{-1}$)	Electrolyte	System	Ref
Cellulose	195`	0.1	1 M H_2SO_4	2 Electrode	[32]
Bagasse	142	0.5	6 M KOH	2 Electrode	[33]
RSFL	150	-	-	2 Electrode	[34]
leonarditefulvic acid	368	0.05	6 M KOH	2 electrode	[35]
Tamarind seed kernel	**191**	**0.5**	**6 M KOH**	**2 Electrode**	**This work**

From the DEIS, CV and GCD results it is clearly evident that the specific surface area and pore size distribution are majorly influencing the specific capacitance and rate capability of the electrode materials, respectively. It is predicted that the specific surface area and pore size distribution of the electrode materials need to be optimized to achieve an excellent electrode material for a supercapacitor application. From above results, we suggest that the DEIS can be an effective preliminary tool to evaluate the electrochemical performance of the newly developed electrode material.

7.3 Conclusions

A combination of micro and mesoporous carbon aerogels was prepared from tamarind seed kernel using a simple synthesis strategy. The textural properties of the carbon aerogels were optimized by varying the carbonization temperature. Particularly, the sample carbonized at 700 °C showed high surface area values of 2645 $m^2\ g^{-1}$ and large volume of mesopores in the range of 2-5 nm. It has been successfully demonstrated that the DEIS method can be an efficient tool to characterize electrode material for supercapacitor. As a proof-of-concept, a newly developed carbon aerogel was evaluated using DEIS. Direct measurements of double layer formation and charge transfer resistance at various voltages are used as parameters to identify the best sample. This is in good agreement with the CV, GCD, and textural properties. The prediction by DEIS results in identifying a sample high double layer capacitance value and low charge transfer at all potential, corresponded well to the sample with optimal micro to mesopores ratio. The GCD results further confirmed a superior capacitance value of 191 $F\ g^{-1}$ at current density of 0.5 $A\ g^{-1}$. In conclusion, this method can be a reliable tool to rapidly

evaluate and identify materials with high capacitance and rate capability from an array of electrode materials in the development for supercapacitor application.

References

[1] Zhang W. L, Xu J. H, Hou D. X, Yin J, Liu D. B, He Y. P, and Lin H. B, *J. Colloid Interface Sci.*, **2018**, *530*, 338.

[2] Long C, Chen X, Jiang L, Zhi L, and Fan Z, *Nano Energy*, **2015**, *12*, 141.

[3] Zhang H, Su H, Zhang L, Zhang B, Chun F, Chu X, He W, and Yang W, *J. Power Sources*, **2016**, *331*, 332.

[4] Ruibin Q, Zhongai H, Yuying Y, Zhimin L, Ning A, Xiaoying R, Haixiong H, and Hongying W, *Electrochim. Acta*, **2018**, *167*, 303.

[5] Liu C, Liu J, Wang J, Li J, Luo R, Shen J, Sun X, Han W, and Wang L, *J. Colloid Interface Sci.*, **2018**, *512*, 713.

[6] Liu M, Wei F, Yang X, Dong S, Li Y, and He X, *New Carbon Mater.*, **2018**, *33*, 316.

[7] Zhang W, Lin N, Liu D, Xu J, Sha J, Yin J, Tan X, Yang H, Lu H, and Lin H, *Energy*, **2017**, *128*, 618.

[8] Ramesh T, Jafri R. I, Reddy N. P, Raveendra N. V, Rajalakshmi N, Dhathathreyan K. S, Tamilarasan P, and Ramaprabhu S, *Adv. Porous Mater.*, **2018**, *6*, 8.

[9] Zhao Y, Xie F, Zhang C, Kong R, Feng S and Jiang J. X, *Microporous Mesoporous Mater.*, **2017**, *240*, 73.

[10] Liu Y, Cao L, Luo J, Peng Y, Ji Q, Dai J, Zhu J, and Liu X, *ACS Sustain. Chem. Eng.*, **2019**, *7*, 2763.

[11] Meng Q, Wu H, Meng Y, Xie K, Wei Z ,and Guo Z, *Adv. Mater.*, **2014**, *26*, 4100.

[12] Chen T, Tang Y, Qiao Y, Liu Z, Guo W, Song J, Mu S, Yu S, Zhao Y and Gao F,*Sci. Rep.*, **2016**,*6*, 1.

[13] Dyatkin B, Osti N. C, Gallegos A, Zhang Y, Mamontov E, Cummings P. T, Wu J, and Gogotsi Y, *Electrochim. Acta*, **2018**,*283*, 882.

[14] Yang C, Zhou M, and Xu Q, *Phys. Chem. Chem. Phys.*, **2013**, *15*, 19730.

[15] Huang Q. A, Tsay K. C, Sun C, Yang C, Zhang L, and Zhang J, *J. Power Sources*,

2018, *400*, 69.

[16] Ma Z, Shao G, Fan Y, Feng M, Shen D, and Wang H, *ACS Sustain. Chem. Eng.*, **2017**, *5*, 4856.

[17] Fletcher S, Black V. J, and Kikpatrick I, *J. Solid State Electrochem.*, **2014**, *18*, 1377.

[18] Jani A and Tripathi S. K, *J. Energy Storage*, **2015**, *4*, 121.

[19] Kang J, Wen J, Jayaram S. H, Yu A, and Wang X, *Electrochim Acta*, **2014**, *115*, 587.

[20] Zhang L, Wang Z, Hu, and Dorrell D. G, *Energy Procedia*., **2015**, *75*, 1888.

[21] Ramesh T, Rajalakshmi N, and Dhathathreyan K. S, *J. Energy Storage*, **2015**, *4*, 89.

[22] Ramesh T, Rajalakshmi N, Dhathathreyan K. S, Reddy L. R. G, *ACS Omega*, **2018**, *3*, 12832.

[23] Sahu S. R, Devi D. P, Phanikumar V. V. N, Ramesh T, Rajalakshmi N, Praveena G, Prakash R, Das B, and Gopalan R, *Ionics*, **2018**, *24*, 3413.

[24] Chandra M. C, Harini K, Vajiha A. B, Priya U. L, Jenita P. M, Babuskin S, Karthikeyan S, Sudarshan K, Renuka V, and Sukumar M, *Carbohydr Polym.*, **2018**, *186*, 394.

[25] Nayak A. K, Pal D and Santra K, *Int. J. Biol. Macromol.*, **2015**, *79*, 756.

[26] Zhuo H, Hu Y, Tong X, Zhong L, Peng X, and Sun R, *Ind. Crop. Prod.*, **2016**, *87*, 229.

[27] Hu Y, Tong X, Zhuo H, Zhong L, Peng X, Wang S, and Sun R, RSC Adv, 2016, 6, 15788–15795

[28] Yu M, Han Y, Li Y, Li J, and Wang L, *CarbonhydratePolym.*, **2018**, *199*, 555.

[29] Lei E, Li W, Ma C, Xu Z, and Liu S, *Appl. Surf. Sci.*, **2018**, *457*, 477.

[30] Zhang H, He X, Gu J, Xie Y, Shui H, Zhang X, Xiao N, and Qiu J, *Fuel Process Technol.*, **2018**, *175*, 10.

[31] Misnon I. I, Zain N. K. M, Aziz R. A, Vidyadharan B, and Jose R, *Electrochim Acta*, **2015**, *174*, 78.

[32] Tian X, Zhu S, Peng J, Zuo Y, Wang G, Guo X, Zhao N, Ma Y, and Ma L, *Electrochim*

Acta, **2017**, *241*, 170.

[33] Hao P, Zhao Z, Tian J, Li H, Sang Y, Yu G, Cai H, Liu H, Wong C. P, and Umar A, *Nanoscale*, **2014**, *6*, 12120.

[34] Halama A, Szubzda B, and Pasciak G, *Electrochim Acta*, **2010**, *55*, 7501.

[35] Ma Y. Z, Guo Y, Zhou C, and Wang C. Y, *Electrochim Acta*, **2016**, *210*, 897.

CHAPTER 8

CONCLUSIONS

In the present thesis, we successfully demonstrated the synthesis of novel porous carbons from agricultural biomass waste for supercapacitor electrode application with improved electrochemical performance and lower device cost. The precursor materials are chosen based on their chemical composition and microstructure. The textural properties of the microstructural carbon materials were modified by the KOH chemical activation and by thermal treatments. The electrochemical performances of these textured materials are investigated and the relationship between porosity and electrochemical properties is studied.

A systematic experimental approach is adopted to improve the electrochemical performance in a progressive manner. Initially, the work was focused on the design of a material with high surface area and high electrical conductivity. Natural jute fibre containing a high volume of lumen content is taken as a precursor and converted into high surface area carbon with micro fibrous structure. It is assumed that the high surface area and fibrous structure will provide maximum scope for ion conduction and electron conducting pathways, respectively. Though the activated carbon fibres prepared from jute could fulfill both the requirements, the specific capacitance was moderate compared to other well-known carbon materials because of its inaccessible pores. In order to improve the accessibility of pores for the electrolyte, carbon microsphere samples were synthesized from tamarind seed kernel with open pores that provide ready accessibility for electrolyte ions. These carbon microsphere samples proved to be promising candidate materials compared to other biomass derived electrode materials in electrochemical performance.

Further, a sample with combination of fibrous and spherical structure was synthesized from tamarind seed coat. The physical (micro-fiber) and chemical (tannin-polyphonols) properties of tamarind seed coat largely helped in achieving the carbon material with micro-fibres decorated with irregular spherical particles. These porous carbon micro-fibres showed high specific capacitance, rate, and retention capability in both aqueous and ionic liquid electrolytes. As a major success of this study, the pore size distribution was understood, which play a significant role in achieving superior electrochemical performance. Also, it is demonstrated that the pore size must be compatible with the solvated ion size of the electrolyte to achieve high capacitance and rate capability.

Further, the role of heteroatoms in enhancing the electrochemical parameters are studied by fabricating the advanced form of carbons incorporated with nitrogen. For this purpose, a tamarind seed kernel was chosen as a precursor which was dissolved in a mixture containing nitrogen salt to obtain an advanced carbon aerogel structure. The resultant carbon aerogel

samples synthesized from tamarind seed kernel showed a significantly high electrochemical performance compared to all the other materials reported in this thesis as well as with other biomass carbons reported in literature, because of its very high surface area, with nearly equal percentage of micropores and mesopores. The salient features and prominent physical and electrochemical properties of the best performing electrode materials fabricated and studied in this work are listed in **Table 8.1**.

Table 8.1 Textural and Electrochemical performance of best performing electrode materials.

Precursor	**Synthesis methods**	**Structure**	**Surface area ($m^2 g^{-1}$)**	**Specific capacitance ($F g^{-1}$)**	**SEM Image**
Jute fibres	Carbonization & Activation	Micro-tubular	1224	114	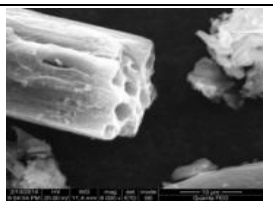
Tamarind kernel	Hydrothermal & Activation	Micro and Mesopores decorated Spheres	1284	160	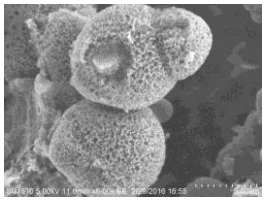
Tamarind seed coat	Hydrothermal & Carbonization & Activation	Hierarchical porous carbon micro-fibres	1702	157(KOH) 76 (IL)	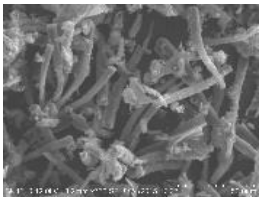
Tamarind kernel	Sol-gel & Carbonization	3D interconnected porous network	2645	191	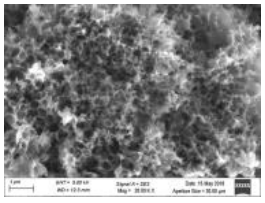

From Table 8.1 it can clearly be understood that each form of carbon material has its own merits compared to the other forms in terms of the experimental complexities and electrochemical performance. Further, a novel technique of using Dynamic Electrochemical Impedance Spectroscopy (DEIS) for rapidly evaluating the performance of new materials in development for supercapacitor application has been developed. It is found that the C_{dl} and R_{ct} values obtained from DEIS measurements linearly varied with the applied potential for the best

performing electrode materials indicating high specific capacitance and high rate capability, respectively. The results clearly demonstrated that the C_{dl} and R_{ct} values depend on the textural (surface area & pore size) properties of the electrode materials. The DEIS results are validated with the conventional CV and GCD results, and the agreement between them was good.

We can clearly see from the Figure 8.1 given below, as the surface area increases the specific capacitance increases. The role of pore volume or pore size are significantly seen in higher scan rates, wherein based on the size of the pores, samples having lower pore size showed higher resistance owing to inaccessibility of electrolyte. Whereas a moderate pore distribution showed an electrolyte retention thereby increase in overall capacitance. This indicates that mere surface area alone cannot be the only parameter to decide the performance of material in supercapacitor.

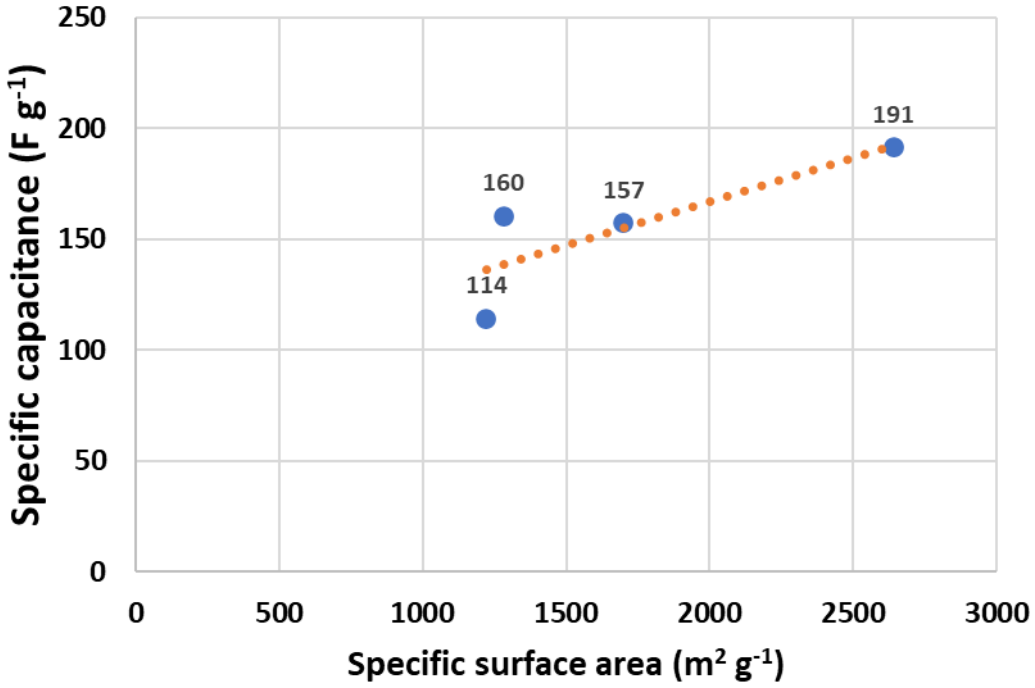

Figure 8.1 The relationship between specific capacitance and specific surface area of the synthesize carbon materials.

The materials synthesized in this work have shown extremely high capacitive performance and cyclic stability, and therefore, can be directly used as supercapacitor electrode and as support material in other electrochemical energy systems.

Scope for future research work

- Large scale production of these carbon materials and its cost analysis for comparison with the commercial activated carbons.
- Development of pouch cells or cylindrical cells with varying capacity ranges from 10 F to 200 F using the high performing electrode materials in aqueous and non-aqueous electrolytes.
- Improving the specific capacitance of the carbon material by incorporating the redox material onto the porous matrix.

In addition, the synthesized carbon materials have exhibited promising electrochemical behavior and the applications of these materials can be extended to other electrochemical systems like batteries, fuel cells, electrolysis, and sensors because of its high catalytic surface area, electrochemical stability, and conductivity.

LIST OF PUBLICATIONS

1. **T. Ramesh**, V. Raman, N. Rajalakshmi, L. Ram Gopal Reddy, Dynamic electrochemical impedance spectroscopy as a rapid screening tool for supercapacitor electrode materials, *J. Mater. Sci.: Mater. Electron*, **2019**, *31*, 1681.
2. **T. Ramesh**, N. Rajalakshmi, K.S. Dhathathreyan, L. Ram Gopal Reddy, Hierarchical porous carbon microfibers derived from tamarind seed coat for high-energy supercapacitor application, ACS Omega, **2018**, 3, *10*, 12832.
3. **T. Ramesh**, V. Raman, N. Rajalakshmi, L. Ram Gopal Reddy, Tamarind based porous carbon microspheres for high performance supercapacitors **(Submitted to Materials Letters)**
4. **T. Ramesh**, N. Rajalakshmi, K.S. Dhathathreyan, L. Ram Gopal Reddy, Activated carbon fibres derived from jute for high performance supercapacitor. **(To be submitted)**

PAPERS PRESNTED IN NATIONAL AND INTERNATIONAL CONFERENCES

1. T. Ramesh, N. Rajalakshmi, K.S. Dhathathreyan, L. Ram Gopal Reddy, Porous carbon microspheres derived tamarind seed kernel for supercapacitor application. Oral presentation in the International Conference on Advanced Materials **(ICAM- 2019)** held at Nirmalagiri College, Kannur, Kerela, India during 12-14th Jun, 2019
2. T. Ramesh, N. Rajalakshmi, K.S. Dhathathreyan, L. Ram Gopal Reddy, Jute derived activated carbon fibres for high performance supercapacitor. Oral presentation in the International Conference on Advanced Nanomaterials for Energy, Environment and Healthcare Applications **(ANEH-2018)** held at K.S.R College of Arts and Science for Women, Tiruchengode, India during 31 Aug- 1 Sep, 2018
3. T. Ramesh, N. Rajalakshmi, K.S. Dhathathreyan, L. Ram Gopal Reddy,Facile synthesis of carbon microspheres/MnO2 composite as highperformance electrodes for supercapacitors. Oral presentation in the National Conference on Recent Developments in Chemical Sciences and Allied Technologies held at National Institute of Technology, Warangal during 29-30, June-2017
4. T. Ramesh, N. Rajalakshmi, K.S. Dhathathreyan, L. Ram Gopal Reddy, Hierarchically porous carbon derived from agricultura l resource for high power supercapacitor applications. Oral presentation in the International Conference on Nanomaterials and Nanotechnology **(ICNANO-2017)** held at VBRI, Allahabad during 01-03, Mar-2017

AWARDS & ACHIEVEMENTS

1. Received "**Best Oral Presenter Award**" for the oral presentation titled "Hierarchically porous carbon derived from agricultural resource for high power supercapacitor applications" at International Conference on Nanomaterials and Nanotechnology **(ICNANO-2017)** 01-03 March 2017